

# Glue in hadrons at medium resolution and the QCD instanton vacuum

Wei-Yang Liu<sup>✉,\*</sup>, Edward Shuryak,<sup>†</sup> and Ismail Zahed<sup>‡</sup>

*Center for Nuclear Theory, Department of Physics and Astronomy,  
Stony Brook University, Stony Brook, New York 11794-3800, USA*

 (Received 11 April 2024; accepted 3 August 2024; published 5 September 2024)

We discuss a general framework for the evaluation of the gluonic form factors in light hadrons at low momentum transfer, in the QCD instanton vacuum. At medium resolution of the order of the inverse mean instanton size, the glue is mostly localized in single or pairs of pseudoparticles and globally constrained by the fluctuations of their topological charges. These pseudoparticles trap light quarks, giving rise to emerging multiflavor 't Hooft interactions. We explicitly evaluate the gluonic scalar, pseudoscalar, energy-momentum tensor (EMT), and the leading  $C$ -odd and  $C$ -even three-gluon hadronic form factors, at next to leading order in the instanton density, including molecular clusters of like and unlike instantons. We use the results for the EMT to address the contribution of the gluons in Ji's mass and spin sum rules, at low resolution. When evolved, our results for the mass and spin composition of the nucleon are shown to be in good agreement with the recently reported lattice results at higher resolution.

DOI: [10.1103/PhysRevD.110.054005](https://doi.org/10.1103/PhysRevD.110.054005)

## I. INTRODUCTION

We will start by explaining the title and by recalling the terminology to be used. In general, form factors are Fourier transforms of distributions of certain charges. The standard example is the electromagnetic form factors describing the electromagnetic charge and current distributions of nucleons and nuclei. However, form factors can be defined for any operator, and we will focus below on gluonic probes, like  $G_{\mu\nu}^2$ .

The form factors are functions of the (spacelike) momentum transfer  $Q$  and reflect on what the probe “sees,” if it has spatial resolution  $\sim 1/Q$ . In Fig. 1, we schematically identify three resolution regimes for QCD probes: hard, semihard, and soft. We now recall the meaning of this terminology.

The hard regime is given by perturbative Feynman diagrams with a number of gluon propagators  $(1/Q^2)^n$ . Physically, it corresponds to a hadron in a very compressed form, so that the quarks are inside the perturbative Coulomb fields of each other. In this regime, there are no dimensional quantities involved, as QCD is asymptotically free, and the power  $n$  can be obtained just by dimensional considerations

(except for certain special cases, e.g., spin flipping amplitudes, where quark masses must also appear).

This paper is about the semihard regime dominated by nonperturbative vacuum fluctuations. The latter are assumed to be semiclassical pseudoparticles, instantons, or their pairs. The ensuing form factors are generically of the form  $\beta_i(Q\rho) \cdot Q^n$  with  $\rho$  being a typical instanton size. At large  $Q\rho \gg 1$ , the form factors decrease exponentially, but they have different shapes in the  $Q\rho \sim O(1)$  region.

In the soft regime, the resolution is too poor to resolve individual instantons. This regime is dominated by “chiral” phenomena related to the appearance of a quark condensate and a “pion cloud” surrounding most hadrons. These chiral properties can be described either by summing multi-instanton chains or by phenomenological chiral Lagrangians. In this regime, the form factors are related to hadronic parameters, e.g., for the scalar channel with the  $2m_\pi$  threshold or the  $\sigma$  meson mass.

Different QCD operators naturally see different distributions. However, because of the self-duality of the instantons, the scalar  $O_S = G_{\mu\nu}^2$  and the pseudoscalar  $O_P = G_{\mu\nu}\tilde{G}_{\mu\nu}$  operators see the same well-localized spherical ball of the shape

$$(G_{a\mu\nu}^{\text{inst}})^2 = \frac{1}{g^2} \frac{192\rho^4}{(x^2 + \rho^2)^4} \quad (1)$$

if an instanton is alone or a similar but more complicated instanton is paired. It is important to note that it is a spot of rather strong field, of a quite small size.

\* Contact author: [wei-yang.liu@stonybrook.edu](mailto:wei-yang.liu@stonybrook.edu)

† Contact author: [edward.shuryak@stonybrook.edu](mailto:edward.shuryak@stonybrook.edu)

‡ Contact author: [ismail.zahed@stonybrook.edu](mailto:ismail.zahed@stonybrook.edu)

*Published by the American Physical Society under the terms of the Creative Commons Attribution 4.0 International license. Further distribution of this work must maintain attribution to the author(s) and the published article's title, journal citation, and DOI. Funded by SCOAP<sup>3</sup>.*

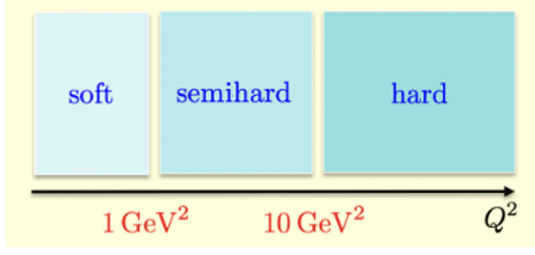


FIG. 1. The soft, semihard, and hard  $Q^2$  regions characterizing different regimes of the hadronic form factors.

Today, the mainstream of a first-principle theory of nonperturbative phenomena is lattice QCD. Therefore, it is important from the start to recall how these three regimes are revealed on the lattice as well. Gauge lattice configurations are dominated by “gluons,” waves with wavelength  $\sim a$ , the lattice UV cutoff. Yet, e.g., the *gradient flow* procedure (cooling) can be used to remove these gluons and reveal genuine nonperturbative fields. After a few coolings, the gluonic landscape looks like a (rather dense) ensemble of strongly correlated instanton–anti-instanton pairs. After further flow time or cooling, these pairs get annihilated, leading to a (rather dilute) ensemble of individual instantons and anti-instantons, which can withstand even “deep cooling.” For a detailed description of this procedure, see, e.g., [1].

For completeness, we briefly recall the history of the “instanton vacuum.” The QCD vacuum consists of semiclassical and topological instantons and anti-instantons (pseudoparticles) [2], that are described by a gluon moduli (quenched) with additional determinantal interactions (unquenched) [3,4]. In the “instanton liquid model” (ILM), one of us suggested that these pseudoparticles have mean size and density [5]

$$\rho \approx \frac{1}{3} \text{fm}, \quad n_{I+A} \approx 1 \text{fm}^{-4}, \quad (2)$$

which gives the dimensionless packing fraction  $\kappa = n_{I+A} \pi^2 \rho^4 \approx 0.1$ . This view of the QCD vacuum is supported by a large body of analytical and numerical results related to chiral symmetry breakings, including many aspects of the pions and the anomalous  $\eta'$  mesons; for a review, see, e.g., [6].

The QCD instanton vacuum does not strictly confine at large distances, although the instanton-induced central potential between heavy quarks is linear within a femtometer [7], before turning to a constant at large distances. However, it breaks spontaneously chiral symmetry by trapping and delocalizing massless left-handed or right-handed quarks, in a narrow zero-mode zone of about 100 MeV around the zero virtuality line. This mechanism is at the origin of mass from no mass and plays a central role in the composition and structure of light hadrons.

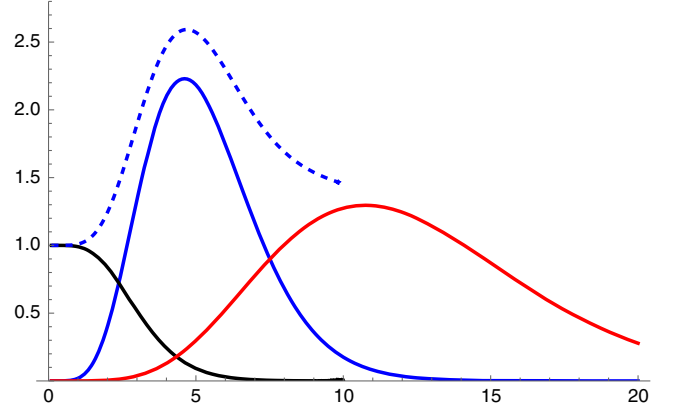


FIG. 2. Spectral function in coordinate space in units of  $\text{GeV}^{-1}$ , with the perturbative contribution (black solid line), the scalar glueball contribution (blue solid line), the scalar meson contribution (red solid line), and their sum (dashed blue line).

Earlier studies involving gluonic operators in the ILM included studies of their vacuum point-to-point correlators [8–10]. In particular, the scalar  $G_{\mu\nu}^2$  and pseudoscalar  $G_{\mu\nu} \tilde{G}_{\mu\nu}$  operators were found to receive large nonperturbative contributions. In contrast, the stress tensor correlator (also quadratic in the gauge field) was observed to be not affected.

In Fig. 2, we show the ratio of the vacuum correlator of two scalar  $G^2$  operators separated by (Euclidean) distance  $x$  (in  $\text{GeV}^{-1}$ ), normalized by the leading perturbative contribution

$$\Pi_{GG}^0(x) = \frac{384g^4}{\pi^4 x^8}. \quad (3)$$

In the coordinate representation, the “hard,” “semihard,” and “soft” regimes appear in the opposite order (left to right) in comparison to momentum representation in Fig. 1. Using estimates from the spectral representation, we show the scalar glueball contribution (blue solid line), the scalar sigma contribution (red solid line), the perturbative contribution (black solid line), and their sum (blue dashed line). The glueball mass and coupling are  $m_{0^{++}} = 1.5 \text{ GeV}$  and  $\lambda_{0^{++}} = 17.2 \text{ GeV}^3$  [8], respectively, while the sigma mass and mixing are, respectively,  $m_\sigma = 0.6 \text{ GeV}$  and  $\lambda_\sigma/\lambda_{0^{++}} \approx 0.066$  [11].

In Fig. 2, all three regimes are on display, with the full spectral function (blue dashed line) versus the distance in  $\text{GeV}^{-1}$  units where 5 is 1 fm. The hard regime is dominant at short distances (black solid line) with a plateau, where perturbation theory holds. The rise in the spectral function for separations  $x = 2\text{--}5 \text{ GeV}^{-1} \approx 0.41\text{--}1 \text{ fm}$  correspond to the semihard regime. The “sigma halo” at large separation  $x > 5 \text{ GeV}^{-1} \approx 1 \text{ fm}$  corresponds to the soft regime, familiar from, e.g., nuclear forces at large distances. In fact, the

transition between the hard and semihard regimes is even stronger in the ILM [6], as we will briefly review below.

Unlike chiral effects, phenomena related to the gauge fields are due not only to well-separated pseudoparticles in the dilute ILM, but also to fields in “incomplete tunneling” or instanton–anti-instanton molecules. In our papers such as [12] (devoted to the electromagnetic pion form factor) and the first paper of these series [7] (potentials in quarkonia), we have found that the “molecular” effects can even be dominant. In this respect, we reformulated the instanton vacuum to that of a “dense instanton ensemble,” where this contribution was included.

In this paper, we will evaluate gauge-invariant matrix elements of select gluonic operators in hadrons. Naturally, their definitions follow from QCD factorization, of inclusive processes [e.g., deep inelastic scattering (DIS)] or semi-inclusive processes (e.g., heavy quark pair production). They also emerge in the effective description of heavy quarkonia and in the standard model when the electroweak and heavy degrees of freedom are integrated out. Physically, they describe how the glue is distributed inside hadrons, mesons, or baryons and, therefore, carry important insights into their structure.

Unfortunately, such gluonic matrix elements are notoriously hard to measure experimentally, owing to the confining character of QCD in the infrared. For a recent investigation of the importance of the glue in semi-inclusive heavy meson production at threshold, see [13,14] (and references therein). So far, most of the evaluations are theoretical. First principle QCD lattice simulations provide a useful framework for their evaluation, but the intricacies of renormalization with operator mixing proves often to be quite formidable.

While the glueball spectra in gluodynamics are known rather well, there are no appropriate “constituent gluon models.” This is not surprising, given the intermittent nature of the vacuum gauge fields. Therefore, the explicit glue will not be treated as separate degrees of freedom (gluons) but as solitonic gauge fields or pseudoparticles of semiclassical nature. The QCD instanton vacuum captures the essentials of these pseudoparticles and provides a well-defined framework for the derivation of the gluonic matrix elements, in vacuum and in hadrons.

The matrix elements of the glue in hadrons using the QCD instanton vacuum was first used in [15] for a few gluonic operators in forward hadronic matrix elements and in [9] for both fermionic and gluonic form factors. We will show below how the methods of [15] can be generalized for nonforward matrix elements, in agreement with [9]. In the process, we will analyze a large class of gluonic operators, some of which are of relevance to select semi-inclusive processes, following factorization. Last but not least, we will show how to include the contributions from pairs of like and unlike instanton molecules.

All matrix elements should be understood as normalized at the “intermediate scale”  $\mu$  fixed by the instanton size

$$\mu^2 \sim \frac{1}{\rho^2} \approx (0.6 \text{ GeV})^2. \quad (4)$$

Sometimes, this scale appears with numerical factors, reaching  $\mu^2 \sim 1 \text{ GeV}^2$ . It should not be confused with the smaller “chiral” scales associated with the pion mass or the much higher scale  $\mu^2 > 4 \text{ GeV}^2$  at which perturbative evolution can be used.

The organization of the paper is as follows: In Sec. II, we summarize our results for a number of gluonic form factors. In Sec. III, we review some aspects of the QCD instanton vacuum and the role played by the zero modes in the spontaneous breaking of chiral symmetry. We briefly note the possible interplay of the  $P$  vortices with the topological pseudoparticles in the QCD vacuum. In Sec. IV, we detail the emergence of the effective quark and gluon interactions in the QCD instanton vacuum, in the single-instanton approximation. In Sec. V, we show how to use the sum ansatz in general, to evaluate the pertinent hadronic form factors at low momentum transfer. In Sec. VI, we detail the derivation of the gluonic scalar form factor at next-to-leading order (NLO) in the instanton density and including instanton molecular configurations. In Sec. VII, we derive the pseudoscalar gluonic form factor at NLO in the instanton density, where the fluctuations in the topological charge are also included. In Sec. IX, we derive the form factor for a general  $C$ -odd and dimension-6 gluonic operator, which appears as a leading twist-3 operator in diffractive production of heavy pseudoscalar mesons. Its  $C$ -even and dimension-6 gluonic operator form factor is also analyzed in Sec. IX. In Sec. X, we analyze the QCD gravitational form factor (GFF) in a hadronic state, in the context of the QCD instanton vacuum. The GFF is split into a traceless and traceful part, each of which are evaluated at NLO in the instanton density. In Sec. XI, we show that all hadronic squared masses satisfy the scale anomaly identity in the QCD instanton vacuum. In Sec. XI, we use Ji’s mass sum rule, to detail the various contributions of the quark and gluons in the QCD instanton vacuum at low resolution. In Sec. XII, we extend this budget analysis to Ji’s spin sum rule for the nucleon. Our conclusions are in Sec. XIV. In Appendix A, we outline the general structure of the emergent multiflavor effective Lagrangian with constitutive gluons. In Appendix B, we show how the multiflavor interactions yield a massive  $\eta'$  and a massless pion for the case of two light flavors and extract the scalar and pseudoscalar singlet couplings to the emerging constituent quarks. In Appendix C, we briefly go over the instanton field and field strength in singular gauge and detail its color moduli. In Appendix D, we detail how the color averaging is performed for the instanton pairs and molecules. In Appendix E, we suggest that the emergent effective vertices

with Lehmann-Symanzik-Zimmermann (LSZ) reduced gluons can be used in Feynman graphs that include small size instantons only. In Appendix F, we briefly show how the canonical ensemble of pseudoparticles can be extended to a grand canonical ensemble, to account for the fluctuations in their number which captures globally the scale and  $U(1)$  anomalies. In Appendix G, we summarize some useful identities for averaging over the color moduli.

## II. SUMMARY OF THE RESULTS

The theory of semi-inclusive and exclusive QCD processes with large momentum transfer  $Q^2$  is rooted in two assumptions (see [16,17] for early work): (i) the factorization of a soft and hard parts of the processes, appearing when  $Q^2$  is larger than any nonperturbative scale, and (ii) the hard part, after it is appropriately “factored out,” can be treated using perturbative QCD.

Unfortunately, there are big discrepancies between such an asymptotic theory and existing experimental data, which remain in the semihard regime (as illustrated in Fig. 1). This is particularly clear from current JLab data on the nucleon electromagnetic form factors [18] and lattice simulations [19]. The measured mesonic and baryonic form factors are well above the predictions of the perturbative QCD scaling laws, even when taken with maximally favorable assumptions (flat distributions and twist corrections included). This is not surprising, since there is a drastic difference between the scales in DIS and jet physics, on one hand, and exclusive processes, on the other. The former are well defined above the scale  $\mu^2 \sim 100 \text{ GeV}^2$  (hard regime), while the exclusive processes are defined at a much smaller scale, within 1–10  $\text{GeV}^2$  (semihard regime).

In this paper, we evaluate a number of gluonic form factors, e.g.,  $GG$ ,  $G\tilde{G}$ ,  $fGGG$ ,  $dGGG$ , and  $T_g^{\mu\nu}$ , in the QCD instanton vacuum at medium resolution, within the semihard regime. At this resolution, the gluons are described by

semiclassical pseudoparticles, with the large gauge space reduced solely to the bosonic and fermionic moduli of these pseudoparticles. Their contribution in a given hadron is amenable to pertinent matrix elements of the collectivized fermionic zero modes in the moduli.

The calculation are carried out to next order in the instanton density in the QCD instanton vacuum, where the contributions of like and unlike pairs of instantons are retained. There are many technical details associated to these calculations, most of which can be found in the subsequent sections and appendixes. Therefore, we decided to present our results first, while leaving their derivations to the rest of the paper.

### A. $GG$ vacuum form factor

The gluonic scalar vacuum form factor captures important aspects of the gluonic correlation function in the QCD vacuum. Since it also shows up as part of the glue in the nucleon scalar form factor, we will start by recalling and then extending some of the results [6,9]. The gluonic scalar vacuum form factor is

$$\Pi_{GG}(q) = \int d^4x e^{-iq \cdot x} \langle GG(x)GG(0) \rangle_c = (32\pi^2)^2 \frac{\sigma_T(q)}{V} \quad (5)$$

with  $\Pi_{GG}(x)$  the point-to-point correlator of the scalar source  $O_S = G_{\mu\nu}^2$ . Equation (5) was discussed in the bosonized ILM in [9] and in the full ILM in [6], with the latter study focusing on the transition between the semihard and the hard or free regime.

In Fig. 3, we show the  $x$ -space point-to-point correlator normalized to the perturbative (two gluon) version. The  $x$ -space spectral function (dashed line) accounts for the scalar sigma, plus the scalar  $0^{++}$  glueball, plus the soft two-pion cut and the hard two-parton cut:

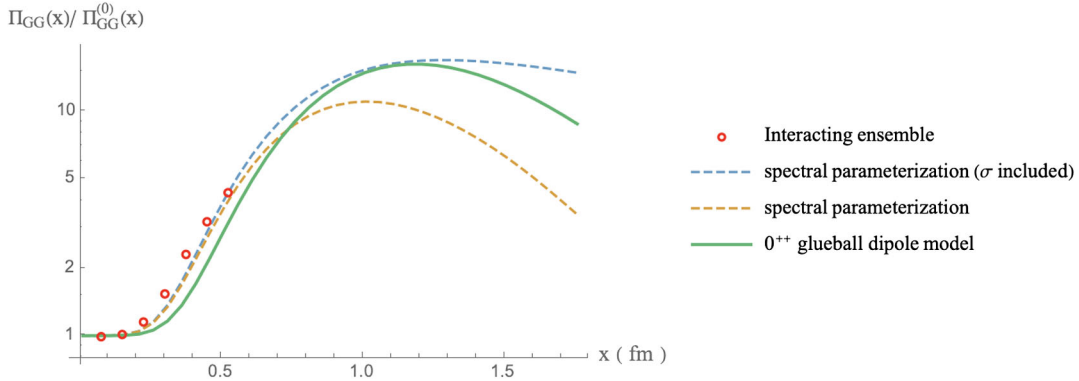


FIG. 3. Spectral function from the ILM (open red circles) [8], normalized by the perturbative contribution 14(c) in coordinate space. The comparison is to the empirical spectral parametrization (6) with the scalar sigma (blue dashed line) and without the scalar sigma (orange dashed line) and the  $0^{++}$  glueball dipole parametrization (8) (green solid line).

$$\begin{aligned} \Pi_{GG}^{(full)}(x) &= \lambda_{0^{++}}^2 D(m_{0^{++}}, x) + \lambda_\sigma^2 D(m_\sigma, x) \\ &+ \int_{4m_\pi^2}^{\Lambda_\chi^2} ds \frac{3}{64\pi^2} \sqrt{1 - \frac{4m_\pi^2}{s}} (s - 2m_\pi^2)^2 D(\sqrt{s}, x) \\ &+ \frac{2g^4}{\pi^2} \int_{s_0}^{\infty} ds s^2 D(\sqrt{s}, x). \end{aligned} \quad (6)$$

The parameters used in the spectral parametrization are  $\lambda_{0^{++}} = 15.6 \text{ GeV}^3$ ,  $\lambda_\sigma = 2.6 \text{ GeV}^3$ ,  $m_{0^{++}} = 1.25 \text{ GeV}$ , and  $m_\sigma = 683.1 \text{ MeV}$  to be consistent with the interacting ensemble calculation [8]. The perturbative threshold is set to  $s_0 = 2.4 \text{ GeV}$  [8], and the chiral symmetry-breaking scale range is  $\Lambda_\chi = 1.1 \text{ GeV}$ . Note that we have reinstated the gauge coupling with a value  $g^2/4\pi = 0.3$ , when accounting for the perturbative contributions.

To account for the dominance of the  $0^{++}$  glueball at low  $Q^2$ , and the free two-parton cut at large  $Q^2$ , we use instead a dipole approximation for the vacuum form factor:

$$\sigma_T(q) \approx \frac{\sigma_T}{(1 + Q^2/m_{0^{++}}^2)^2}, \quad (7)$$

where  $m_{0^{++}} = 1.25 \text{ GeV}$  [8]. When translated to  $x$  space plus the free contribution, it reads

$$\begin{aligned} \Pi_{GG}^{(dipole)}(x) &= \frac{384g^4}{\pi^4 x^8} + \frac{128\pi^2}{b} \langle G^2 \rangle \\ &\times \int \frac{d^4 q}{(2\pi)^4} \frac{1}{(1 + q^2/m_{0^{++}}^2)^2} e^{-iq \cdot x}. \end{aligned} \quad (8)$$

$$\begin{aligned} \frac{1}{32\pi^2} \langle P'S | g^2 G_{\mu\nu}^2 | PS \rangle &= - \left[ \frac{1}{4} M_{\text{inv}}^{(0)} \frac{\sigma_T (2\pi)^4}{\bar{N} V} \delta^4(q) \right] \bar{u}_s(P') u_s(P) \\ &- \left[ \frac{1}{N_c} \left( \frac{2\kappa}{\rho^2 m^{*2}} \right) \beta_{2g}^{(I)}(\rho q) + \frac{1}{2N_c(N_c^2 - 1)} \left( \frac{2\kappa}{\rho^2 m^{*2}} \right)^2 3\rho^2 m^2 T_{II} \beta_{2g}^{(II)}(\rho q) \right] \langle P'S | m \bar{\psi} \psi | PS \rangle \\ &+ \frac{1}{2N_c(N_c^2 - 1)} \left( \frac{2\kappa}{\rho^2 m^{*2}} \right)^2 \frac{\rho^4 m^2}{9} T_{IA} \beta_{2g}^{(IA)}(\rho q) q_\mu q_\nu \langle P'S | \bar{\psi} \left( \gamma_{(\mu} i \overleftrightarrow{\partial}_{\nu)} - \frac{1}{4} g_{\mu\nu} i \overleftrightarrow{\not{D}} \right) \psi | PS \rangle, \end{aligned} \quad (10)$$

where packing fraction  $\kappa$  is the dimensionless vacuum parameter defined as

$$\kappa = n_{I+A} \pi^2 \rho^4. \quad (11)$$

Here, the dependence on  $Q^2$  is given via induced nonlocal form factors, normalized to 1 and derived from certain instanton-based diagrams. Their analytic form is defined in (87) and their specific form illustrated in Fig. 4. The quark hopping integral is defined in (88).

At large  $x$  or small  $Q^2$ , the scalar point-to-point correlator captures the fluctuations of the number of pseudo-particles in the ILM, and its value at  $Q^2 = 0$  is related to the

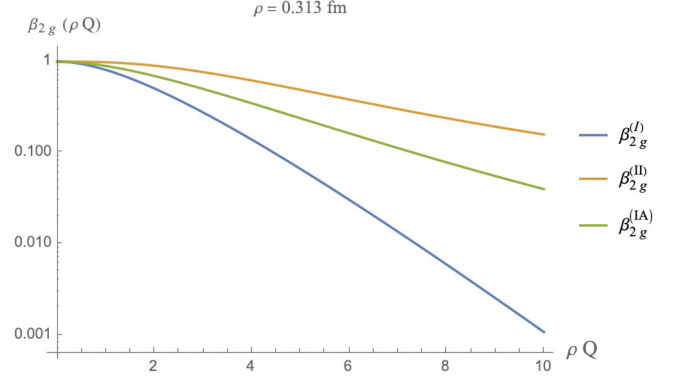


FIG. 4. Induced pseudoparticle form factors  $\beta_{2g}^{(I)}$ ,  $\beta_{2g}^{(II)}$ , and  $\beta_{2g}^{(IA)}$  versus  $Q\rho$ , from lower to upper, respectively.

In Fig. 3, we show (8) (green solid line), which lies between the full spectral representation with the sigma meson (dashed blue line) and without the sigma meson (dashed orange line).

## B. GG nucleon form factor

The nucleon gluonic scalar form factor following from the trace of the energy-momentum tensor (EMT) is defined as

$$- \frac{b}{32\pi^2} \langle P'S | g^2 G_{\mu\nu}^2 | PS \rangle = M_N G_N(Q^2) \bar{u}_s(P') u_s(P) \quad (9)$$

with in and out momenta  $P$  and  $P' = P + Q$ . Our main result for (9) in the ILM is

scale anomaly relation, which we will discuss in Sec. III A. It allows us to fix the normalization of the form factor. This effect can be included in (10) via the substitution

$$\frac{\sigma_T (2\pi)^4}{\bar{N} V} \delta^4(q) \rightarrow \frac{\sigma_T(q)}{\bar{N}}, \quad (12)$$

which shows how the glue in the scalar vacuum form factor exports to the nucleon scalar form factor.

In Fig. 5, we show the result for the gluonic contribution to the trace of the EMT in the nucleon (9) and (10) prior to the substitution (12) (red solid line), and after the substitution (green solid line). The comparison is to the recent

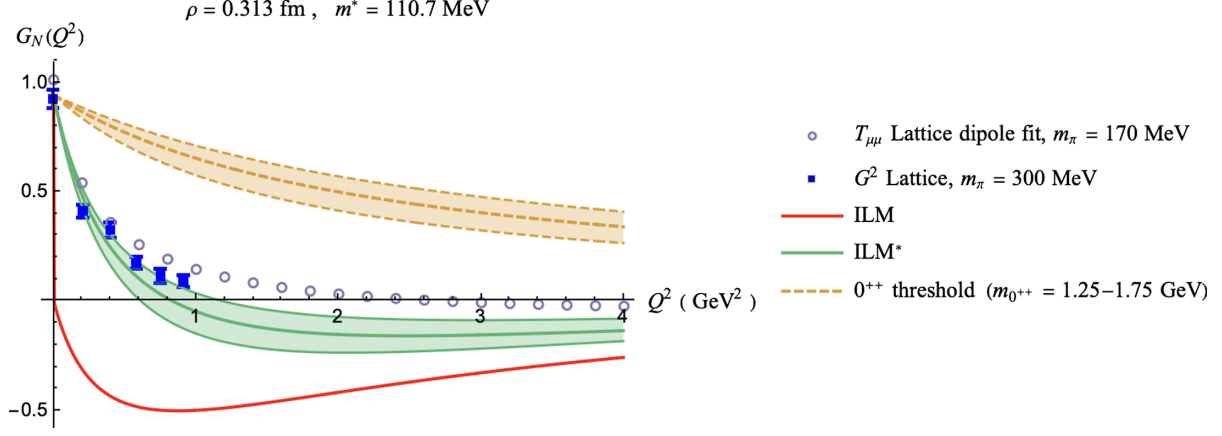


FIG. 5. Nucleon gluonic scalar form factor (9) (red solid line) and after the substitution (12) (green solid line) versus the lattice results (blue data points) [20]. The lattice dipole fits to the  $A$ ,  $D$  EMT form factors from [21] are used to reconstruct the nucleon gluonic scalar form factor (gray open circles), along with the  $0^{++}$  dipole form factor (12) (dashed brown line) with the glueball mass band  $m_{0^{++}}$  ranging from 1.25 to 1.75 GeV based on the various lattice calculations on the glueball mass [8,22,23]. The upper band corresponds to  $m_{0^{++}} = 1.75$  GeV, and lower band represents  $m_{0^{++}} = 1.25$  GeV.

lattice results (blue squares) from [20]. The lattice results for the nucleon  $A$ - and  $D$ -form factors from [21] can be used to reconstruct the gluonic contribution to the trace of the EMT in the nucleon (gray open circles). As expected, our results in the semihard region (red solid curve) when supplemented with the  $0^{++}$ -dipole glueball contribution in the soft region (dashed brown line) yield a good account of the reported and reconstructed lattice results in both the soft and semihard regions (green solid line).

### C. $G\tilde{G}$ nucleon form factor

The gluonic pseudoscalar form factor in a hadron state is defined as

$$\frac{1}{32\pi^2} \langle P'S | g^2 G_{\mu\nu} \tilde{G}_{\mu\nu} | PS \rangle = M_N \tilde{G}_N(Q^2) \bar{u}_s(P') i\gamma^5 u_s(P). \quad (13)$$

In the ILM at NLO in the instanton density, the result is

$$\begin{aligned} \frac{1}{32\pi^2} \langle P'S | g^2 G_{\mu\nu}^a \tilde{G}_{\mu\nu}^a | PS \rangle &= \left[ M_q(0) \frac{\chi_t(2\pi)^4}{\tilde{N}} \delta^4(q) \right] \bar{u}_{s'}(P') i\gamma^5 u_s(P) \\ &+ \left[ \frac{1}{N_c} \left( \frac{2\kappa}{\rho^2 m^{*2}} \right) \tilde{\beta}_{2g}^{(I)}(\rho q) + \frac{1}{2N_c(N_c - 1)} \left( \frac{2\kappa}{\rho^2 m^{*2}} \right)^2 3\rho^2 m^2 T_{II} \tilde{\beta}_{2g}^{(II)}(\rho q) \right] \langle P'S | m\bar{\psi} i\gamma^5 \psi | PS \rangle \\ &- \frac{1}{16N_c(N_c - 1)} \left( \frac{2\kappa}{\rho^2 m^{*2}} \right)^2 \rho^2 m^2 T_{IA} \tilde{\beta}_{2g}^{(IA)}(\rho q) i q_\mu \langle P'S | \bar{\psi} \gamma_\mu \gamma^5 \psi | PS \rangle, \end{aligned} \quad (14)$$

where the nonlocal form factors are given in (107) and the hopping between pseudoparticles is defined in (88). The first contribution in (14) captures the fluctuations of the topological charge of the pseudoparticles in the ILM in (37) in the large volume limit, which we can recast as

$$\frac{\chi_t(q)}{V} = \int d^4x e^{-iq \cdot x} \left\langle \frac{1}{32\pi^2} G\tilde{G}(x) \frac{1}{32\pi^2} G\tilde{G}(0) \right\rangle_c \quad (15)$$

with  $\chi_t(0) \approx \chi_t$  in the zero momentum limit. In Fig. 6, we show the result (14) (red solid line) for the gluonic pseudoscalar form factor in the nucleon state where the gluonic pseudoscalar form factor is defined in (13).

The expected behavior in the soft regime, near  $Q = 0$ , now stems from the screened topological charge fluctuations in the large volume limit, in the leading order in the

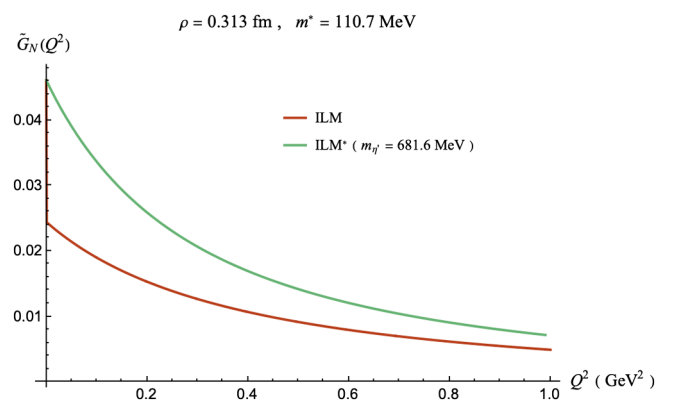


FIG. 6. Nucleon gluonic pseudoscalar form factor (14) in the QCD instanton vacuum (red solid line) and after the substitution (17) (green solid line).

pseudoparticle density. One expects this screening to be less singular than in the scalar case. Neglecting the three-pion continuum, its range is related with the (significantly heavier)  $\eta'$  meson

$$\chi_t(q) \approx \frac{\chi_t}{1 + Q^2/m_{\eta'}^2}. \quad (16)$$

[For consistency of the setting, we use  $m_{\eta'} \approx 681.6$  MeV for two flavors (B8).]

In Fig. 5, we show the result for the topological form factor (green solid line) following from (14) after the substitution

$$\frac{\chi_t (2\pi)^4}{\bar{N} V} \delta^4(q) \rightarrow \frac{\chi_t(q)}{\bar{N}}. \quad (17)$$

#### D. $dGGG$ nucleon form factor

The result for the  $C$ -odd gluonic operator  $d^{abc}G^aG^bG^c$  in a hadronic state at NLO in the instanton density is given by

$$\begin{aligned} \langle P' | g^3 d^{abc} G_{\mu\nu}^a G_{\rho\alpha}^b G_{\lambda\alpha}^c | P \rangle = & -\frac{N_c - 2}{2N_c^2(N_c^2 - 1)} \left( \frac{2\kappa}{\rho^2 m^{*2}} \right)^2 \frac{8\pi^2 m}{9} \rho^2 m^2 T_{II} \beta_{3g}^{(II)}(\rho q) \frac{1}{2} q^2 \delta_{\rho\lambda} \langle P' | \bar{\psi} \sigma_{\mu\nu} \psi | P \rangle \\ & + \frac{N_c - 2}{2N_c^2(N_c^2 - 1)} \left( \frac{2\kappa}{\rho^2 m^{*2}} \right)^2 \frac{8\pi^2 m}{9} \rho^2 m^2 T_{II} \beta_{3g}^{(II)}(\rho q) (\delta_{\mu\alpha} q_\beta q_\nu - \delta_{\nu\alpha} q_\beta q_\mu) \delta_{\rho\lambda} \langle P' | \bar{\psi} \sigma_{\alpha\beta} \psi | P \rangle \\ & - \frac{N_c - 2}{2N_c^2(N_c^2 - 1)} \left( \frac{2\kappa}{\rho^2 m^{*2}} \right)^2 \rho^2 m^2 T_{IA} \frac{4\pi^2}{45} \beta_{3g}^{(IA)}(\rho q) \\ & \times \left[ \epsilon_{\beta\gamma\lambda\sigma} q_\sigma q_\nu \delta_{\mu\rho} - \epsilon_{\beta\gamma\nu\sigma} q_\sigma q_\lambda \delta_{\mu\rho} - \frac{1}{2} \epsilon_{\beta\gamma\lambda\nu} q^2 \delta_{\mu\rho} + (\rho \leftrightarrow \lambda) - (\mu \leftrightarrow \nu) \right] \langle P' | \bar{\psi} \gamma_{[\beta} i \overleftrightarrow{\partial}_{\gamma]} \gamma^5 \psi | P \rangle \\ & - \frac{N_c - 2}{2N_c^2(N_c^2 - 1)} \left( \frac{2\kappa}{\rho^2 m^{*2}} \right)^2 \rho^2 m^2 T_{IA} \frac{4\pi^2}{15} \beta_{3g}^{(IA)}(\rho q) \delta_{\rho\lambda} \\ & \times \left( \epsilon_{\beta\gamma\mu\sigma} q_\sigma q_\nu - \epsilon_{\beta\gamma\nu\sigma} q_\sigma q_\mu - \frac{1}{2} \epsilon_{\beta\gamma\mu\nu} q^2 \right) \langle P' | \bar{\psi} \gamma_{[\beta} i \overleftrightarrow{\partial}_{\gamma]} \gamma^5 \psi | P \rangle \\ & - \frac{N_c - 2}{2N_c^2(N_c^2 - 1)} \left( \frac{2\kappa}{\rho^2 m^{*2}} \right)^2 \rho^2 m^2 T_{IA} \frac{8\pi^2}{45} \beta_{3g}^{(IA)}(\rho q) \\ & \times \left[ \epsilon_{\mu\nu\rho\alpha} (\delta_{\beta\lambda} q_\gamma q_\alpha - \delta_{\beta\alpha} q_\gamma q_\lambda) - \frac{1}{2} \epsilon_{\mu\nu\rho\gamma} q^2 \delta_{\beta\lambda} + (\rho \leftrightarrow \lambda) \right] \langle P' | \bar{\psi} \gamma_{[\beta} i \overleftrightarrow{\partial}_{\gamma]} \gamma^5 \psi | P \rangle, \end{aligned} \quad (18)$$

where the form factors normalized to unity are given in (118). The details of the derivation of (18) can be found in Sec. IX.

#### E. $fGGG$ nucleon form factor

The general result for the  $C$ -even gluonic form factor  $f^{abc}G^aG^bG^c$  in a hadronic state at NLO in the instanton density reads

$$\begin{aligned} \frac{5\rho^2}{384\pi^2} \langle P' S | g^3 f^{abc} G_{\mu\nu}^a G_{\nu\rho}^b G_{\rho\mu}^c | P S \rangle = & - \left[ \frac{1}{4} M_{\text{inv}}^{(0)} \frac{\sigma_T (2\pi)^4}{\bar{N} V} \delta^4(q) \right] \bar{u}_s(P') u_s(P) \\ & - \left[ \frac{1}{N_c} \left( \frac{2\kappa}{\rho^2 m^{*2}} \right) - \frac{1}{2N_c(N_c^2 - 1)} \left( \frac{2\kappa}{\rho^2 m^{*2}} \right)^2 3\rho^2 m^2 T_{II} \right] \tilde{\beta}_{3g}(\rho q) \langle P' S | m \bar{\psi} \psi | P S \rangle, \end{aligned} \quad (19)$$

where the instanton-induced form factors are given in (135), with the details of the derivation given in Sec. IX. The  $fGGG$  form factor is defined as

$$\langle P' S | g^3 f^{abc} G_{\mu\nu}^a G_{\nu\rho}^b G_{\rho\mu}^c | P S \rangle = M_N^3 A_{3g}^N(Q^2) \bar{u}_s(P') u_s(P). \quad (20)$$

In Fig. 7, we show the behavior of the  $C$ -even three-gluon form factor (19) using the QCD instanton vacuum parameter (red solid curve). The jump at  $Q = 0$  follows from the additional contribution stemming from the fluctuations

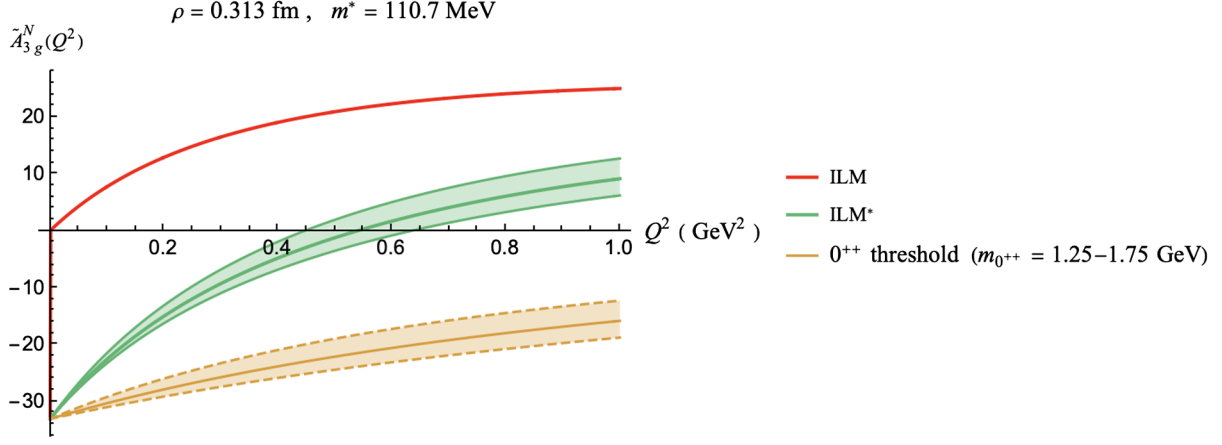


FIG. 7.  $C$ -even form factor in (19) (red solid curve) and after the substitution (Sec. IX) (green solid curve), along with the  $0^{++}$  dipole form substitution (12) (dashed brown line) where the glueball mass band  $m_{0^{++}}$  ranges from 1.25 to 1.75 GeV based on the various lattice calculations on the glueball mass [8,22,23]. The upper band corresponds to  $m_{0^{++}} = 1.75$  GeV, and the lower band represents  $m_{0^{++}} = 1.25$  GeV.

of the pseudoparticles number in the large volume limit in leading order in the density. It is screened by higher-order corrections (green solid curve) following the substitution (12).

#### F. $T_g^{\mu\nu}$ nucleon form factor

The hadronic form factor related to the tensor combination of gluonic field strengths is a very special case, since

the semiclassical instanton fields have a vanishing stress tensor. This implies a behavior that is very different from the previous cases, as seen already in vacuum point-to-point correlators [8].

The gluon energy-momentum form factor in a hadron state appears only due to instanton–anti-instanton “molecules.” In the pseudoparticle moduli, this form factor is amenable to quark-based observables

$$\begin{aligned}
\langle P'S | g^2 \bar{T}_{\mu\nu}^g | PS \rangle &= \frac{1}{2N_c(N_c^2 - 1)} \left( \frac{2\kappa}{\rho^2 m^{*2}} \right)^2 \rho^2 m^2 T_{IA} \left\{ \frac{16\pi^2}{3} \beta_{T_g,1}^{(IA)}(\rho q) \langle P'S | \bar{\psi} \left( \gamma_{(\mu} i \overleftrightarrow{\partial}_{\nu)} - \frac{1}{4} g_{\mu\nu} i \overleftrightarrow{\not{D}} \right) \psi | PS \rangle \right. \\
&\quad - \frac{4\pi^2 \rho^2}{9} \beta_{T_g,2}^{(IA)}(\rho q) \left( q_\mu q_\rho g_{\nu\lambda} + q_\nu q_\rho g_{\mu\lambda} - \frac{1}{2} g_{\mu\nu} q_\rho q_\lambda \right) \langle P'S | \bar{\psi} \left( \gamma_{(\rho} i \overleftrightarrow{\partial}_{\lambda)} - \frac{1}{4} g_{\rho\lambda} i \overleftrightarrow{\not{D}} \right) \psi | PS \rangle \\
&\quad \left. - 4\pi^2 \rho^4 \beta_{T_g,3}^{(IA)}(\rho q) \left( q_\mu q_\nu - \frac{1}{4} q^2 g_{\mu\nu} \right) q_\rho q_\lambda \langle P'S | \bar{\psi} \left( \gamma_{(\rho} i \overleftrightarrow{\partial}_{\lambda)} - \frac{1}{4} g_{\rho\lambda} i \overleftrightarrow{\not{D}} \right) \psi | PS \rangle \right\} \\
&\quad + \frac{1}{2N_c(N_c^2 - 1)} \left( \frac{2\kappa}{\rho^2 m^{*2}} \right)^2 \rho^2 m^2 T_{II} \frac{8\pi^2 \rho^2}{9} \beta_{T_g}^{(II)}(\rho q) \left( q_\mu q_\nu - \frac{1}{4} q^2 g_{\mu\nu} \right) \langle P'S | m \bar{\psi} \psi | PS \rangle. \quad (21)
\end{aligned}$$

The induced pseudoparticle form factors normalized to 1 are given in (149). The details regarding the derivation of (21) in the QCD instanton vacuum can be found in Sec. X with the supporting appendixes. Figure 14(c) can be used to analyze the gluonic energy-momentum form factors of the nucleon, in terms of the nucleon quark form factors. These form factors constrain the nucleon generalized parton distributions at zero skewness. They will be discussed elsewhere. Here, we will make use of (21) to budget the mass and spin content of the nucleon in the QCD instanton vacuum as we now summarize.

#### G. Ji’s mass sum rule

How the nucleon mass may be assigned to the quarks and gluons is resolution dependent. The QCD instanton vacuum at low resolution provides for a budgeting based on semiclassics. Using Ji’s mass decomposition, whereby the nucleon mass is split to

$$M_N = M_Q^N + M_G^N + M_A^N + M_m^N \quad (22)$$

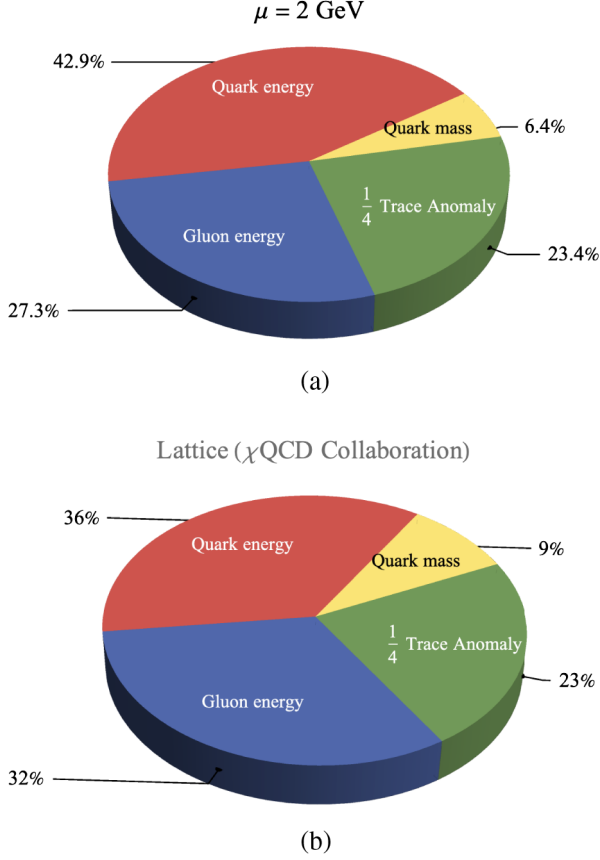


FIG. 8. Mass decomposition using Ji's nucleon mass sum rule, in the QCD instanton vacuum after DGLAP evolution at a resolution  $\mu = 2$  GeV (a) and the lattice results at the same resolution from [26].

with the quark and gluon contributions identified in (167), in particular, at NLO in the instanton density and a resolution of  $\mu \approx 1/\rho \approx 600$  MeV, we obtain

$$\begin{aligned}
 \frac{M_Q^N}{M_N} &= \frac{3}{4} \left( A_q(0) - \frac{\sigma_{\pi N}}{M_N} \right) \approx 69.19\%, \\
 \frac{M_G^N}{M_N} &= \frac{3}{4} A_g(0) \approx 1.01\%, \\
 \frac{M_A^N}{M_N} &= \frac{1}{4} \left( 1 - \frac{\sigma_{\pi N}}{M_N} \right) \approx 23.40\%, \\
 \frac{M_m^N}{M_M} &= \frac{\sigma_{\pi N}}{M_N} \approx 6.39\%
 \end{aligned} \tag{23}$$

with all the details given in Sec. XI. Fixing the pion-nucleon sigma term [24,25] shows that 69% of the nucleon mass is in the valence quarks (hopping zero modes), 23.4% in the condensate (displaced vacuum instanton field), and 1% in the moduli gluons. This budgeting evolves with the resolution. Using Dokshitzer-Gribov-Lipatov-Altarelli-Parisi (DGLAP) evolution to  $\mu \approx 2$  GeV yields a redistribution of the mass in favor of the gluons, with

$$\begin{aligned}
 \frac{M_Q^N}{M_N} &\approx 42.91\%, \\
 \frac{M_G^N}{M_N} &\approx 27.29\%.
 \end{aligned} \tag{24}$$

There is no change in the anomalous and mass contributions. In Fig. 8, we show comparative pie charts for the evolved ILM results (170) and (171) at the resolution of  $\mu \approx 2$  GeV, with the lattice results in [26] at the same resolution.

### H. Ji's spin sum rule

Similarly to the mass decomposition, the spin decomposition can be addressed using Ji's spin sum rule

$$S_N = \frac{1}{2} \Sigma_q + L_q + J_g, \tag{25}$$

where the quark angular momentum contribution is split into the intrinsic quark spin  $\Sigma_q$  plus orbital momentum  $L_q$ . In the QCD instanton vacuum, the leading LO contribution to the intrinsic quark spin is mostly from the vacuum topological susceptibility. In the QCD instanton vacuum with two flavors at a resolution  $\mu \approx 1/\rho \approx 600$  MeV, the budgeting is

$$\begin{aligned}
 \frac{\frac{1}{2} \Sigma_q}{S_N} &= \Delta \tilde{q} - \frac{g^2}{8\pi^2} N_f \Delta g \approx 10.5\%, \\
 \frac{L_q}{S_N} &= A_q(0) + B_q(0) - \frac{\frac{1}{2} \Sigma_q}{S_N} \approx 88.2\%, \\
 \frac{J_g}{S_N} &= A_g(0) + B_g(0) \approx 1.4\%
 \end{aligned} \tag{26}$$

with most of the derivation given in Sec. XII. Here, we assumed  $B_{q,g}(0) = 0$  [27]. Again, these assignments are resolution dependent and change with increasing  $\mu$ . In particular, for  $\mu \approx 2$  GeV, we obtain

$$\begin{aligned}
 \frac{\frac{1}{2} \Sigma_q}{S_N} &\approx 10.5\%, \\
 \frac{L_q}{S_N} &\approx 53.1\%, \\
 \frac{J_g}{S_N} &\approx 36.4\%.
 \end{aligned} \tag{27}$$

In Fig. 9(a), we show the histograms for the spin assignments (195), in the QCD instanton vacuum with two flavors before evolution at  $\mu = 0.56$  GeV and after evolution at  $\mu = 2$  GeV. They are to be compared to the lattice results in Fig. 9(b) from the  $\chi$ QCD Collaboration [28] and the ETMC Collaboration [29], both at the resolution of  $\mu = 2$  GeV.

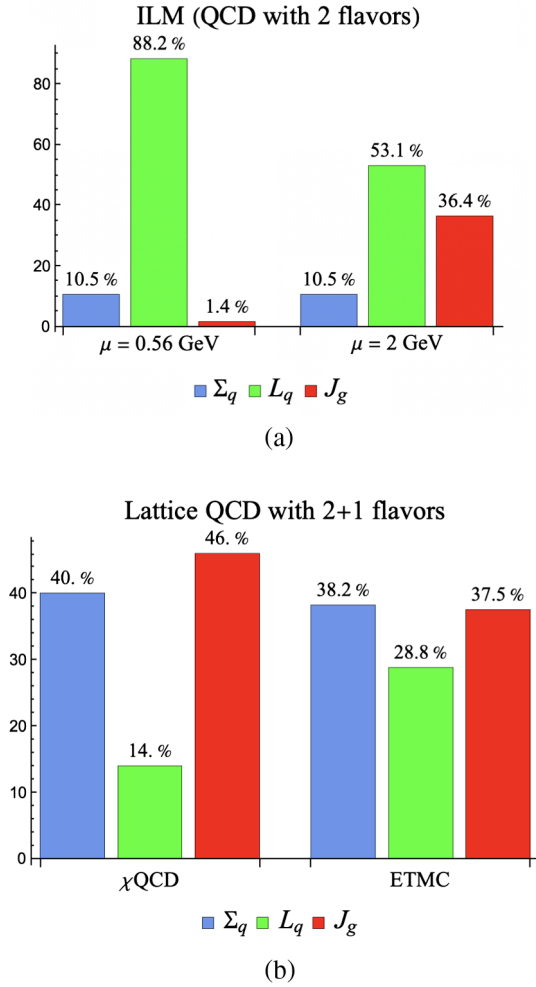


FIG. 9. (a) Nucleon spin decomposition using Ji’s spin sum rule, in the QCD instanton vacuum with two flavors at  $\mu = 0.56$  GeV (left) and  $\mu = 2$  GeV (right). (b) The same decomposition from the  $\chi$ QCD Lattice Collaboration [28] (left) and the ETMC Lattice Collaboration [29] (right), at a resolution of  $\mu = 2$  GeV.

### III. SEMICLASSICAL GLUE IN THE QCD VACUUM

Understanding of any quantum system starts with understanding of its ground state and predefining its excitations. Similarly, understanding hadrons requires an understanding of the QCD vacuum. The central aspects of the QCD vacuum are twofold: the quantum breaking of conformal symmetry and the spontaneous breaking of chiral symmetry, both of which are tied to the topological nature of the gauge configurations at low resolution.

The size distribution of the pseudoparticles is well captured semiempirically by the original ILM [5], confirmed then by various mean-field studies [30,31] and statistical simulations of the ensemble [6]. This distribution can be written as

$$n(\rho) \sim \frac{1}{\rho^5} (\rho \Lambda_{\text{QCD}})^b e^{-\#\rho^2/R^2} \quad (28)$$

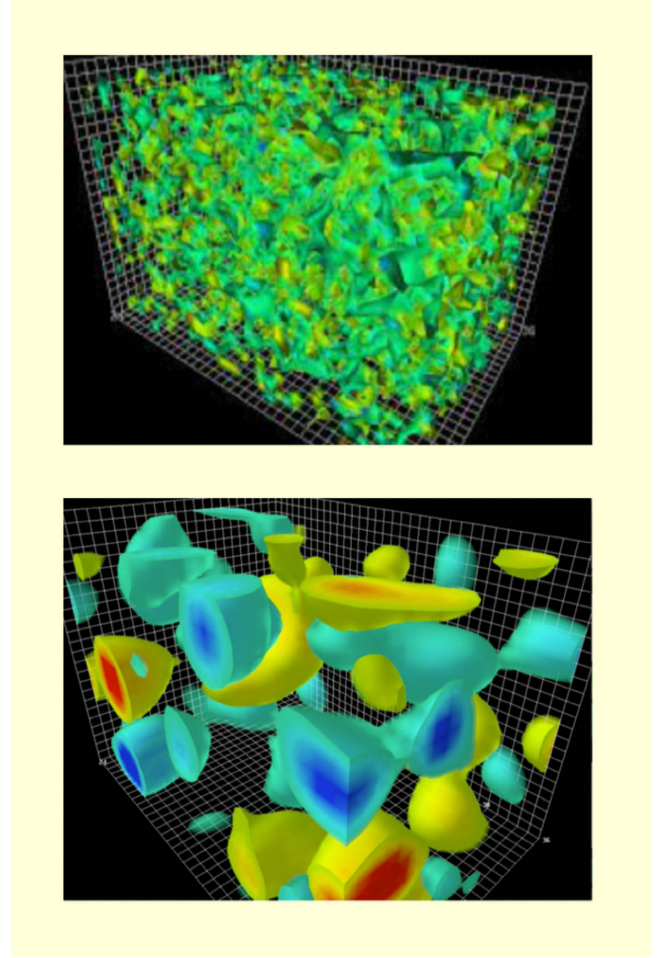


FIG. 10. Visualization of the vacuum in gluodynamics, before cooling at a resolution of about  $\frac{1}{10}$  fm (top) and after “deep cooling” at a resolution of about  $\frac{1}{3}$  fm (bottom) [35], where the pseudoparticles emerge.

with  $b = 11N_c/3 - 2N_f/3$  (one loop). The small size distribution follows from the conformal nature of the instanton moduli and perturbation theory. The large size distribution is nonperturbative but cut off by  $R$  the mean separation of the instantons (anti-instantons) in the vacuum. Detailed lattice simulations using the gradient flow method [32,33] find that the mean tunneling rate and quasiparticle size are

$$n_{I+A} = \frac{\bar{N}}{V} \equiv \frac{1}{R^4} \approx \frac{1}{\text{fm}^4}, \quad \frac{\bar{\rho}}{R} \approx \frac{1}{3}. \quad (29)$$

This distribution, as well as values of the size and density, has been many times confirmed by lattice works, using various versions of “deep cooling” of configurations. In Fig. 10, we show, e.g., results from lattice simulations by Leinweber and his collaborators [34], using the gradient flow (cooling) method. At high resolution as illustrated in Fig. 10 (top), the vacuum is dominated by quantum or zero point motion, but as the resolution is decreased, as

illustrated in Fig. 10 (bottom), a much smoother landscape emerges, composed essentially of instantons and anti-instantons. These are tunneling pseudoparticles, between vacua with different Chern-Simons numbers.

Most of the hadronic correlation functions in the QCD vacuum are little affected by the removal of the quantum gluons by gradient flow, an indication of the central role played by these pseudoparticles [6,36]. The dimensional parameters (29) combine in the dimensionless parameter packing fraction  $\kappa \equiv \pi^2 \bar{\rho}^4 n_{I+A} \approx 0.1$ , a small emerging parameter that allows for a many-body analysis.

### A. Scale anomaly

The quantum breaking of conformal symmetry is best captured by the anomalous part of the trace of the energy-momentum tensor

$$T^\mu{}_\mu \approx -\frac{b}{32\pi^2} G_{\mu\nu}^a G^{a\mu\nu} + m\bar{\psi}\psi. \quad (30)$$

Throughout, we will use the rescaling  $gG \rightarrow G$  for operators in the instanton or anti-instanton gauge fields. In the QCD instanton vacuum, the gluonic operators

$$\begin{aligned} G^2/(32\pi^2) &\rightarrow (N_+ + N_-)/V = N/V, \\ G\tilde{G}/(32\pi^2) &\rightarrow (N_+ - N_-)/V = \Delta N/V \end{aligned} \quad (31)$$

count the number-sum (first) and number-difference (second) of instantons plus anti-instantons in the 4-volume  $V$ . In the canonical ensemble with zero theta angle, the former is fixed by the mean instanton density with  $N_\pm/V \rightarrow \bar{N}/2V$  and  $\Delta N = 0$ . As a result, the expectation value of (30) in the Yang-Mills vacuum illustrated in Fig. 10 is

$$\langle T^\mu{}_\mu \rangle \approx -bn_{I+A} \approx -10 \text{ fm}^{-4} \quad (32)$$

in leading order in the packing fraction and chiral limit. The emerging gluon condensate  $\langle G^2 \rangle$ , which is positive, is at the origin of most hadronic mass in the Universe [37].

### B. Fluctuating pseudoparticles

In Fig. 10, the tunneling quasiparticles fluctuate in numbers. Remarkably, these fluctuations are universally captured by the distributions [9,15,31]

$$\mathbb{P}(N_+, N_-) \propto \left[ e^{\frac{bN}{4}} \left( \frac{\bar{N}}{N} \right)^{\frac{bN}{4}} \right] \left[ \frac{1}{(2\pi\chi_t)^{\frac{1}{2}}} e^{-\frac{\Delta N^2}{2\chi_t}} \right] \quad (33)$$

with mean  $\bar{N}$ , in agreement with low-energy theorems [38]. The dominant second moments are

$$\begin{aligned} \sigma_T &= \langle (N - \bar{N})^2 \rangle_{\mathbb{P}}, \\ \chi_t &= \langle (N_+ - N_-)^2 \rangle_{\mathbb{P}}. \end{aligned} \quad (34)$$

The variance in  $N$  or vacuum compressibility,

$$\sigma_T = V \int d^4x \left\langle \frac{1}{32\pi^2} GG(x) \frac{1}{32\pi^2} GG(0) \right\rangle_{\mathbb{P}}, \quad (35)$$

vanishes in the large  $N_c$  limit:

$$\sigma_T = \frac{4\bar{N}}{b}. \quad (36)$$

The large volume topological susceptibility is

$$\chi_t = V \int d^4x \left\langle \frac{1}{32\pi^2} G\tilde{G}(x) \frac{1}{32\pi^2} G\tilde{G}(0) \right\rangle_{\mathbb{P}}. \quad (37)$$

In quenched QCD,  $\chi_t \rightarrow \chi_t^{(0)}$  is given by the Witten-Veneziano formula [39,40]

$$\frac{\chi_t^{(0)}}{V} = \lim_{V \rightarrow \infty} \frac{\langle \Delta N^2(V) \rangle_{\mathbb{P}}}{V} = \frac{f_\pi^2 M_1^2}{2N_f} \quad (38)$$

with  $M_1$  the quenched singlet mass,

$$M_1^2 = m_\eta^2 + m_\eta^2 - 2m_K^2, \quad (39)$$

and Eqs. (38) and (39) hold in the QCD instanton vacuum [6,30,31]. In the unquenched QCD instanton vacuum, (38) is very sensitive to the presence of light quarks with the substitution  $M_1^2 \rightarrow m_\pi^2$  (see below) and vanishes in the chiral limit [9,15].

### C. Light quarks and zero modes

When a light quark crosses a tunneling configuration, it develops a zero mode that is single handed [41], an amazing phenomenon protected by topology and the Atiyah-Singer theorem. It is the delocalization of these zero modes and their interactions that is at the origin of the spontaneous breaking of chiral symmetry and the emergence of the light hadronic spectrum. Remarkably, this topological mechanism for mass generation leaves behind a distinct fingerprint: universal conductancelike fluctuations in the quark spectrum, predicted by random matrix theory [42] and confirmed by lattice simulations [43].



FIG. 11. A quark zero mode propagating through an instanton enters left handed and exits right handed, to maintain a null quasispin  $\vec{\tau} + \vec{\sigma} = \vec{0}$  (left). The opposite takes place through an anti-instanton (right).

In Fig. 11, we show how a light up-quark helicity in a zero mode is flipped when crossing an instanton (left) or anti-instanton (right). (In the zero mode, the quark spin  $\vec{\sigma}$  is locked to the color  $\vec{z}$ , in a hedgehoglike configuration with  $\vec{\sigma} + \vec{z} = \vec{0}$ .) This flipping is captured by the 't Hooft vertex for a single quark flavor [41]. Specifically, the LSZ reduced forward scattering matrix for the zero mode in Fig. 11 is in Euclidean signature

$$n_I \left\langle \psi_R^\dagger(p) p \cdot \sigma^\dagger [\varphi'(p) \hat{p} \cdot \sigma \epsilon U] \frac{1}{m} [\varphi'(p) (\hat{p} \cdot \sigma \epsilon U)^\dagger] p \cdot \sigma \psi_L(p) \right\rangle_U + (I, L) \leftrightarrow (\bar{I}, R) \quad (40)$$

with the Weyl notation subsumed ( $p \cdot \sigma = p_\mu \sigma_\mu$ ), where  $\sigma_\mu = (-i\vec{\sigma}, 1)$ , and the normalized quark zero mode

$$\phi_{aI}^i(p) = \varphi'(p) (\hat{p} \cdot \sigma \epsilon U)_\alpha^i \equiv [\pi \rho^2 (I_0 K_0(z) - I_1 K_1(z))'_{z=\rho p/2}] (\hat{p} \cdot \sigma \epsilon U)_\alpha^i. \quad (41)$$

Here, the matrix element  $(\epsilon U)_a^i = \epsilon^i_b U_{ab}$  carries spin  $i$  and color  $a$ , with  $\epsilon^i_b$  a real antisymmetric tensor (hedgehog in spin color) and  $U$  an  $SU(N_c)$  valued color matrix. The averaging in (41) is carried over  $U$ . Equation (40) can be recast in the form

$$M_q(p) \left( \frac{N}{N} \psi^\dagger(p) \psi(p) - \frac{\Delta N}{N} \psi^\dagger(p) \gamma^5 \psi(p) \right) \rightarrow \psi^\dagger(p) \left[ M_q(p) \left( 1 - \frac{\Delta N}{N} \gamma^5 \right) \right] \psi(p) \quad (42)$$

with the running constituent quark mass [44,45] [ $\tilde{\kappa} = \kappa/(2\pi^2 N_c)$ ]

$$M_q(p) = \tilde{\kappa} \frac{|p\varphi'(p)|^2}{m\rho^4} \rightarrow \frac{\sqrt{\tilde{\kappa}}}{\sqrt{2}\rho^2} \frac{|p\varphi'(p)|^2}{\|q\varphi'\|^2}. \quad (43)$$

The singular  $1/m$  effect is removed by disordering, with  $M_q(0) = 383 \pm 39$  MeV [45], which is comparable to the numerical result  $M_q(0) \approx 300$  MeV [6,46]. In the QCD instanton vacuum, the running quark mass is fixed by the same scale as the gluon condensate or  $M_u(0) \approx 1/R$ , since  $\bar{\rho} \approx R/3$ , with the size distribution (28) still controlled by  $R$ . This ensures the renormalization group invariance of all mass scales.

The emergent quark mass (43) in the QCD instanton vacuum may remind us of the constituent quark mass from the Nambu-Jona-Lasinio (NJL) model [47,48] (and references therein). However, it is important to stress that the latter is a pre-QCD model, while the former is rooted in QCD and is now supported by even numerical QCD lattice visualizations as in Fig. 10. The canonical NJL model, although useful, does not explain the vacuum gluon condensate, the running quark mass, the  $\eta'$  mass (unless modified), and the universal spectral conductance fluctuations [42]. More importantly, the gluonic operators, their correlations, and mixing with the quarks are readily described in the QCD instanton vacuum. For completeness, we note the nontopological approach to the hadronic mass scale in [49] (and references therein), where also a running quark mass emerges by resumming gluon rainbow diagrams.

#### D. Center $P$ vortices

The topologically active quasiparticles give rise to a linearly rising central potential till about 1 fm, before the potential flattens out at larger distances [7]. Strong lattice evidence for the disordering of large Wilson loops, points to the center-projected vortices (center  $P$  vortices) [50–52]. Center  $P$  vortices can link with large Wilson loops through  $Z_{N_c}$  fluxes, leading to an emergent string tension  $\sigma_T$  fixed by the planar density of  $N_V/\sqrt{V}$  of center  $P$  vortices. More specifically,  $\sigma_T = 1/(2\pi l_s^2)$  with a string length  $l_s \approx 0.2$  fm, so that  $N_V/\sqrt{V} \approx 4/\text{fm}^2$ .

The center  $P$  vortices are characterized by a number of branching points (monopoles), which are likely anchors of topological structures or quasiparticles. Yet the latter carry much stronger chromoelectric and -magnetic fields  $\sqrt{E} = \sqrt{B} \approx 2.5/\bar{\rho} \approx 1.5$  GeV, in comparison to  $\sigma_T \bar{\rho} \approx 0.3$  GeV carried by a center  $P$  vortex. This suggests that the quantum breaking of conformal and chiral symmetry is strongly mediated by the quasiparticles for the low-lying hadrons in their ground state. The radial and orbitally excited states have larger sizes and, hence, are more susceptible to piercing by  $Z_{N_c}$  fluxes threading the center  $P$  vortices. Throughout, we will focus on the pseudoparticles for the low-lying hadrons.

#### IV. EFFECTIVE THEORY OF INSTANTON ENSEMBLE

For a more quantitative description of the QCD vacuum at low resolution, we will focus on the pseudoparticles illustrated in Fig. 10. We designate by  $N_+$  the number of pseudoparticles and by  $N_-$  the number of pseudoparticles with opposite charges. For fixed numbers  $N_\pm$ , the canonical partition function  $Z_{N_\pm}$  is

$$Z_{N_{\pm}} = \frac{1}{N_{+}!N_{-}!} \int \prod_{I=1}^{N_{+}+N_{-}} d\Omega_I n_0(\rho_I) \rho_I^{N_f} e^{-S_{\text{int}}} \times \prod_f \text{Det}(\not{D} + m_f)_{\text{low}}, \quad (44)$$

where  $d\Omega_I = d\rho_I d^4z_I dU_I$  is the conformal measure (size  $\rho_I$ , center  $z_I$ , and color orientation  $U_I$ ) for each single (anti-)instanton. The mean tunneling rate is

$$n_0(\rho) = C_{N_c} (1/\rho^5) (8\pi^2/g^2)^{2N_c} e^{-8\pi^2/g^2(\rho)}$$

with  $C_{N_c}$  is the number dependent on color number  $N_c$  and the gauge interaction between instantons and anti-instantons is  $S_{\text{int}}$ .

### A. Emergent 't Hooft vertices

The fermion determinant receives contribution from the high-momentum modes as well as the low-momentum modes. The contribution of the higher modes are localized on the pseudoparticles. They renormalize the mean-density rate, with an additional factor of  $\rho^{N_f}$ . The low-momentum modes, in the form of quasizero modes, are delocalized among the pseudoparticles. The chief result of the delocalization is the emerging constituent mass (42) and (43) and 't Hooft vertices [6,15,30,53]:

$$\Theta_I = \prod_f \left[ \frac{m_f}{4\pi^2\rho^2} + i\psi_f^\dagger(x) U_I \frac{1}{2} \left( 1 + \frac{1}{4} \tau^a \bar{\eta}_{\mu\nu}^a \sigma^{\mu\nu} \right) U_I^\dagger \frac{1-\gamma^5}{2} \psi_f(x) \right] e^{-\frac{2\pi^2}{g} \rho^2 R^{ab}(U_I) \bar{\eta}_{\mu\nu}^b G_{\mu\nu}^a},$$

$$\Theta_A = \prod_f \left[ \frac{m_f}{4\pi^2\rho^2} + i\psi_f^\dagger(x) U_A \frac{1}{2} \left( 1 + \frac{1}{4} \tau^a \eta_{\mu\nu}^a \sigma^{\mu\nu} \right) U_A^\dagger \frac{1+\gamma^5}{2} \psi_f(x) \right] e^{-\frac{2\pi^2}{g} \rho^2 R^{ab}(U_A) \eta_{\mu\nu}^b G_{\mu\nu}^a} \quad (45)$$

to lowest order in the current quark masses  $m_f$ . The gluonic field strength  $G_{\mu\nu}^a$  follows from the LSZ reduction of pseudoparticle field strength and is sourced by the color-magnetic moment [54,55]. The rigid color rotation  $R^{ab}(U)$  is defined as

$$R^{ab}(U) = \frac{1}{2} \text{Tr}(\tau^a U \tau^b U^\dagger).$$

With this in mind, the ensuing canonical partition function  $Z_{N_{\pm}}$  in (44) reads

$$Z_{N_{\pm}} = Z_{N_{\pm}}^{(g)} \int \prod_{I=1}^{N_{+}+N_{-}} d^4z_I dU_I \frac{(4\pi^2\rho^3)^{N_f}}{V} \times \int \mathcal{D}\psi \mathcal{D}\psi^\dagger \mathcal{D}A_\mu \left( \prod_{I=1}^{N_{+}} \Theta_I \prod_{A=1}^{N_{-}} \Theta_A \right) \times \exp \left[ - \int d^4x \left( -\psi^\dagger i \not{D} \psi + \frac{1}{4} (G_{\mu\nu}^a)^2 \right) \right] \quad (46)$$

with

$$Z_{N_{\pm}}^{(g)} = \frac{1}{N_{+}!N_{-}!} \left( \int d\rho n_{+}(\rho) V \right)^{N_{+}} \left( \int d\rho n_{-}(\rho) V \right)^{N_{-}} e^{-\bar{S}_{\text{int}}}. \quad (47)$$

Here,  $n_{\pm}(\rho)$  is the effective instanton size distribution, including the pseudoparticle binary interaction  $\bar{S}_{\text{int}}$ , which can be estimated by Feynman variational principle [15,56].

### B. Single-instanton approximation

Since most of the gluonic matrix elements will be assessed in hadronic states, we can ignore  $\bar{S}_{\text{int}}$ , and each emerging vertex  $\Theta_{I,A}$  in (46) can be randomly averaged over the single-pseudoparticle moduli with mean size fixed:

$$\theta_{\pm} = \int d^4z_{I,A} dU_{I,A} \Theta_{I,A}. \quad (48)$$

The explicit form of the vertices in the single-instanton approximation (SIA) can be found in Appendix A. In the large volume limit with fixed pseudoparticle density, the emergent vertices  $\theta_{\pm}$  exponentiate, giving

$$Z_{N_{\pm}} = Z_{N_{\pm}}^{(g)} \int \mathcal{D}\psi \mathcal{D}\psi^\dagger \mathcal{D}A_\mu \exp(-S_{\text{eff}}), \quad (49)$$

where the effective action in Euclidean space reads

$$S_{\text{eff}}(N_{+}, N_{-}) = \int d^4x \left[ -\psi^\dagger (i \not{D} - m_f^*) \psi + \frac{1}{4} (G_{\mu\nu}^a)^2 \right] - G(1+\delta)\theta_{+} - G(1-\delta)\theta_{-}. \quad (50)$$

The emergent parameters  $G$  and  $\delta$  are fixed by the saddle point approximation. The effective coupling  $G$

$$G = \frac{N (4\pi^2\rho^3)^{N_f}}{2V \prod_f (\rho m_f^*)} \quad (51)$$

TABLE I. Emergent parameters.

	Covariant	Light front [60]
$G$	610.3 GeV <sup>-2</sup>	567.8 GeV <sup>-2</sup>
$m$	12.2 MeV	16.17 MeV
$m^*$	110.70 MeV	114.76 MeV
$M_q(0)$	395.17 MeV	398.17 MeV
$\langle\bar{\psi}_f\psi_f\rangle$	-(208.39 MeV) <sup>3</sup>	-(208.58 MeV) <sup>3</sup>

is tied to the mean instanton size  $\rho$ , density  $N/V$ , and determinantal mass  $m_f^*$  [7,57,58]

$$m_f^* = m_f - \frac{2\pi^2\rho^2}{N_c} \langle\bar{\psi}_f\psi_f\rangle. \quad (52)$$

It follows from the mean-field approximation to the effective action in the SIA summarized in Appendix A.

We note that the determinantal mass  $m_f^*$  does not run with momentum and is much smaller than the running constituent quark mass  $M_q(0)$  used in [59,60] (and references therein). The latter resums all pseudoparticle contributions (close and far) to the quark propagator in leading order in the packing fraction.

The determinantal mass follows from the SIA, by retaining only the closest pseudoparticle in the inverted quark propagator, for a given zero mode [see [58] and Eqs. (72)–(74) in [7]]. It is appropriate for the description of the hopping of fermions at distances  $|x-y| \leq R \approx 1$  fm, e.g., in the local clustering of the zero modes in the effective 't Hooft vertices and pairing of pseudoparticles in molecules. The larger constituent quark mass  $M_q(0)$  describes long-range propagation of the emerging quarks for  $|x-y| \gg R \approx 1$  fm and is more appropriate in the description of long-range hadronic correlators.

The screened topological charge  $\delta$  is fixed to

$$\delta = \frac{\Delta N}{N} \sum_f \frac{m_f^*}{m_f}. \quad (53)$$

For a canonical ensemble of pseudoparticles, the instanton number sum  $N$  and difference  $\Delta N$  are fixed to  $N = Vn_{I+A}$  and  $\Delta N = 0$ , respectively. In a grand canonical ensemble, the instanton number sum and difference are allowed to fluctuate.

Using (49), the mean values of the instanton determinantal vertices  $\langle\theta_{\pm}\rangle$  are

$$\langle\theta_{\pm}\rangle = \prod_f \left( \frac{m_f^*}{4\pi^2\rho^2} \right) V. \quad (54)$$

The effective instanton vertices are composed of the  $2N_f$ -quark 't Hooft interaction and the emission of multiple gluons. The effective action can be decomposed

into the fermionic instanton-induced interactions ('t Hooft Lagrangian), with or without multigluon tail emission. The corresponding effective Lagrangian is given in Appendix A. Note that multigluon tail emissions are further suppressed by the small instanton size  $\rho$ .

The vacuum parameters are fixed to  $\rho = 0.313$  fm and  $n_{I+A} = 1$  fm<sup>-4</sup>. The table for the parameters used in ILM is shown in Table I.

The determinantal mass is to be compared to the heavier constituent quark mass  $M_q(0) \approx 395$  MeV. Both masses are close those used in [7,58–60]. The quark condensate  $\langle\bar{\psi}\psi\rangle$  is also close to the one given in [61]. The values of the current quark mass and quark condensate can also be compared to the FLAG lattice calculation by renormalization group evolution. At  $\mu = 2$  GeV, the current mass is  $m \simeq 6.9$  MeV, and the quark condensate is  $\langle\bar{\psi}_f\psi_f\rangle \simeq -(251.7 \text{ MeV})^3$  comparable to the result in FLAG lattice  $N_f = 2 + 1 + 1$  calculation [62]. For completeness, we refer to [6,15], for more details regarding the phenomenology of the QCD instanton vacuum.

### C. Pseudoparticle form factors

The emergent vertices (45) can be generalized to include further finite size effects of the pseudoparticles. More specifically, each quark field in the interaction vertices  $\Theta_{I,A}$  gets dressed:

$$\psi(k) \rightarrow \sqrt{\mathcal{F}(\rho k)}\psi(k) \quad (55)$$

with

$$\sqrt{\mathcal{F}(k)} = z \frac{d}{dz} [I_0(z)K_0(z) - I_1(z)K_1(z)] \Big|_{z=\frac{k}{2}}, \quad (56)$$

which is essentially the profiling of the instanton by the quark zero mode.

Also, each emitted gluon gets dressed by an induced nonlocal form factor. For that, we recall that the Belavin-Polyakov-Schwartz-Tyupkin instanton in singular gauge is given by

$$A_{\mu}^a(x) = \frac{1}{g} \frac{2\bar{\eta}_{\mu\nu}^a x_{\nu} \rho^2}{x^2(x^2 + \rho^2)}, \quad (57)$$

which is seen to satisfy both fixed-point and covariant gauge. In momentum space, it reads

$$gA_{\mu}^a(q) = i4\pi^2 \frac{\bar{\eta}_{\mu\nu}^a q_{\nu}}{q^2} \mathcal{F}_g(\rho q) \quad (58)$$

with the gluonic form factor induced by the finite instanton size [63,64]

$$\mathcal{F}_g(q) = \frac{4}{q^2} - 2K_2(q). \quad (59)$$

As a result, each instanton in the interaction vertices  $\Theta_{I,A}$  is regulated by

$$\frac{2\pi^2}{g} \bar{\eta}_{\mu\nu}^a \rightarrow \frac{2\pi^2}{g} \bar{\eta}_{\mu\nu}^a \mathcal{F}_g(\rho q), \quad (60)$$

which follows from (58) by LSZ reduction.

The use of the gluonic vertices  $\Theta_{I,A}$  is justified in momentum space diagrams, when the exchange ‘‘tail’’ gluons carry energies below the sphaleron mass (the top of the tunneling barrier)

$$M_S = \int d^3x \frac{1}{8} G_{\mu\nu}^2(0, \vec{x}) = \frac{3\pi}{4\alpha_s \rho}. \quad (61)$$

Using the above vacuum parameters, we have  $8\pi^2/g^2(\rho) = 10\text{--}15$  [6]. This fixes the sphaleron mass  $M_S \sim 2.5$  GeV, for  $\alpha_s(1/\rho) \sim 0.42\text{--}0.7$ .

## V. HADRONIC FORM FACTORS

The hadronic form factors are characterized by several regimes: (i) a soft energy regime with  $Q^2 < 1$  GeV<sup>2</sup>, where meson exchanges induced by the emerging vacuum interactions are dominant; (ii) a semihard regime with  $1 < Q^2 < 10$  GeV<sup>2</sup>, where scaling is still largely violated, where nonperturbative vacuum fields are still important [65]; and (iii) a hard regime  $Q^2 \gg 10$  GeV<sup>2</sup> where perturbative scaling ultimately takes place. Here, we will focus on the soft energy regime, where the emergent multiflavor interactions in the QCD vacuum at low resolution are dominant and manifest in the form of effective meson exchanges.

With this in mind, and to evaluate the pertinent hadronic form factors with gluonic operators in the QCD instanton vacuum, we will trade matrix elements of the gluonic operators for effective fermionic operators. This can be done in two ways, either by averaging the gluonic operators

in the presence of the zero modes for forward matrix elements [66] or by using the semiclassical bosonization for forward and off-forward matrix elements [9]. This trading was shown to be exact in two-dimensional QCD in the large  $N_c$  limit in [67] [see Eqs. (91) and (92)]. Here, we will show how to generalize [66], by showing how it can be extended to off-forward matrix elements, and also at NLO in the mean instanton density to account for like and unlike instanton molecules. The latter play a dominant role in the gluonic contribution to the energy-momentum tensor and, in general, most gluonic operators on the light front.

### A. Sum ansatz

Let  $\mathcal{O}[A]$  be a generic gluonic operator, sourced by a multipseudoparticle gluon field given by the sum ansatz

$$A(x) = \sum_{I=1}^{N_++N_-} A_I(x). \quad (62)$$

The ensuing gluonic operator  $\mathcal{O}[A]$  is seen to split into a sum of multi-instanton contributions

$$\mathcal{O}[A] = \sum_I \mathcal{O}[A_I] + \sum_{I \neq J} \mathcal{O}[A_I, A_J] + \dots \quad (63)$$

of increasing complexity. In the QCD instanton vacuum, the gauge fields and their quark zero modes are reduced to a quantum moduli. The vacuum averaging over the quantum moduli in the absence of source is the effective Lagrangian given in Appendix A. In the presence of the split form of the gluonic source (63), the averaging over the quantum moduli trades the gluonic source for multi-flavored fermionic vertices.

### B. Vacuum averages

The vacuum averages of local gluonic operators using (46) for fixed- $N_{\pm}$  configurations (canonical ensemble) follow from

$$\langle \mathcal{O}[A] \rangle_{N_{\pm}} = \frac{Z^{(g)}_{N_{\pm}}}{Z_{N_{\pm}}} \int \prod_{I=1}^{N_++N_-} d^4z_I dU_I \frac{(4\pi^2 \rho^3)^{N_f}}{V} \int \mathcal{D}\psi \mathcal{D}\psi^\dagger \mathcal{D}A_\mu \mathcal{O}[A] \left( \prod_{I=1}^{N_+} \Theta_I \prod_{A=1}^{N_-} \Theta_A \right) e^{-\int d^4x (-\psi^\dagger i \not{D} \psi + \frac{1}{4} (G_{\mu\nu}^a)^2)}. \quad (64)$$

The evaluation of the gluonic operators from the instanton vacuum is twofold. When the operator probes the gluonic content inside the hadronic state with a momentum transfer, the contribution can be calculated by replacing the gluonic field in the operator by the semiclassical background of the instantons [15,66]. The averages over the operators and the quark-instantonic vertices convert the gluonic operator into

the corresponding effective quark operator. Thus, in the instanton ensemble, the gluonic operators are mapped into some effective fermionic operators associated with the multi-instanton configuration in the instanton vacuum.

Using (63), the vacuum expectation value of  $\mathcal{O}[A]$  in the instanton ensemble can be organized in diluteness contributions using the instanton density  $n_{I+A}$ :

$$\begin{aligned}
\langle \mathcal{O}[A] \rangle_{N_{\pm}} &= \sum_{n=1}^{\infty} \frac{1}{n!} \left[ \sum_{k=0}^n \binom{n}{k} N_+^{n-k} N_-^k \frac{\langle \mathcal{O}_{++\dots} \rangle_{\text{eff}}}{\langle \theta_+ \rangle^{n-k} \langle \theta_- \rangle^k} \right] \\
&= N_+ \frac{\langle \mathcal{O}_+ \rangle_{\text{eff}}}{\langle \theta_+ \rangle} + N_- \frac{\langle \mathcal{O}_- \rangle_{\text{eff}}}{\langle \theta_- \rangle} + \frac{N_+^2}{2} \frac{\langle \mathcal{O}_{++} \rangle_{\text{eff}}}{\langle \theta_+ \rangle^2} + N_+ N_- \frac{\langle \mathcal{O}_{+-} \rangle_{\text{eff}}}{\langle \theta_+ \rangle \langle \theta_- \rangle} + \frac{N_-^2}{2} \frac{\langle \mathcal{O}_{--} \rangle_{\text{eff}}}{\langle \theta_- \rangle^2} + \dots, \quad (65)
\end{aligned}$$

where the effective fermionic operator  $\mathcal{O}_{++\dots}$  is obtained by simultaneously connecting  $\mathcal{O}[A]$  to the  $n$  instantons by sharing the classical fields:

$$\mathcal{O}_{++\dots} = \int d^4 z_{I_1} dU_{I_1} \dots d^4 z_{I_n} dU_{I_n} \mathcal{O}[A_{I_1}, A_{I_2}, \dots, A_{I_n}] \Theta_{I_1} \dots \Theta_{I_n}. \quad (66)$$

Now the canonical ensemble average effectively reduces to the path integral of the effective field theory. The calculations become the vacuum expectation values of a bunch of effective multi-instanton fermionic operators over the effective Lagrangian  $\mathcal{L}_{\text{eff}}$ . This is the consequences of the diluteness of the instanton vacuum. The calculations now can be done order by order in the framework of the instanton density expansion. As the same idea of the diluteness, the correlation between the instantons becomes irrelevant. Therefore, the fermion and gluon exchanges among the instanton vertices  $\Theta_I$  will be neglected. The extension to a grand canonical ensemble

of pseudoparticles with varying  $N_{\pm}$  will follow by inspection (see below).

### C. Form factors

The preceding arguments for the vacuum averages can be extended to hadronic matrix elements, provided that the resulting effective vertices are localized within the hadronic size. This is true for most light hadrons, since the instanton size is comparable to even to the pion, the smallest of all light hadrons. With this in mind, the transition matrix element of the gluon operator  $\mathcal{O}[A]$  in a hadron state will be given by an ensemble average similar to (65) with in-out on-shell hadronic states:

$$\begin{aligned}
\langle P' | \mathcal{O}[A] | P \rangle_{N_{\pm}} &= \sum_{n=1}^{\infty} \frac{1}{n!} \left[ \sum_{k=0}^n \binom{n}{k} \left( \frac{N_+}{\langle \theta_+ \rangle} \right)^{n-k} \left( \frac{N_-}{\langle \theta_- \rangle} \right)^k \langle P' | \mathcal{O}_{++\dots} | P \rangle_{\text{eff}} \right] \\
&= \frac{N_+}{\langle \theta_+ \rangle} \langle P' | \mathcal{O}_+ | P \rangle_{\text{eff}} + \frac{N_-}{\langle \theta_- \rangle} \langle P' | \mathcal{O}_- | P \rangle_{\text{eff}} + \frac{1}{2} \frac{N_+^2}{\langle \theta_+ \rangle^2} \langle P' | \mathcal{O}_{++} | P \rangle_{\text{eff}} \\
&\quad + \frac{N_+}{\langle \theta_+ \rangle} \frac{N_-}{\langle \theta_- \rangle} \langle P' | \mathcal{O}_{+-} | P \rangle_{\text{eff}} + \frac{1}{2} \frac{N_-^2}{\langle \theta_- \rangle^2} \langle P' | \mathcal{O}_{--} | P \rangle_{\text{eff}} + \dots. \quad (67)
\end{aligned}$$

The form factors following from (67) can be expanded systematically, in terms of the instanton density, which is commensurate with a bookkeeping in  $1/N_c$ . Translational symmetry relates the hadronic matrix element of  $\mathcal{O}[A]$  to the momentum transfer between the hadronic states:

$$\langle P' | \mathcal{O}[A] | P \rangle = \frac{1}{V} \int d^4 x \langle P | \mathcal{O}[A(x)] | P \rangle e^{-iq \cdot x} \quad (68)$$

The recoiling hadron momentum is defined as  $P' = P + q$ , and the forward limit follows from  $q \rightarrow 0$ . Equation (67) generalizes the arguments in [66] to off-forward and multi-instanton contributions.

Graphically, the color averaging in (66) connects  $\mathcal{O}[A]$  to  $n$  instantons through the classical field backgrounds. Each matrix element in (67) is evaluated by the effective Lagrangian  $\mathcal{L}_{\text{eff}}$ , with only the connected diagrams retained. The hadronic matrix element effectively reduces to the path integral of the effective field theory, thanks to the diluteness of the pseudoparticles in the vacuum state. The calculations can be carried order by order in the instanton density expansion.

More specifically, each of the external fermion (anti-fermion) lines in the diagram contributes a pair of  $UU^\dagger$  in the color group integral. Each of the  $UU^\dagger$  pair gives a  $1/N_c$  factor in the large  $N_c$  limit. Therefore, the  $1/N_c$  counting of each diagram is  $1/N_c^{N_f}$ , where  $N_f$  is the external unattached

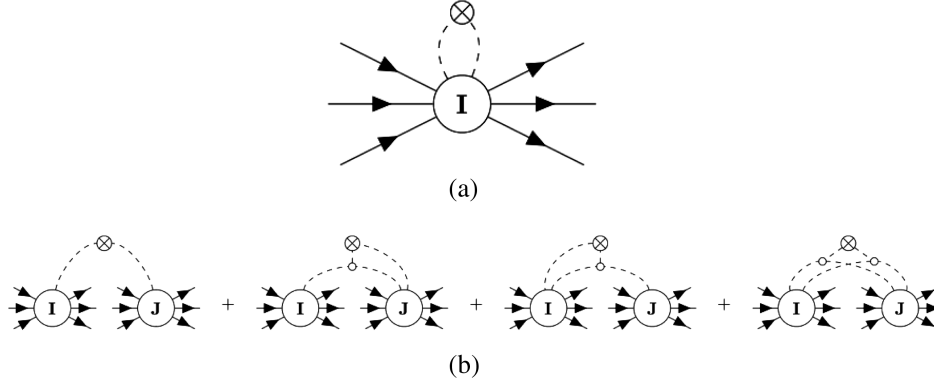


FIG. 12. (a) The diagrams of  $\mathcal{O}[I]$  in the multi-instanton expansion of the two-gluon operator  $\mathcal{O}_{2g}$  and  $\tilde{\mathcal{O}}_{2g}$ . Each dashed line connected to the instanton represents the classical background field. (b) The diagrams of  $\mathcal{O}[A_I, A_J]$  in the multi-instanton expansion of the two-gluon operator  $\mathcal{O}_{2g}$  and  $\tilde{\mathcal{O}}_{2g}$ . Each line connected to the instantons  $I$  and  $J$  represents the gluon fields in the operator. Each of the ring dots in the diagrams represents the insertion of the non-Abelian cross term  $G_{\mu\nu}[A_I, A_J]$  in (C5).

fermion number [the number of the external (anti-)fermion line unattached to the operator]. Note that in some cases the leading  $1/N_c$  contribution gives the disconnected diagrams in the matrix element [15]. In this case, the fluctuation in the instanton numbers comes into play, and the ensemble formulation has to be generalized to the grand canonical ensemble.

## VI. GLUONIC SCALAR FORM FACTORS

We will start our analysis by illustrating how this averaging carries for the simplest two-gluon scalar operator

$$\mathcal{O}_{2g}[A] = G_{\mu\nu}^2(x). \quad (69)$$

### A. One-instanton contribution

In leading order in the density expansion, the effective fermionic operator for  $\mathcal{O}_{2g}$  is obtained by averaging the leading expansion of  $\mathcal{O}_{2g}$  with one instanton vertex:

$$\frac{1}{V} \int d^4x \mathcal{O}_{2g\pm}(x) e^{-iq \cdot x} = \frac{1}{V} \int d^4x F_{2g}^{(I,A)}(x) e^{-i\rho q \cdot x} \left[ \left( \frac{m^*}{4\pi^2 \rho^2} \right)^{N_f} (2\pi)^4 \delta^4(q) - \frac{1}{N_c} \left( \frac{m^*}{4\pi^2 \rho^2} \right)^{N_f-1} \int d^4z \bar{\psi}(z) \frac{1 \mp \gamma^5}{2} \psi(z) e^{-iq \cdot z} \right], \quad (71)$$

where the profile function for the single (anti-)instanton  $I$  ( $A$ ) is defined as

$$F_{2g}^{(I,A)}(x) = \frac{192}{(x^2 + 1)^4}. \quad (72)$$

The leading-order contribution of the  $1/N_c$  expansion comes from the diagrams where all of the  $N_f$  flavors looped

$$\mathcal{O}_{2g\pm}(x) = \int d^4z_I dU_I \mathcal{O}_{2g}[A_I] \Theta_I \quad (70)$$

with  $\mathcal{O}_{2g}[A_I] = G_{\mu\nu}^2[A_I]$ . The classical field of the single instanton plays an important role in the expectation value of the gluonic operators, due to its strong and localized nature.

The calculations are illustrated by the diagrammatic contribution in Fig. 12(a), where each of the dashed lines denotes the replacement of the instanton classical fields into the gluon field in the operator. In the Feynman diagram, each of the external fermion flavors  $N_f$  contributes a pair of  $UU^\dagger$  in the color group integral, giving a  $1/N_c$  factor. The  $1/N_c$  counting of each diagram is  $1/N_c^{N_f}$ . Hence, we consider only the one-flavor contribution at each order of the instanton density expansion.

In leading order in the instanton density, the  $1/N_c$  expansion of the result in (123) gives

up. These diagrams do not have any contribution in the canonical ensemble, as they are disconnected from the hadronic source. Similar to the calculation of the  $G_{\mu\nu}^2$  operator in [15], we have to consider the fluctuations in the instanton vacuum. However, this part will contribute only to the forward matrix element. In the off-forward matrix element, the nontrivial contribution has to be connected to the hadronic source and, therefore, is down by  $1/N_c$ .

### B. Two-instanton contribution

At next-to-leading order of the instanton density expansion, the effective fermionic operator for  $\mathcal{O}_{2g}$  can be obtained by averaging the leading expansion of  $\mathcal{O}_{2g}$  with a two-instanton vertex

$$\begin{aligned} & \mathcal{O}_{2g\pm\pm}(x) \\ &= \int d^4z_I d^4z_J dU_I dU_J \mathcal{O}_{2g}[A_I, A_J] \Theta_I \Theta_J \end{aligned} \quad (73)$$

with

$$\begin{aligned} \mathcal{O}_{2g}[A_I, A_J] &= 2G_{\mu\nu}^a[I]G_{\mu\nu}^a[J] + 2G_{\mu\nu}^a[J]G_{\mu\nu}^a[I, J] \\ &+ 2G_{\mu\nu}^a[I]G_{\mu\nu}^a[I, J] + G_{\mu\nu}^a[I, J]G_{\mu\nu}^a[I, J]. \end{aligned} \quad (74)$$

Here,  $G_{\mu\nu}[I]$  is short for  $G_{\mu\nu}[A_I]$ , the single-instanton field strength.

In Fig. 12(b), we also show the diagrams that contribute to the gluonic scalar operator  $\mathcal{O}_{2g}$  at the second order in the instanton density. Each diagram corresponds to each term of the terms given in (142). Each of the dashed lines denotes the replacement of the instanton classical fields by the gluon field in the operator. In the case of a two-instanton cluster, at the leading order in the  $1/N_c$  contribution, each instanton with the  $N_f - 1$  flavors contracted will dominate the contribution in the hadronic matrix element. The effective operator produces two types of coupling due to the chirality. The operator produced by  $II$  or  $AA$  clusters corresponds to a chiral-flipping process

$$\begin{aligned} \frac{1}{V} \int d^4x \mathcal{O}_{2g++,-}(x) e^{-iq \cdot x} &= \frac{1}{2N_c(N_c^2 - 1)} \left( \frac{m^*}{4\pi^2 \rho^2} \right)^{2N_f - 2} \int d^4z_I d^4z_J \frac{1}{8} \text{tr}\{S(z_I - z_J)\} \\ &\times \frac{1}{V} \int d^4x e^{-iq \cdot x} F_{2g}^{(II, AA)}(x - z_I, x - z_J) \left[ \bar{\psi}(z_I) \frac{1 \mp \gamma^5}{2} \psi(z_J) + \bar{\psi}(z_J) \frac{1 \mp \gamma^5}{2} \psi(z_I) \right], \end{aligned} \quad (75)$$

where the profile function for the  $II$  cluster is defined as

$$\begin{aligned} F_{2g}^{(II)}(x - z_I, x - z_J) &= 2G_{\mu\nu}^a(x - z_I)G_{\mu\nu}^a(x - z_J) + 4\epsilon^{acd}G_{\mu\nu}^c(x - z_I)A_\mu^d(x - z_I)A_\nu^a(x - z_J) \\ &+ 4\epsilon^{acd}G_{\mu\nu}^c(x - z_J)A_\mu^d(x - z_J)A_\nu^a(x - z_I) \end{aligned} \quad (76)$$

and the profile function for the  $AA$  cluster is equal

$$F_{2g}^{(II)}(x - z_I, x - z_J) = F_{2g}^{(AA)}(x - z_I, x - z_J). \quad (77)$$

The operator produced by  $IA$  molecules corresponds to a chiral-conserving process:

$$\begin{aligned} \frac{1}{V} \int d^4x \mathcal{O}_{2g+-}(x) e^{-iq \cdot x} &= -\frac{1}{2N_c(N_c^2 - 1)} \left( \frac{m^*}{4\pi^2 \rho^2} \right)^{2N_f - 2} \int d^4z_I d^4z_J \frac{1}{4} \text{tr}\{S(z_I - z_J)\gamma_\mu\} \\ &\times \frac{1}{V} \int d^4x e^{-iq \cdot x} F_{2g, \mu\nu}^{(IA)}(x - z_I, x - z_J) \left[ \bar{\psi}(z_I)\gamma_\nu \frac{1 + \gamma^5}{2} \psi(z_J) - \bar{\psi}(z_J)\gamma_\nu \frac{1 - \gamma^5}{2} \psi(z_I) \right], \end{aligned} \quad (78)$$

where the profile function for the  $IA$  molecule is defined as

$$\begin{aligned} F_{2g, \rho\lambda}^{(IA)}(x - z_I, x - z_J) &= \frac{1}{2} \bar{\eta}_{\rho\beta}^a \eta_{\lambda\beta}^b [2G_{\mu\nu}^a(x - z_I)G_{\mu\nu}^b(x - z_J) + 4\epsilon^{acd}G_{\mu\nu}^c(x - z_I)A_\mu^d(x - z_I)A_\nu^b(x - z_J) \\ &+ 4\epsilon^{bcd}G_{\mu\nu}^c(x - z_J)A_\mu^d(x - z_J)A_\nu^a(x - z_I)]. \end{aligned} \quad (79)$$

Generally, the operators induced by the instanton clusters are nonlocal. However, as a result of the diluteness in the instanton ensemble, the highly localized nature of the instantons allows us to approximate the nonlocal quark operators by local operators, using the expansion in terms of the relative distance between the instanton pairs  $R = z_I - z_J$ . The relevant contribution to those matrix

elements at higher order of the instanton density comes from the close clusters. Therefore, we can extract the leading contribution by the  $R$  expansion (the local approximation)

$$\bar{\psi}(z_I)\psi(z_J) \simeq \bar{\psi}(z)\psi(z) - R_\mu \bar{\psi}(z) \overleftrightarrow{\partial}_\mu \psi(z) + \dots$$

Note that the quark line connecting the instanton  $I$  and  $J$  produces the Euclidean quark propagator with a determinantal mass  $m^*$  in the SIA, as opposed to the constituent quark mass in the mean-field approximation, i.e.,

$$S(x-y) \sim \int \frac{d^4k}{(2\pi)^4} \frac{i\not{k} + m^*}{k^2 + m^{*2}} \mathcal{F}(\rho k) e^{-ik \cdot (x-y)}. \quad (80)$$

$$\frac{1}{32\pi^2} \frac{\langle PS | g^2 G_{\mu\nu}^2 | PS \rangle}{2M_N} = -\frac{\sigma_T}{\bar{N}} \frac{1}{4} M_{\text{inv}}^{(0)} - \left[ \frac{1}{N_c} \left( \frac{2\kappa}{\rho^2 m^{*2}} \right) + \frac{1}{2N_c(N_c^2 - 1)} \left( \frac{2\kappa}{\rho^2 m^{*2}} \right)^2 \rho^2 m^2 T_{II} \right] \frac{\langle PS | m \bar{\psi} \psi | PS \rangle}{2M_N}. \quad (81)$$

The first term comes from the instanton number fluctuation, and the second term comes from the quark-instanton interaction in the SIA. The topological compressibility  $\sigma_T$  can be estimated by the QCD low-energy theorem [15,38]. The value is given by

$$\sigma_T = \langle (N - \bar{N})^2 \rangle_{\text{P}} = \frac{4}{b} \bar{N}, \quad (82)$$

where  $b = \frac{11}{3} N_c$  is the one-loop beta function in  $1/N_c$  limit (quenched QCD).

In QCD, the gluonic scalar operator is tied to the nucleon mass due by the conformal anomaly. In the chiral limit, the nucleon mass is saturated by the contribution from the anomalous mass (invariant mass  $M_{\text{inv}}$ ) induced by the spontaneous breaking of chiral symmetry:

$$M_N(m \rightarrow 0) \equiv M_{\text{inv}} = -\frac{b}{32\pi^2} \frac{\langle PS | g^2 G_{\mu\nu}^2 | PS \rangle}{2M_N}. \quad (83)$$

In the large  $N_c$  limit, the invariant mass follows by dimension

$$M_{\text{inv}}^{(0)} = C \left( \frac{\bar{N}}{V} \right)^{1/4}. \quad (84)$$

As in quenched QCD ( $N_c \rightarrow \infty$ ), the instanton density is the only scale in the QCD instanton vacuum. It is the analog of  $\Lambda_{\text{QCD}}$  for the gauge configurations in the QCD

### C. Forward matrix element

To make the physics more transparent, we properly normalize the hadronic matrix element in the forward limit  $q \rightarrow 0$ . With the consideration of the instanton fluctuations, the hadronic matrix element reads

vacuum, after cooling through gradient flow. Beyond the quenched limit, quarks start to contribute. The invariant mass will start to run due to the mixing between the gluon scalar and the quark scalar operator, induced by the quark-instanton interaction. The result to second order in the instanton density is

$$M_{\text{inv}} = M_{\text{inv}}^{(0)} + \left( \frac{b}{N_c} \left( \frac{2\kappa}{\rho^2 m^{*2}} \right) + \frac{b}{2N_c(N_c^2 - 1)} \right) \times \left( \frac{2\kappa}{\rho^2 m^{*2}} \right)^2 3\rho^2 m^2 T_{II} \frac{\langle PS | m \bar{\psi} \psi | PS \rangle}{2M_N}. \quad (85)$$

The invariant mass is renormalized by the quark mixing, in the instanton density expansion. With the invariant mass renormalized, the generalization to the off-forward matrix element is now straightforward, as we now detail.

### D. Off-forward matrix element

In the small size limit with momenta  $\rho q \ll 1$ , the detailed instanton structure is not probed. In this case, the gluonic operators are reduced to effective quark operators, and the momentum transfer dependence is dominated by quarks. However, when the momentum transfer becomes large enough to probe the instanton size, the momentum transfer dependence will be corrected by the instanton profiles. Hence, the off-forward hadronic matrix element

$$\begin{aligned} \frac{1}{32\pi^2} \langle P'S | g^2 G_{\mu\nu}^2 | PS \rangle &= - \left[ \frac{1}{4} M_{\text{inv}}^{(0)} \frac{\sigma_T}{\bar{N}} \frac{(2\pi)^4}{V} \delta^4(q) \right] \bar{u}_s(P') u_s(P) \\ &- \left[ \frac{1}{N_c} \left( \frac{2\kappa}{\rho^2 m^{*2}} \right) \beta_{2g}^{(I)}(\rho q) + \frac{1}{2N_c(N_c^2 - 1)} \left( \frac{2\kappa}{\rho^2 m^{*2}} \right)^2 3\rho^2 m^2 T_{II} \beta_{2g}^{(II)}(\rho q) \right] \langle P'S | m \bar{\psi} \psi | PS \rangle \\ &+ \frac{1}{2N_c(N_c^2 - 1)} \left( \frac{2\kappa}{\rho^2 m^{*2}} \right)^2 \frac{\rho^4 m^2}{9} T_{IA} \beta_{2g}^{(IA)}(\rho q) q_\mu q_\nu \langle P'S | \bar{\psi} \left( \gamma_{(\mu} i \overleftrightarrow{\partial}_{\nu)} - \frac{1}{4} g_{\mu\nu} i \overleftrightarrow{\not{D}} \right) \psi | PS \rangle, \end{aligned} \quad (86)$$

where the nonlocal form factors induced by the finite instanton size effect are defined as

$$\begin{aligned}\beta_{2g}^{(I)}(q) &= \frac{1}{q} \int_0^\infty dx \frac{24x^2}{(x^2+1)^4} J_1(qx) = \frac{q^2}{2} K_2(q), \\ \beta_{2g}^{(II)}(q) &= \frac{1}{q} \int_0^\infty dx \frac{8(2-x^2)}{(1+x^2)^4} J_1(qx) = \frac{16}{q^2} - \frac{1}{6} q^2 (K_2(q) + 2K_4(q)), \\ \beta_{2g}^{(IA)}(q) &= \frac{1}{q} \int_0^\infty dx \frac{576x^2}{(1+x^2)^4} \frac{J_3(qx)}{q^2 x^2} = 12[48(-32+q^2) \\ &\quad + q^2(768+72q^2+q^4)K_0(q) + 12q(128+28q^2+q^4)K_1(q)]/q^6\end{aligned}\quad (87)$$

and are normalized to unity in the forward limit. We plotted them in Fig. 4.

The quark hopping integral between the instanton and anti-instanton  $T_{IA}(\rho m^*)$  is defined as

$$\begin{aligned}T_{II} &= \int \frac{d^4 R}{4\pi^2 R} \int_0^\infty dk \mathcal{F}(k) J_1(kR) \Big|_{R < \frac{1}{\rho\sqrt{m_{I+A}}}}, \\ T_{IA} &= \int \frac{d^4 R}{16\pi^2} \int_0^\infty dk k \mathcal{F}(k) J_2(kR) \Big|_{R < \frac{1}{\rho\sqrt{m_{I+A}}}}.\end{aligned}\quad (88)$$

With the vacuum parameters, we have  $T_{II} = 1.666$  and  $T_{IA} = 0.5834$ .

It is clear that the universal fluctuation dominates the gluonic scalar form factor at the leading order of the  $1/N_c$  expansion. The  $\delta^4(q)$  contribution reflects on the scalar glueball decorrelator with the glueballs sourced solely by the localized and semiclassical instanton and anti-instanton fields:

$$\frac{\sigma_T (2\pi)^4}{\bar{N} V} \delta^4(q) = \frac{1}{32\pi^2 \langle G^2 \rangle} \int d^4 x e^{-iq \cdot x} \langle G^2(x) G^2(0) \rangle_c.\quad (89)$$

At nonzero momentum transfer, (86) shows that the gluonic  $G^2$  in a hadron mixes with the scalar meson ( $\sigma$ ) and tensor meson ( $t$ ) in the hadron. The mixing with the quark traceless tensor operator is penalized further by the instanton size.

$$\frac{1}{V} \int d^4 x \mathcal{O}_{2g\pm}(x) e^{-iq \cdot x} = \frac{1}{V} \int d^4 x \tilde{F}_{2g}^{(I,A)}(x) e^{-i\rho q \cdot x} \left[ \left( \frac{m^*}{4\pi^2 \rho^2} \right)^{N_f} (2\pi)^4 \delta^4(q) - \frac{1}{N_c} \left( \frac{m^*}{4\pi^2 \rho^2} \right)^{N_f-1} \int d^4 z \bar{\psi}(z) \frac{1 \mp \gamma^5}{2} \psi(z) e^{-iq \cdot z} \right],\quad (94)$$

where the profile function for the single (anti-)instanton  $I$  ( $A$ ) is defined as

$$\tilde{F}_{2g}^{(I,A)}(x) = \pm \frac{192}{(x^2+1)^4}.\quad (95)$$

## VII. GLUONIC PSEUDOSCALAR FORM FACTOR

The preceding calculation can be straightforwardly extended to the gluonic pseudoscalar operator, which enters the spin sum rule in hadrons through the U(1) anomaly (see below)

$$\tilde{\mathcal{O}}_{2g}[A] = G_{\mu\nu}^a(x) \tilde{G}_{\mu\nu}^a(x),\quad (90)$$

where the dual field strength is defined as

$$\tilde{G}_{\mu\nu}^a(x) = \frac{1}{2} \epsilon_{\mu\nu\rho\lambda} G_{\rho\lambda}^a(x).\quad (91)$$

### A. One-instanton contribution

At leading order in the instanton density, the effective quark operator for  $\tilde{\mathcal{O}}_{2g}$  can be obtained using

$$\tilde{\mathcal{O}}_{2g\pm}(x) = \int d^4 z_J dU_J \tilde{\mathcal{O}}_{2g}[A_J] \Theta_J,\quad (92)$$

where

$$\tilde{\mathcal{O}}_{2g}[A_J] = G_{\mu\nu}^a[A_J] \tilde{G}_{\mu\nu}^a[A_J].\quad (93)$$

The evaluation of (92) is also illustrated by the same diagrammatic contributions in Fig. 12(a). The profile function for the single (anti-)instanton  $I$  ( $A$ ) in the gluonic pseudoscalar operator can be deduced from the scalar by using the identity  $\tilde{G}_{\mu\nu}^a[I, A] = \pm G_{\mu\nu}^a[I, A]$ . More specifically, we have

Again, the contribution is dominated by the disconnected diagrams where all of the  $N_f$  flavors looped up. The LO contribution for the pseudoscalar follows from the instanton vacuum fluctuations in the forward limit.

### B. Two-instanton contribution

The contribution at the NLO instanton density  $c$  is given as

$$\tilde{\mathcal{O}}_{2g\pm\pm}(x) = \int d^4z_I d^4z_J dU_I dU_J \tilde{\mathcal{O}}_{2g}[A_I, A_J] \Theta_I \Theta_J \quad (96)$$

$$\begin{aligned} \frac{1}{V} \int d^4x \tilde{\mathcal{O}}_{2g++,-}(x) e^{-iq \cdot x} &= \frac{1}{2N_c(N_c^2 - 1)} \left( \frac{m^*}{4\pi^2 \rho^2} \right)^{2N_f - 2} \int d^4z_I d^4z_J \frac{1}{8} \text{tr}\{S(z_I - z_J)\} \\ &\times \frac{1}{V} \int d^4x e^{-iq \cdot x} \tilde{F}_{2g}^{(II,AA)}(x - z_I, x - z_J) \left[ \bar{\psi}(z_I) \frac{1 \mp \gamma^5}{2} \psi(z_J) + \bar{\psi}(z_J) \frac{1 \mp \gamma^5}{2} \psi(z_I) \right], \end{aligned} \quad (98)$$

where the profile functions for the  $II$  and  $AA$  clusters are, respectively,

$$\tilde{F}_{2g}^{(II)}(x - z_I, x - z_J) = F_{2g}^{(II)}(x - z_I, x - z_J) \quad (99)$$

and

$$\tilde{F}_{2g}^{(AA)}(x - z_I, x - z_J) = -F_{2g}^{(II)}(x - z_I, x - z_J). \quad (100)$$

The operator produced by the  $IA$  molecules corresponds to a chiral-conserving process:

$$\begin{aligned} \frac{1}{V} \int d^4x \tilde{\mathcal{O}}_{2g+-}(x) e^{-iq \cdot x} &= -\frac{1}{2N_c(N_c^2 - 1)} \left( \frac{m^*}{4\pi^2 \rho^2} \right)^{2N_f - 2} \int d^4z_I d^4z_J \frac{1}{4} \text{tr}\{S(z_I - z_J) \gamma_\mu\} \\ &\times \frac{1}{V} \int d^4x e^{-iq \cdot x} \tilde{F}_{2g,\mu\nu}^{(IA)}(x - z_I, x - z_J) \left[ \bar{\psi}(z_I) \gamma_\nu \frac{1 + \gamma^5}{2} \psi(z_J) - \bar{\psi}(z_J) \gamma_\nu \frac{1 - \gamma^5}{2} \psi(z_I) \right], \end{aligned} \quad (101)$$

where the profile function for the  $IA$  molecule is defined as

$$\tilde{F}_{2g,\rho\lambda}^{(IA)}(x - z_I, x - z_J) = 2\bar{\eta}_{\rho\beta}^a \eta_{\lambda\beta}^b [e^{acd} G_{\mu\nu}^c(x - z_I) A_\mu^d(x - z_I) A_\nu^b(x - z_J) - e^{bcd} G_{\mu\nu}^c(x - z_J) A_\mu^d(x - z_J) A_\nu^a(x - z_I)]. \quad (102)$$

Again, we approximate the nonlocal quark operators by local operators, by expanding in terms of the relative distance between the instanton pairs  $R = z_I - z_J$ .

### C. Forward matrix element

For the gluonic pseudoscalar, the naive forward limit of the hadronic matrix element vanishes due to the parity selection rule. To extract the forward form factor, we choose a different normalization for the forward matrix element by tilting the hadron slightly off forward and properly normalizing the matrix element with spin, before

with

$$\begin{aligned} \tilde{\mathcal{O}}_{2g}[A_I, A_J] &= 2G_{\mu\nu}^a[I] \tilde{G}_{\mu\nu}^a[J] + 2G_{\mu\nu}^a[I] \tilde{G}_{\mu\nu}^a[I, J] \\ &+ 2G_{\mu\nu}^a[J] \tilde{G}_{\mu\nu}^a[I, J] + G_{\mu\nu}^a[I, J] \tilde{G}_{\mu\nu}^a[I, J]. \end{aligned} \quad (97)$$

The instanton pair contribution is similar to the one illustrated in Fig. 12(b). The effective operator produces two types of coupling due to the chirality. The one produced by the  $II$  or  $AA$  clusters corresponds to a chiral-flipping process:

taking the forward limit. Without loss of generality, we assume that the initial state of the nucleon is in the rest frame. Now, we can rewrite the nucleon spinor product as

$$\bar{u}_s(P') i\gamma^5 u_s(P) \simeq 2M_N s_v$$

with the helicity defined as  $s_v = -\chi_s^\dagger \frac{i}{2} \vec{\sigma} \cdot \vec{v} \chi_s$ , where the final state nucleon carries a small recoiled velocity  $\vec{v} \simeq \vec{q}/M_N$ . Thus, the forward limit of the matrix element can be defined as

$$\frac{\langle PS|\mathcal{O}|PS\rangle}{2M_N s_v} = \lim_{P' \rightarrow P} \frac{\langle P'S|\mathcal{O}|PS\rangle}{2M_N s_v}. \quad (103)$$

With the proper normalization to the matrix element, the result of the hadronic matrix element in the forward limit reads

$$\begin{aligned} \frac{1}{32\pi^2} \frac{\langle PS|g^2 G_{\mu\nu}^a \tilde{G}_{\mu\nu}^a|PS\rangle}{2M_N s_v} &= M_q(0) \frac{\chi_t}{\bar{N}} + \left[ \frac{1}{N_c} \left( \frac{2\kappa}{\rho^2 m^{*2}} \right) + \frac{1}{2N_c(N_c^2 - 1)} \left( \frac{2\kappa}{\rho^2 m^{*2}} \right)^2 3\rho^2 m^2 T_{II} \right] \frac{\langle PS|m\bar{\psi}i\gamma^5\psi|PS\rangle}{2M_N s_v} \\ &\quad - \frac{1}{16N_c(N_c^2 - 1)} \left( \frac{2\kappa}{\rho^2 m^{*2}} \right)^2 \rho^2 m^2 T_{IA} i q_\mu \frac{\langle P'S|\bar{\psi}\gamma_\mu\gamma^5\psi|PS\rangle}{2M_N s_v}, \end{aligned} \quad (104)$$

where  $M_q(0) \approx 395$  MeV is the constituent quark mass in (43) and the value is estimated in [59,60]. Here, we assumed the nucleon as a quark-scalar-diquark composite, to capture part of the correlations in the nucleon but not all [57,68], e.g.,  $(uud)_\uparrow \approx u_\uparrow[ud]_0$  for a spin-up proton. It follows that the mixing of the proton spin with the axial charge is mostly through the unpaired  $u$  quark.

The result parallels the gluonic scalar matrix element. The first term stems from the fluctuation of the number difference in the ensemble, and the second term stems from the quark-instanton interaction. The topological susceptibility  $\chi_t$  can be estimated by the QCD low-energy theorem [9,15,38]. When recast in terms of the determinantal mass, the result is

$$\chi_t = \langle \Delta N^2 \rangle_{\mathbb{P}} \sim \bar{N} \left( 1 + N_f \frac{m^*}{m} \right)^{-1}. \quad (105)$$

In quenched QCD or gluodynamics, the value in (105) is about  $\bar{N}$  (Poisson), a result supported by quenched lattice simulations [69]. A similar estimate follows from the Witten-Veneziano formula in (38) and (39) with  $\chi_t^{(0)}/\bar{N} \sim 1.95/N_f$  for a singlet mass  $M_1 \approx 0.85$  GeV. In unquenched QCD, (105) is significantly screened by the quarks and vanishes in the chiral limit  $\chi_t/\bar{N} \sim m/N_f m^*$ . This result holds in the QCD instanton vacuum [9,15,70,71] and is in agreement with chiral perturbation theory [72–74] and random matrix theory [75].

The gluonic pseudoscalar operator is tied to the quark intrinsic spin by the Adler-Bell-Jackiw (ABJ) anomaly. In the chiral limit, the quark intrinsic spin in the nucleon is saturated by the gluonic helicity induced by the ABJ anomaly. This point will be detailed below.

#### D. Off-forward matrix element

The generalization to the off-forward matrix element is straightforward, with the result

$$\begin{aligned} \frac{1}{32\pi^2} \langle P'S|g^2 G_{\mu\nu}^a \tilde{G}_{\mu\nu}^a|PS\rangle &= \left[ M_q(0) \frac{\chi_t}{\bar{N}} \frac{(2\pi)^4}{V} \delta^4(q) \right] \bar{u}_s(P') i\gamma^5 u_s(P) \\ &\quad + \left[ \frac{1}{N_c} \left( \frac{2\kappa}{\rho^2 m^{*2}} \right) \tilde{\beta}_{2g}^{(I)}(\rho q) + \frac{1}{2N_c(N_c^2 - 1)} \left( \frac{2\kappa}{\rho^2 m^{*2}} \right)^2 3\rho^2 m^2 T_{II} \tilde{\beta}_{2g}^{(II)}(\rho q) \right] \langle P'S|m\bar{\psi}i\gamma^5\psi|PS\rangle \\ &\quad - \frac{1}{16N_c(N_c^2 - 1)} \left( \frac{2\kappa}{\rho^2 m^{*2}} \right)^2 \rho^2 m^2 T_{IA} \tilde{\beta}_{2g}^{(IA)}(\rho q) i q_\mu \langle P'S|\bar{\psi}\gamma_\mu\gamma^5\psi|PS\rangle, \end{aligned} \quad (106)$$

where the nonlocal form factors induced by the finite instanton size effect are defined as

$$\begin{aligned} \tilde{\beta}_{2g}^{(I)}(q) &= \frac{1}{q} \int_0^\infty dx \frac{24x^2}{(x^2 + 1)^4} J_1(qx), \\ \tilde{\beta}_{2g}^{(II)}(q) &= \frac{1}{q} \int_0^\infty dx \frac{8(2 - x^2)}{(1 + x^2)^4} J_1(qx), \\ \tilde{\beta}_{2g}^{(IA)}(q) &= \frac{1}{q} \int_0^\infty dx \frac{192x^2}{(1 + x^2)^5} \frac{J_2(qx)}{qx} \end{aligned} \quad (107)$$

and are normalized to unity in the forward limit. The quark hopping integral between the instanton and anti-instanton  $T_{IA}(\rho m^*)$  is defined in (88). Note that the ultralocal  $\delta^4(q)$  contribution can be written as

$$\frac{\chi_t}{\bar{N}} \frac{(2\pi)^4}{V} \delta^4(q) = \frac{1}{32\pi^2 (G^2)} \int d^4 x e^{-iq \cdot x} \langle G\tilde{G}(x)G\tilde{G}(0) \rangle. \quad (108)$$

The nonzero momentum transfer induces emergent meson-nucleon couplings in (106), with the pseudoscalar mesons ( $\eta'$ ) and axial vector mesons ( $f_1$ ).

### VIII. C-ODD THREE-GLUON FORM FACTOR

Another class of gluonic operator of interest is the C-odd three-gluon operator

$$\mathcal{O}_{3g}[A] = d^{abc} G_{\mu\nu}^a(x) G_{\rho\alpha}^b(x) G_{\lambda\alpha}^c(x), \quad (109)$$

which is found to be the leading operator in the photo-production process of heavy pseudoscalar mesons [76]. A similar but not identical operator was considered recently in [66], to estimate Weinberg's CP-odd contribution to the nucleon matrix element. We now proceed to evaluate it in the QCD instanton vacuum, through the substitution of the sum ansatz (62) and the ensuing averaging over the moduli.

#### A. One-instanton contribution

Since  $d^{abc}$  is a symmetric  $SU(3)$  structure constant which with no support on the  $SU(2)$  subgroup, in LO of the instanton density, it follows that all associated color orientations of the gluonic fields rotate congruently in the moduli. Therefore, the structure constant  $d^{abc}$  would reduce to  $\text{tr}(\tau^a \{\tau^b, \tau^c\}) = 0$ , with zero contribution.

#### B. Two-instanton contribution

In NLO in the instanton density expansion, some of the two-instanton terms in  $\mathcal{O}_{3g}[A]$  involve the nontrivial relative color rotation  $U_I^\dagger U_J = U_{IJ}$  between  $\tau^a$  and  $\mathbb{1}_2$  in the  $SU(2)$  subgroup, with nonzero net color structure

$$\text{tr}(U_I \tau^a U_I^\dagger \{U_J \tau^b U_J^\dagger, U_J \tau^c U_J^\dagger\}) = \text{tr}(\tau^a U_I^\dagger U_J \mathbb{1}_2 U_J^\dagger U_I) \delta^{bc}. \quad (110)$$

This means contributions from the single-instanton fields  $G_{\mu\nu}[A_I]$  and  $G_{\mu\nu}[A_J]$ , as well as the overlap between pairs of instanton fields  $G_{\mu\nu}[A_I, A_J]$ , a consequence of the non-Abelian gauge nature. (See Appendix C.) The evaluation of the latter appears involved. Fortunately, the calculation can be simplified, as the  $d^{abc}$  color structure has support only when two different  $SU(2)$  subgroups in  $SU(N_c)$  overlap through their relative color orientations. To obtain a non-trivial relative color rotation, the crossing term  $G_{\mu\nu}[I, J]$  has to be combined with both  $G_{\mu\nu}[I]$  and  $G_{\mu\nu}[J]$  to carry the same color rotation along either  $I$  or  $J$ :

$$\mathcal{O}_{3g\pm\pm}(x) = \int d^4 z_I d^4 z_J d^4 U_I d^4 U_J \mathcal{O}_{3g}[A_I, A_J] \Theta_I \Theta_J, \quad (111)$$

where

$$\begin{aligned} \mathcal{O}_{3g}[A_I, A_J] = & d^{abc} \left( G_{\mu\nu}^a[I] G_{\rho\alpha}^b[I] G_{\lambda\alpha}^c[J] + G_{\mu\nu}^a[I] G_{\rho\alpha}^b[J] G_{\lambda\alpha}^c[I] + G_{\mu\nu}^a[J] G_{\rho\alpha}^b[I] G_{\lambda\alpha}^c[I] + G_{\mu\nu}^a[J] G_{\rho\alpha}^b[J] G_{\lambda\alpha}^c[I] \right. \\ & + G_{\mu\nu}^a[J] G_{\rho\alpha}^b[I] G_{\lambda\alpha}^c[J] + G_{\mu\nu}^a[J] G_{\rho\alpha}^b[J] G_{\lambda\alpha}^c[I] + G_{\mu\nu}^a[I] G_{\rho\alpha}^b[J] G_{\lambda\alpha}^c[I, J] + G_{\mu\nu}^a[J] G_{\rho\alpha}^b[I] G_{\lambda\alpha}^c[I, J] \\ & \left. + G_{\mu\nu}^a[I] G_{\rho\alpha}^b[I, J] G_{\lambda\alpha}^c[J] + G_{\mu\nu}^a[J] G_{\rho\alpha}^b[I, J] G_{\lambda\alpha}^c[I] + G_{\mu\nu}^a[I, J] G_{\rho\alpha}^b[I] G_{\lambda\alpha}^c[J] + G_{\mu\nu}^a[I, J] G_{\rho\alpha}^b[J] G_{\lambda\alpha}^c[I] \right). \quad (112) \end{aligned}$$

Here,  $G_{\mu\nu}[I]$  is short for  $G_{\mu\nu}[A_I]$ . In the case of a two-instanton cluster and in LO in  $1/N_c$  counting, each instanton with  $N_f - 1$  flavors looped up dominates the contribution in the hadronic matrix element. The effective operator produces two types of coupling due to the chirality. The operator produced by  $II$  or  $AA$  clusters corresponds to a chiral-flipping process:

$$\begin{aligned} \frac{1}{V} \int d^4 x e^{-iq \cdot x} \mathcal{O}_{3g^{++}, --}(x) = & -\frac{N_c - 2}{2N_c^2(N_c^2 - 1)} \left( \frac{m^*}{4\pi^2 \rho^2} \right)^{2N_f - 2} \int d^4 z_I d^4 z_J \frac{1}{8} \text{tr}\{S(z_I - z_J)\} \\ & \times \frac{1}{V} \int d^4 x e^{-iq \cdot x} F_{3g, \mu\nu\rho\lambda\alpha\beta}^{(II)}(x - z_I, x - z_J) \left[ \bar{\psi}(z_I) \frac{1 \mp \gamma^5}{2} \sigma_{\alpha\beta} \psi(z_J) + \bar{\psi}(z_J) \frac{1 \mp \gamma^5}{2} \sigma_{\alpha\beta} \psi(z_I) \right], \quad (113) \end{aligned}$$

where the profile function for the  $II$  or  $AA$  pairs is defined as

$$\begin{aligned} F_{3g, \mu\nu\rho\lambda\alpha\beta}^{(II)}(x - z_I, x - z_J) = & \frac{1}{2} \bar{\eta}_{\beta\gamma}^a [G_{\mu\nu}^b(x - z_I) G_{\rho\alpha}^b(x - z_I) G_{\lambda\alpha}^a(x - z_J) + G_{\mu\nu}^b(x - z_I) G_{\rho\alpha}^a(x - z_J) G_{\lambda\alpha}^b(x - z_I) \\ & + G_{\mu\nu}^a(x - z_J) G_{\rho\alpha}^b(x - z_I) G_{\lambda\alpha}^b(x - z_I)] + (I \leftrightarrow J) \\ & + \frac{1}{2} \bar{\eta}_{\beta\gamma}^a \frac{1}{4(N_c + 2)} [\epsilon^{acd} G_{\mu\nu}^c(x - z_I) [A_\rho^d(x - z_I) A_\alpha^b(x - z_J) - A_\alpha^d(x - z_I) A_\rho^b(x - z_J)] G_{\lambda\alpha}^b(x - z_J) \\ & + \epsilon^{acd} G_{\rho\alpha}^c(x - z_I) [A_\lambda^d(x - z_I) A_\alpha^b(x - z_J) - A_\alpha^d(x - z_I) A_\lambda^b(x - z_J)] G_{\mu\nu}^b(x - z_J) \\ & + \epsilon^{acd} G_{\lambda\alpha}^c(x - z_I) [A_\mu^d(x - z_I) A_\nu^b(x - z_J) - A_\nu^d(x - z_I) A_\mu^b(x - z_J)] G_{\rho\alpha}^b(x - z_J) + (\rho \leftrightarrow \lambda)]. \quad (114) \end{aligned}$$

The operator produced by  $IA$  clusters corresponds to a chiral-conserving process:

$$\begin{aligned} \frac{1}{V} \int d^4x e^{-iq \cdot x} \mathcal{O}_{3g+-}(x) &= -\frac{N_c - 2}{2N_c^2(N_c^2 - 1)} \left( \frac{m^*}{4\pi^2 \rho^2} \right)^{2N_f - 2} \int d^4z_I d^4z_J \frac{i}{4} \text{tr} \{ S(z_I - z_J) \gamma_\alpha \} \\ &\times \frac{1}{V} \int d^4x e^{-iq \cdot x} F_{3g, \mu\nu\rho\lambda\alpha\beta}^{(IA)}(x - z_I, x - z_J) \left[ \bar{\psi}(z_I) \gamma_\beta \frac{1 + \gamma^5}{2} \psi(z_J) + \bar{\psi}(z_J) \gamma_\beta \frac{1 - \gamma^5}{2} \psi(z_I) \right], \end{aligned} \quad (115)$$

where the profile function for the instanton clusters is defined as

$$\begin{aligned} F_{3g, \mu\nu\rho\lambda, \beta\gamma}^{(IA)}(x - z_I, x - z_J) &= \frac{1}{2} \bar{n}_{\beta\gamma}^a \left[ G_{\mu\nu}^b(x - z_I) G_{\rho\alpha}^b(x - z_I) G_{\lambda\alpha}^a(x - z_J) + G_{\mu\nu}^b(x - z_I) G_{\rho\alpha}^a(x - z_J) G_{\lambda\alpha}^b(x - z_I) \right. \\ &+ G_{\mu\nu}^a(x - z_J) G_{\rho\alpha}^b(x - z_I) G_{\lambda\alpha}^b(x - z_I) \left. \right] - (I \leftrightarrow J) \\ &+ \frac{1}{2} \bar{n}_{\beta\gamma}^a \frac{1}{4(N_c + 2)} \left[ \epsilon^{acd} G_{\mu\nu}^c(x - z_I) [A_\rho^d(x - z_I) A_\alpha^b(x - z_J) - A_\alpha^d(x - z_I) A_\rho^b(x - z_J)] G_{\lambda\alpha}^b(x - z_J) \right. \\ &+ \epsilon^{acd} G_{\rho\alpha}^c(x - z_I) [A_\lambda^d(x - z_I) A_\alpha^b(x - z_J) - A_\alpha^d(x - z_I) A_\lambda^b(x - z_J)] G_{\mu\nu}^b(x - z_J) \\ &+ \left. \epsilon^{acd} G_{\lambda\alpha}^c(x - z_I) [A_\mu^d(x - z_I) A_\nu^b(x - z_J) - A_\nu^d(x - z_I) A_\mu^b(x - z_J)] G_{\rho\alpha}^b(x - z_J) + (\rho \leftrightarrow \lambda) \right]. \end{aligned} \quad (116)$$

In the SIA, these correlation functions can be simplified as single-point profile functions. The renormalization-group invariant result for the hadronic matrix element is

$$\begin{aligned} \langle P' | g^3 d^{abc} G_{\mu\nu}^a G_{\rho\alpha}^b G_{\lambda\alpha}^c | P \rangle &= -\frac{N_c - 2}{2N_c^2(N_c^2 - 1)} \left( \frac{2\kappa}{\rho^2 m^{*2}} \right)^2 \frac{8\pi^2 m}{9} \rho^2 m^2 T_{II} \beta_{3g}^{(II)}(\rho q) \frac{1}{2} q^2 \delta_{\rho\lambda} \langle P' | \bar{\psi} \sigma_{\mu\nu} \psi | P \rangle \\ &+ \frac{N_c - 2}{2N_c^2(N_c^2 - 1)} \left( \frac{2\kappa}{\rho^2 m^{*2}} \right)^2 \frac{8\pi^2 m}{9} \rho^2 m^2 T_{II} \beta_{3g}^{(II)}(\rho q) (\delta_{\mu\alpha} q_\beta q_\nu - \delta_{\nu\alpha} q_\beta q_\mu) \delta_{\rho\lambda} \langle P' | \bar{\psi} \sigma_{\alpha\beta} \psi | P \rangle \\ &- \frac{N_c - 2}{2N_c^2(N_c^2 - 1)} \left( \frac{2\kappa}{\rho^2 m^{*2}} \right)^2 \rho^2 m^2 T_{IA} \frac{4\pi^2}{45} \beta_{3g}^{(IA)}(\rho q) \\ &\times \left[ \epsilon_{\beta\gamma\lambda\sigma} q_\sigma q_\nu \delta_{\mu\rho} - \epsilon_{\beta\gamma\nu\sigma} q_\sigma q_\lambda \delta_{\mu\rho} - \frac{1}{2} \epsilon_{\beta\gamma\lambda\nu} q^2 \delta_{\mu\rho} + (\rho \leftrightarrow \lambda) - (\mu \leftrightarrow \nu) \right] \langle P' | \bar{\psi} \gamma_{[\beta} i \overleftrightarrow{\partial}_{\gamma]} \gamma^5 \psi | P \rangle \\ &- \frac{N_c - 2}{2N_c^2(N_c^2 - 1)} \left( \frac{2\kappa}{\rho^2 m^{*2}} \right)^2 \rho^2 m^2 T_{IA} \frac{4\pi^2}{15} \beta_{3g}^{(IA)}(\rho q) \delta_{\rho\lambda} \\ &\times \left( \epsilon_{\beta\gamma\mu\sigma} q_\sigma q_\nu - \epsilon_{\beta\gamma\nu\sigma} q_\sigma q_\mu - \frac{1}{2} \epsilon_{\beta\gamma\mu\nu} q^2 \right) \langle P' | \bar{\psi} \gamma_{[\beta} i \overleftrightarrow{\partial}_{\gamma]} \gamma^5 \psi | P \rangle \\ &- \frac{N_c - 2}{2N_c^2(N_c^2 - 1)} \left( \frac{2\kappa}{\rho^2 m^{*2}} \right)^2 \rho^2 m^2 T_{IA} \frac{8\pi^2}{45} \beta_{3g}^{(IA)}(\rho q) \\ &\times \left[ \epsilon_{\mu\nu\rho\alpha} (\delta_{\beta\lambda} q_\gamma q_\alpha - \delta_{\beta\alpha} q_\gamma q_\lambda) - \frac{1}{2} \epsilon_{\mu\nu\rho\gamma} q^2 \delta_{\beta\lambda} + (\rho \leftrightarrow \lambda) \right] \langle P' | \bar{\psi} \gamma_{[\beta} i \overleftrightarrow{\partial}_{\gamma]} \gamma^5 \psi | P \rangle, \end{aligned} \quad (117)$$

where

$$\begin{aligned} \beta_{3g}^{(II)}(\rho q) &= \frac{1}{q} \int_0^\infty dx \frac{9}{2} \frac{640x^4}{(1+x^2)^6} \frac{J_3(qx)}{q^2 x^2}, \\ \beta_{3g}^{(IA)}(\rho q) &= \frac{1}{q} \int_0^\infty dx \frac{2880x^4}{(1+x^2)^6} \frac{J_3(qx)}{q^2 x^2}, \end{aligned} \quad (118)$$

which is seen to vanish in the forward direction.

### 1. Light front twist-3

This operator is of special interest on the light front as a leading twist-3 that sources the coherent photoproduction of  $1^{++}$  heavy mesons off the nucleon state [76]. In light front signature, it contributes

$$\begin{aligned} \langle P' | g^3 d^{abc} G^{a+i}(x) G^{b+j}(x) G^{c+}_j(x) | P \rangle &= \frac{N_c - 2}{8N_c^2(N_c^2 - 1)(N_c + 2)} \left( \frac{2\kappa}{\rho^2 m^{*2}} \right)^2 \rho^4 m^3 T_{II}(q^+){}^2 \beta_{3g}^+(\rho q) \langle P' S | \bar{\psi} \\ &\times \left( \sigma^{i\alpha} q^+ q_\alpha - \sigma^{+\alpha} q^i q_\alpha - \frac{1}{2} q^2 \sigma^{+i} \right) \psi | PS \rangle, \end{aligned} \quad (119)$$

where

$$\beta_{3g}^+(\rho q) = \frac{4\pi^2}{q} \int_0^\infty dx \frac{512x^4}{(1+x^2)^6} \frac{J_5(qx)}{q^4 x^4}. \quad (120)$$

### 2. Gravity dual twist-5

The gluonic  $C$ -odd operator  $d^{abc} G_{\mu\nu}^a G_{\rho\lambda}^b G_{\rho\lambda}^c$  as a twist-5 boundary operator is argued to be dual of the supergravity B field in diffractive hadron-hadron scattering with odderon exchange [77]. In particular, its off-forward matrix element is

$$\begin{aligned} \langle P' | g^3 d^{abc} G_{\mu\nu}^a G_{\rho\lambda}^b G_{\rho\lambda}^c | P \rangle &= -\frac{N_c - 2}{2N_c^2(N_c^2 - 1)} \left( \frac{2\kappa}{\rho^2 m^{*2}} \right)^2 \rho^2 m^2 T_{II} \frac{16\pi^2}{9} q^2 \langle P' | m \bar{\psi} \sigma_{\mu\nu} \psi | P \rangle \\ &+ \frac{N_c - 2}{2N_c^2(N_c^2 - 1)} \left( \frac{2\kappa}{\rho^2 m^{*2}} \right)^2 \rho^2 m^2 T_{II} \frac{32\pi^2}{9} (\delta_{\mu\alpha} q_\beta q_\nu - \delta_{\nu\alpha} q_\beta q_\mu) \langle P' | m \bar{\psi} \sigma_{\alpha\beta} \psi | P \rangle \\ &- \frac{N_c - 2}{2N_c^2(N_c^2 - 1)} \left( \frac{2\kappa}{\rho^2 m^{*2}} \right)^2 \rho^2 m^2 T_{IA} \frac{32\pi^2}{45} \beta_{3g}^{(IA)}(\rho q) \\ &\times \left( \epsilon_{\beta\gamma\mu\sigma} q_\sigma q_\nu - \epsilon_{\beta\gamma\nu\sigma} q_\sigma q_\mu - \frac{1}{2} \epsilon_{\beta\gamma\mu\nu} q^2 \right) \langle P' | m \bar{\psi} \gamma_{[\beta} i \overleftrightarrow{\partial}_{\gamma]} \gamma^5 \psi | P \rangle \\ &- \frac{N_c - 2}{2N_c^2(N_c^2 - 1)} \left( \frac{2\kappa}{\rho^2 m^{*2}} \right)^2 \rho^2 m^2 T_{IA} \frac{32\pi^2}{45} \beta_{3g}^{(IA)}(\rho q) \left( \epsilon_{\mu\nu\beta\alpha} q_\gamma q_\alpha - \frac{1}{4} \epsilon_{\mu\nu\beta\gamma} q^2 \right) \langle P' | m \bar{\psi} \gamma_{[\beta} i \overleftrightarrow{\partial}_{\gamma]} \gamma^5 \psi | P \rangle. \end{aligned} \quad (121)$$

## IX. C-EVEN THREE-GLUON FORM FACTOR

As a parity check on the preceding calculation, we now consider the  $C$ -odd analog of (109):

$$\tilde{\mathcal{O}}_{3g}[A] = f^{abc} G_{\mu\nu}^a(x) G_{\nu\rho}^b(x) G_{\rho\mu}^c(x). \quad (122)$$

Equation (122) can again be evaluated semiclassically through the substitution of the gluonic field in (62).

A rerun of the preceding steps gives

$$\begin{aligned} \frac{1}{V} \int d^4 x \tilde{\mathcal{O}}_{3g\pm}(x) e^{-iq \cdot x} &= \frac{1}{\rho^2 V} \int d^4 x \tilde{F}_{3g}^{(I,A)}(x) e^{-i\rho q \cdot x} \left[ \left( \frac{m^*}{4\pi^2 \rho^2} \right)^{N_f} (2\pi)^4 \delta^4(q) \right. \\ &\left. - \frac{1}{N_c} \left( \frac{m^*}{4\pi^2 \rho^2} \right)^{N_f-1} \int d^4 z \bar{\psi}(z) \frac{1 \mp \gamma^5}{2} \psi(z) e^{-iq \cdot z} \right], \end{aligned} \quad (125)$$

### A. One-instanton contribution

In LO in the density expansion, the effective fermionic operator for  $\tilde{\mathcal{O}}_{3g}$  follows from the modular averaging

$$\tilde{\mathcal{O}}_{3g\pm}(x) = \int d^4 z_I dU_I \tilde{\mathcal{O}}_{3g}[A_I] \Theta_I \quad (123)$$

with

$$\tilde{\mathcal{O}}_{3g}[A_I] = \epsilon^{abc} G_{\mu\nu}^a[A_I] G_{\nu\rho}^b[A_I] G_{\rho\mu}^c[A_I]. \quad (124)$$

where the profile function for the single (anti-)instanton  $I$  ( $A$ ) is defined as

$$\tilde{F}_{3g}^{(I,A)}(x) = \frac{1536}{(x^2 + 1)^6}. \quad (126)$$

### B. Two-instanton contribution

At NLO in the density expansion, the effective fermionic operator for  $\tilde{\mathcal{O}}_{3g}$  is obtained by averaging the leading

expansion of  $\tilde{\mathcal{O}}_{3g}$  with a two-instanton vertex:

$$\tilde{\mathcal{O}}_{3g\pm\pm}(x) = \int d^4z_I d^4z_J dU_I dU_J \tilde{\mathcal{O}}_{3g}[A_I, A_J] \Theta_I \Theta_J \quad (127)$$

with

$$\begin{aligned} \tilde{\mathcal{O}}_{3g}[A_I, A_J] \simeq e^{abc} & \left( G_{\mu\nu}^a[I] G_{\rho\alpha}^b[J] G_{\lambda\alpha}^c[J] + G_{\mu\nu}^a[J] G_{\rho\alpha}^b[I] G_{\lambda\alpha}^c[I] + G_{\mu\nu}^a[I] G_{\rho\alpha}^b[J] G_{\lambda\alpha}^c[I] + G_{\mu\nu}^a[J] G_{\rho\alpha}^b[I] G_{\lambda\alpha}^c[J] \right. \\ & \left. + G_{\mu\nu}^a[J] G_{\rho\alpha}^b[I] G_{\lambda\alpha}^c[J] + G_{\mu\nu}^a[I] G_{\rho\alpha}^b[J] G_{\lambda\alpha}^c[I] \right). \end{aligned} \quad (128)$$

Here, we dropped the contributions associated to  $G_{\mu\nu}[I, J]$  as they are subleading in power counting.

The emerging fermionic operators are twofold: chiral conserving and flipping. The chiral-flipping operators are produced by  $II$  or  $AA$  clusters:

$$\begin{aligned} \frac{1}{V} \int d^4x \tilde{\mathcal{O}}_{3g++,-}(x) e^{-iq \cdot x} &= \frac{1}{2N_c(N_c^2 - 1)} \left( \frac{m^*}{4\pi^2 \rho^2} \right)^{2N_f - 2} \int d^4z_I d^4z_J \frac{1}{8} \text{tr}\{S(z_I - z_J)\} \\ &\times \frac{1}{V} \int d^4x e^{-iq \cdot x} \tilde{F}_{3g}^{(II,AA)}(x - z_I, x - z_J) \left[ \bar{\psi}(z_I) \frac{1 \mp \gamma^5}{2} \psi(z_J) + \bar{\psi}(z_J) \frac{1 \mp \gamma^5}{2} \psi(z_I) \right], \end{aligned} \quad (129)$$

where the profile function for the  $II$  cluster is defined as

$$\tilde{F}_{3g}^{(II)}(x - z_I, x - z_J) = 3e^{abc} G_{\mu\nu}^a(x - z_J) G_{\nu\rho}^b(x - z_I) G_{\rho\mu}^c(x - z_I) + 3e^{abc} G_{\mu\nu}^a(x - z_I) G_{\nu\rho}^b(x - z_J) G_{\rho\mu}^c(x - z_J) \quad (130)$$

and the profile function for the  $AA$  cluster is

$$\tilde{F}_{3g}^{(II)}(x - z_I, x - z_J) = \tilde{F}_{3g}^{(AA)}(x - z_I, x - z_J). \quad (131)$$

The chiral-preserving operators are produced by the  $IA$  molecules:

$$\begin{aligned} \frac{1}{V} \int d^4x \tilde{\mathcal{O}}_{3g+-}(x) e^{-iq \cdot x} &= -\frac{1}{2N_c(N_c^2 - 1)} \left( \frac{m^*}{4\pi^2 \rho^2} \right)^{2N_f - 2} \int d^4z_I d^4z_J \frac{1}{4} \text{tr}\{S(z_I - z_J) \gamma_\mu\} \\ &\times \frac{1}{V} \int d^4x e^{-iq \cdot x} \tilde{F}_{3g,\mu\nu}^{(IA)}(x - z_I, x - z_J) \left[ \bar{\psi}(z_I) \gamma_\nu \frac{1 + \gamma^5}{2} \psi(z_J) - \bar{\psi}(z_J) \gamma_\nu \frac{1 - \gamma^5}{2} \psi(z_I) \right], \end{aligned} \quad (132)$$

where the profile function for the  $IA$  molecule is defined as

$$\tilde{F}_{3g,\rho\lambda}^{(IA)}(x - z_I, x - z_J) = \frac{1}{2} \bar{\eta}_{\rho\beta}^a \eta_{\lambda\beta}^b \left[ 3e^{acd} G_{\mu\nu}^b(x - z_J) G_{\nu\rho}^c(x - z_I) G_{\rho\mu}^d(x - z_I) + 3e^{bcd} G_{\mu\nu}^a(x - z_I) G_{\nu\rho}^c(x - z_J) G_{\rho\mu}^d(x - z_J) \right] = 0 \quad (133)$$

and is seen to vanish. We again approximated the nonlocal quark operators by local operators, by expanding in the relative distance between close instanton pairs  $R = z_I - z_J$ .

### C. Off-forward matrix element

The general off-forward hadronic matrix element of the  $C$ -even three-gluon operator is

$$\begin{aligned} \frac{5\rho^2}{384\pi^2} \langle P'S | g^3 f^{abc} G_{\mu\nu}^a G_{\nu\rho}^b G_{\rho\mu}^c | PS \rangle &= - \left[ \frac{1}{4} M_{\text{inv}}^{(0)} \frac{\sigma_T}{N} \frac{(2\pi)^4}{V} \delta^4(q) \right] \bar{u}_{s'}(P') u_s(P) - \left[ \frac{1}{N_c} \left( \frac{2\kappa}{\rho^2 m^{*2}} \right) - \frac{1}{2N_c(N_c^2 - 1)} \right] \\ &\times \left( \frac{2\kappa}{\rho^2 m^{*2}} \right)^2 3\rho^2 m^2 T_{II} \left] \tilde{\beta}_{3g}(\rho q) \langle P'S | m\bar{\psi}\psi | PS \rangle, \end{aligned} \quad (134)$$

where the nonlocal form factors induced by the finite instanton size effect are defined as

$$\tilde{\beta}_{3g}(q) = \frac{1}{q} \int_0^\infty dx \frac{80x^2}{(x^2 + 1)^6} J_1(qx) \quad (135)$$

with the normalization to 1 in the forward limit.

### X. GLUONIC GRAVITATIONAL FORM FACTORS

Another gluonic operator of interest is the gluonic tensor tied to the QCD EMT. To evaluate the QCD energy-momentum tensor using local or nonlocal effective formulations is subtle; for a recent discussion, see [78]. In the present approach, it follows the same reasoning as that for the scalar and pseudoscalar operators discussed above.

With this in mind, the EMT in QCD is given by

$$T_{\mu\nu} = T_{\mu\nu}^g + T_{\mu\nu}^q, \quad (136)$$

where  $T_{\mu\nu}^g$  is the gluonic EMT and  $T_{\mu\nu}^q$  is the quark EMT. All issues of operator renormalization are understood in the sense of a gradient flow cooling to the semiclassical point with fixed topological charge per 4-volume, with the instanton density as the sole scale. The energy-momentum tensor can be decomposed as the sum of a traceless and traceful part [79,80]:

$$T_{\mu\nu} = \bar{T}_{\mu\nu} + \frac{1}{4} g_{\mu\nu} T_{\alpha\alpha}, \quad (137)$$

where the traceless part includes the gluonic tensor

$$\bar{T}_{\mu\nu}^g = \frac{1}{4} g_{\mu\nu} G_{\lambda\rho}^2 - G_{\mu\lambda}^a G_{\nu\lambda}^a \quad (138)$$

and

$$\bar{T}_{\mu\nu}^q = \bar{\psi} \left( \gamma_{(\mu} i \overleftrightarrow{D}_{\nu)} - \frac{1}{4} g_{\mu\nu} m \right) \psi \quad (139)$$

and the traceful part  $T_{\alpha\alpha}$  is given by the trace anomaly in (30). Both contributions belong to different irreducible representations of the Lorentz group. Thus, they do not mix in the renormalization.

In the chiral limit, the traceful part is related to the gluonic scalar by the conformal anomaly, and in  $1/N_c$  counting rule, it is independent of the quarks. We note that this decomposition is commensurate with the analysis of the energy-momentum tensor in holographic QCD, through dual gravitons in bulk [81]. (Holography is a good example of a strong coupling description of a gauge theory via its gravity dual, where the partonic structure is elusive.) The traceful and traceless parts of the energy-momentum tensor correspond to the spin-2 and spin-0 representations of the Lorentz group, respectively, and do not mix under renormalization by symmetry.

The calculation of the gluonic scalar form factor can be easily generalized to the gluonic gravitational form factor. The matrix element vanishes in leading order of the instanton density expansion, due to self-duality. Purely tunneling vacuum configurations do not carry energy-momentum. This is best seen in light front signature with

$$G^{a+i} G^{a+i} = -\frac{1}{2} \left( \vec{E}_\perp^a \cdot \vec{E}_\perp^a + 2\hat{z} \cdot (\vec{E}_\perp^a \times \vec{B}_\perp^a) + \vec{B}_\perp^a \cdot \vec{B}_\perp^a \right). \quad (140)$$

Since the instanton and anti-instanton are self-dual, it means the tunneling configuration of the field strength in Minkowski space satisfies  $\vec{E}^a = \mp i\vec{B}^a$  for all  $I = 1, \dots, N_\pm$ . Therefore, the instanton contribution in the leading order of the instanton density in (63) vanishes. The nontrivial instanton contribution starts from the higher orders of instanton density and, thus, is penalized by an extra factor denoted by  $\kappa = \pi^2 \rho^4 n_{I+A}$ , the packing fraction of the instanton vacuum.

#### A. Two-instanton contribution

At NLO in the instanton density expansion, the effective fermionic operator for  $\mathcal{O}_{2g}$  can be obtained by averaging the leading expansion of  $\mathcal{O}_{2g}$  with a two-instanton vertex:

$$\bar{T}_{\mu\nu\pm\pm}^g(x) = \int d^4 z_I d^4 z_J dU_I dU_J \bar{T}_{\mu\nu}^g[A_I, A_J] \Theta_I \Theta_J \quad (141)$$

with

$$\bar{T}_{\mu\nu}^g[A_I, A_J] = G_{\mu\alpha}^a[I]G_{\nu\alpha}^a[J] + G_{\mu\alpha}^a[I]G_{\nu\alpha}^a[I, J] + G_{\mu\alpha}^a[I, J]G_{\nu\alpha}^a[I] + (I \leftrightarrow J) + G_{\mu\alpha}^a[I, J]G_{\nu\alpha}^a[I, J] - \frac{1}{4}\delta_{\mu\nu}\mathcal{O}_{2g}[A_I, A_J]. \quad (142)$$

The effective operator produces two types of coupling due to the chirality. The operator produced by  $II$  or  $AA$  clusters corresponds to a chiral-flipping process:

$$\begin{aligned} \frac{1}{V} \int d^4x \bar{T}_{\mu\nu^{++,-}}^g(x) e^{-iq \cdot x} &= \frac{1}{2N_c(N_c^2 - 1)} \left( \frac{m^*}{4\pi^2 \rho^2} \right)^{2N_f - 2} \int d^4z_I d^4z_J \frac{1}{8} \text{tr}\{S(z_I - z_J)\} \\ &\times \frac{1}{V} \int d^4x e^{-iq \cdot x} F_{T_g, \mu\nu}^{(II, AA)}(x - z_I, x - z_J) \left[ \bar{\psi}(z_I) \frac{1 \mp \gamma^5}{2} \psi(z_J) + \bar{\psi}(z_J) \frac{1 \mp \gamma^5}{2} \psi(z_I) \right], \end{aligned} \quad (143)$$

where the profile function for  $II$  cluster is defined as

$$\begin{aligned} F_{T_g, \mu\nu}^{(II)}(x - z_I, x - z_J) &= G_{\mu\alpha}^a(x - z_I)G_{\nu\alpha}^a(x - z_J) - \frac{1}{4}\delta_{\mu\nu}G_{\alpha\beta}^a(x - z_I)G_{\alpha\beta}^a(x - z_J) \\ &+ \epsilon^{acd}G_{\mu\alpha}^c(x - z_I)[A_\nu^d(x - z_I)A_\alpha^a(x - z_J) - A_\alpha^d(x - z_I)A_\nu^a(x - z_J)] \\ &+ \epsilon^{acd}G_{\nu\alpha}^c(x - z_I)[A_\mu^d(x - z_I)A_\alpha^a(x - z_J) - A_\alpha^d(x - z_I)A_\mu^a(x - z_J)] \\ &- \delta_{\mu\nu}\epsilon^{acd}G_{\alpha\beta}^c(x - z_I)[A_\alpha^d(x - z_I)A_\beta^b(x - z_J)] + (I \leftrightarrow J) + \mathcal{O}(1/N_c) \end{aligned} \quad (144)$$

and the profile function for  $AA$  cluster is equal

$$F_{T_g, \mu\nu}^{(II)}(x - z_I, x - z_J) = F_{T_g, \mu\nu}^{(AA)}(x - z_I, x - z_J). \quad (145)$$

Here, we dropped the contributions associated to  $G_{\mu\alpha}^a[I, J]G_{\nu\alpha}^a[I, J]$  as they are subleading in power counting.

The operator produced by  $IA$  molecules corresponds to a chiral-conserving process:

$$\begin{aligned} \frac{1}{V} \int d^4x \bar{T}_{\mu\nu^{+-}}^g(x) e^{-iq \cdot x} &= -\frac{1}{2N_c(N_c^2 - 1)} \left( \frac{m^*}{4\pi^2 \rho^2} \right)^{2N_f - 2} \int d^4z_I d^4z_J \frac{1}{4} \text{tr}\{S(z_I - z_J)\gamma_\rho\} \\ &\times \frac{1}{V} \int d^4x e^{-iq \cdot x} F_{T_g, \mu\nu\rho\lambda}^{(IA)}(x - z_I, x - z_J) \left[ \bar{\psi}(z_I)\gamma_\lambda \frac{1 + \gamma^5}{2} \psi(z_J) - \bar{\psi}(z_J)\gamma_\lambda \frac{1 - \gamma^5}{2} \psi(z_I) \right], \end{aligned} \quad (146)$$

where the profile function for  $IA$  molecule is defined as

$$\begin{aligned} F_{T_g, \mu\nu\rho\lambda}^{(IA)}(x - z_I, x - z_J) &= \frac{1}{2}\bar{n}_{\rho\beta}^a n_{\lambda\beta}^b \left[ G_{\mu\alpha}^a(x - z_I)G_{\nu\alpha}^b(x - z_J) - \frac{1}{4}\delta_{\mu\nu}G_{\alpha\beta}^a(x - z_I)G_{\alpha\beta}^b(x - z_J) \right. \\ &+ \epsilon^{acd}G_{\mu\alpha}^c(x - z_I)[A_\nu^d(x - z_I)A_\alpha^b(x - z_J) - A_\alpha^d(x - z_I)A_\nu^b(x - z_J)] \\ &+ \epsilon^{acd}G_{\nu\alpha}^c(x - z_I)[A_\mu^d(x - z_I)A_\alpha^b(x - z_J) - A_\alpha^d(x - z_I)A_\mu^b(x - z_J)] \\ &\left. - \delta_{\mu\nu}\epsilon^{acd}G_{\alpha\beta}^c(x - z_I)A_\alpha^d(x - z_I)A_\beta^b(x - z_J) + \left( \begin{array}{c} I \leftrightarrow J \\ a \leftrightarrow b \end{array} \right) \right] + \mathcal{O}(1/N_c). \end{aligned} \quad (147)$$

### B. Off-forward matrix element

The off-forward hadronic matrix element of the traceless gluonic energy-momentum tensor reads

$$\begin{aligned}
\langle P'S|g^2\bar{T}_{\mu\nu}^g|PS\rangle &= \frac{1}{2N_c(N_c^2-1)}\left(\frac{2\kappa}{\rho^2m^{*2}}\right)^2\rho^2m^2T_{IA}\left\{\frac{16\pi^2}{3}\beta_{T_{g,1}}^{(IA)}(\rho q)\langle P'S|\bar{\psi}\left(\gamma_{(\mu}i\overleftrightarrow{\partial}_{\nu)}-\frac{1}{4}g_{\mu\nu}i\overleftrightarrow{\not{D}}\right)\psi|PS\rangle\right. \\
&\quad -\frac{4\pi^2\rho^2}{9}\beta_{T_{g,2}}^{(IA)}(\rho q)\left(q_\mu q_\rho g_{\nu\lambda}+q_\nu q_\rho g_{\mu\lambda}-\frac{1}{2}g_{\mu\nu}q_\rho q_\lambda\right)\langle P'S|\bar{\psi}\left(\gamma_{(\rho}i\overleftrightarrow{\partial}_{\lambda)}-\frac{1}{4}g_{\rho\lambda}i\overleftrightarrow{\not{D}}\right)\psi|PS\rangle \\
&\quad \left.-4\pi^2\rho^4\beta_{T_{g,3}}^{(IA)}(\rho q)\left(q_\mu q_\nu-\frac{1}{4}q^2g_{\mu\nu}\right)q_\rho q_\lambda\langle P'S|\bar{\psi}\left(\gamma_{(\rho}i\overleftrightarrow{\partial}_{\lambda)}-\frac{1}{4}g_{\rho\lambda}i\overleftrightarrow{\not{D}}\right)\psi|PS\rangle\right\} \\
&\quad +\frac{1}{2N_c(N_c^2-1)}\left(\frac{2\kappa}{\rho^2m^{*2}}\right)^2\rho^2m^2T_{II}\frac{8\pi^2\rho^2}{9}\beta_{T_g}^{(II)}(\rho q)\left(q_\mu q_\nu-\frac{1}{4}q^2g_{\mu\nu}\right)\langle P'S|m\bar{\psi}\psi|PS\rangle, \tag{148}
\end{aligned}$$

where the nonlocal form factors are defined as

$$\begin{aligned}
\beta_{T_{g,1}}^{(IA)}(q) &= \frac{1}{q}\int_0^\infty dx\left[\frac{24}{(1+x^2)^4}J_1(qx)+\frac{24x^2}{(1+x^2)^4}J_3(qx)\right. \\
&\quad \left.-\frac{192}{(1+x^2)^3}\frac{J_3(qx)}{q^2x^2}\right], \tag{149}
\end{aligned}$$

$$\begin{aligned}
\beta_{T_{g,2}}^{(IA)}(q) &= \frac{1}{q}\int_0^\infty dx9x^2\left[\frac{128x^2}{(1+x^2)^4}\frac{J_3(qx)}{q^2x^2}\right. \\
&\quad \left.-\frac{512}{(1+x^2)^3}\frac{J_4(qx)}{q^3x^3}\right], \tag{150}
\end{aligned}$$

$$\beta_{T_{g,3}}^{(IA)}(q) = \frac{1}{q}\int_0^\infty dx\frac{256x^4}{(1+x^2)^3}\frac{J_5(qx)}{q^4x^4}, \tag{151}$$

$$\beta_{T_g}^{(II)}(q) = \frac{1}{q}\int_0^\infty dx\frac{576x^2}{(1+x^2)^4}\frac{J_3(qx)}{q^2x^2} \tag{152}$$

and are normalized to 1. For the quark traceless EMT, the matching is even simpler and straightforward at the leading order of the instanton density expansion

$$\begin{aligned}
\langle P'S|\bar{T}_{\mu\nu}^q|PS\rangle &= \langle P'S|\bar{\psi}\left(\gamma_{(\mu}i\overleftrightarrow{\partial}_{\nu)}-\frac{1}{4}g_{\mu\nu}i\overleftrightarrow{\not{D}}\right)\psi|PS\rangle \\
&\quad +\mathcal{O}(n_{I+A}). \tag{153}
\end{aligned}$$

The traceless gluonic and quark EMT now is matched to the effective traceless quark energy-momentum tensor derived from the effective field theory (50). It is expected, as they are under the same Lorentz irreducible representation. The finite-sized instanton profile also induces the mixing of the scalar quark operator.

In the nucleon states, we can parametrize the matrix element for the effective quark traceless EMT operator and the scalar operator

$$\begin{aligned}
\langle P'S|\bar{T}_{\mu\nu}^{q,g}|PS\rangle &= \bar{u}_{s'}(P')\left(A_{q,g}(q)\left(\gamma^{(\mu}\bar{P}^{\nu)}-\frac{1}{4}g^{\mu\nu}M_N\right)+B_{q,g}(q)\left(\frac{i\bar{P}^{(\mu}\sigma^{\nu)\alpha}q_\alpha}{2M_N}-g^{\mu\nu}\frac{q^2}{16M_N}\right)\right. \\
&\quad \left.+C_{q,g}(q)\frac{1}{M_N}\left(q^\mu q^\nu-\frac{1}{4}g^{\mu\nu}q^2\right)\right)u_s(P) \tag{154}
\end{aligned}$$

and the scalar form factor

$$\langle P'S|m\bar{\psi}\psi|PS\rangle = \sigma(q)\bar{u}_{s'}(P')u_s(P). \tag{155}$$

The gluonic gravitational form factors are related to the effective quark form factors as

$$A_g(q) = \frac{1}{2N_c(N_c^2-1)}\left(\frac{2\kappa}{\rho^2m^{*2}}\right)^2\rho^2m^2T_{IA}(\rho m^*)\frac{16\pi^2}{3}\beta_{T_{g,1}}^{(IA)}(\rho q)A_q(q), \tag{156}$$

$$B_g(q) = \frac{1}{2N_c(N_c^2-1)}\left(\frac{2\kappa}{\rho^2m^{*2}}\right)^2\rho^2m^2T_{IA}(\rho m^*)\frac{16\pi^2}{3}\beta_{T_{g,1}}^{(IA)}(\rho q)B_q(q), \tag{157}$$

$$C_g(q) = \frac{1}{2N_c(N_c^2 - 1)} \left( \frac{2\kappa}{\rho^2 m^{*2}} \right)^2 \rho^2 m^2 T_{IA}(\rho m^*) \left\{ \frac{16\pi^2}{3} \beta_{T_g,1}^{(IA)}(\rho q) C_q(q) + \frac{2\pi^2 \rho^2}{9} M_N^2 \left( \beta_{T_g,2}^{(IA)}(\rho q) + \frac{9}{2} \rho^2 q^2 \beta_{T_g,3}^{(IA)}(\rho q) \right) \right. \\ \left. \times \left( A_q + B_q \frac{q^2}{4M_N^2} - C_q \frac{3q^2}{M_N^2} \right) \right\} + \frac{1}{2N_c(N_c^2 - 1)} \left( \frac{2\kappa}{\rho^2 m^{*2}} \right)^2 \rho^2 m^2 T_{II} \frac{4\pi^2 \rho^2 M_N^2}{9} \beta_{T_g}^{(II)}(\rho q) \frac{\sigma(q)}{M_N}. \quad (158)$$

### C. Gravitational charges: $A_{qg}(\mathbf{0})$

In the forward limit  $q \rightarrow 0$ , the gluonic traceless part (154) is

$$\langle PS | g^2 \bar{T}_{\mu\nu}^q | PS \rangle = \frac{1}{2N_c(N_c^2 - 1)} \left( \frac{n_{I+A} 4\pi^2 \rho^2}{2 m^*} \right)^2 \rho^2 T_{IA}(\rho m^*) \\ \times \frac{16\pi^2}{3} \langle PS | \bar{T}_{\mu\nu}^q | PS \rangle, \quad (159)$$

and the quark traceless part dominates the matrix element at the LO in the density expansion:

$$\langle PS | \bar{T}_{\mu\nu}^q | PS \rangle = 2 \left( P_\mu P_\nu - \frac{1}{4} g_{\mu\nu} M_N^2 \right) A_q(0). \quad (160)$$

Poincaré symmetry guarantees the energy-momentum conservation of the  $A$ -form factor in the zero momentum limit

$$A_q(0) + A_g(0) = 1$$

with

$$A_g(0) = \frac{1}{2N_c(N_c^2 - 1)} \left( \frac{2\kappa}{\rho^2 m^{*2}} \right)^2 \frac{16\pi^2 \rho^2 m^2}{3} T_{IA}(\rho m^*) \\ \times \left[ 1 + \frac{1}{2N_c(N_c^2 - 1)} \right. \\ \left. \times \left( \frac{2\kappa}{\rho^2 m^{*2}} \right)^2 \frac{16\pi^2 \rho^2 m^2}{3} T_{IA}(\rho m^*) \right]^{-1}.$$

The gluonic contribution to the nucleon gravitational charge  $A_g(0)$  receives a contribution from the instanton-anti-instanton molecules at NLO. Using the QCD instanton vacuum parameters [59,60] (and references therein), we have at the resolution  $\mu \approx 1/\rho$

$$A_q(0) = 0.9865, \quad A_g(0) = 0.0135.$$

These estimates are consistent with those given in [37].

To compare with other results, we can evolve the result from  $\mu_0 = 0.56 \text{ GeV} \approx 1/\rho$ , where the evolution starts to resolve the instanton vacuum [59,60] with DGLAP equation [82]

$$\mu \frac{d}{d\mu} \begin{pmatrix} A_q(0) \\ A_g(0) \end{pmatrix}_\mu = \frac{\alpha_s}{4\pi} \begin{pmatrix} -\frac{16}{3} C_F & \frac{4}{3} N_f \\ \frac{16}{3} C_F & -\frac{4}{3} N_f \end{pmatrix} \begin{pmatrix} A_q(0) \\ A_g(0) \end{pmatrix}_\mu, \quad (161)$$

where  $C_F = \frac{N_c^2 - 1}{2N_c}$ . The asymptotic form, thus, is given by the solution at  $\mu \rightarrow \infty$ :

$$A_q(0) = \frac{N_f}{4C_F + N_f}$$

and

$$A_g(0) = \frac{4C_F}{4C_F + N_f}.$$

At  $\mu = 2 \text{ GeV}$ , the results are shown in the table below.

	$A_q(0)$	$A_g(0)$
ILM (this work)	0.560	0.364
Asymptotic [83,84]	0.529	0.471
Skyrmion [85]	0.5	0.5
Lattice (dipole, 2018) [86]	0.46(8)	0.54(8)
Lattice (dipole, 2023) [21]	0.510(25)	0.501(27)
Lattice (tripole) [87]	0.57(4)	0.429(39)
Lattice (Extended Twisted Mass Collaboration) [29]	0.618(60)	0.427(92)
Global analysis [88]	0.58(1)	0.414(8)

In the second and fourth lattice results,  $A_q(0)$  is obtained by imposing the momentum conservation  $A_q(0) = 1 - A_g(0)$ . Extended Twisted Mass Collaboration is using physical pion mass.

### D. Gravitational charges: $C_{qg}(\mathbf{0})$

The  $C$ -form factor at zero momentum transfer is given by

$$C_g(0) = \frac{1}{2N_c(N_c^2 - 1)} \left( \frac{2\kappa}{\rho^2 m^{*2}} \right)^2 \rho^2 m^2 T_{IA} \\ \times \left\{ \frac{16\pi^2}{3} C_q(0) + \frac{2\pi^2 \rho^2}{9} M_N^2 A_q(0) \right\} \\ + \frac{1}{2N_c(N_c^2 - 1)} \left( \frac{2\kappa}{\rho^2 m^{*2}} \right)^2 \rho^2 m^2 T_{II} \frac{4\pi^2 \rho^2}{9} M_N \sigma_{\pi N}. \quad (162)$$

The estimate follows by saturating the scalar and flavor-singlet nucleon form factor, by the  $\sigma$  exchange, with the result

$$\sigma_{\pi N} \equiv \frac{\langle PS | m \bar{\psi} \psi | PS \rangle}{2M_N} = 3m \times \frac{M_q(0) g_{\sigma qq}^2 / G_\sigma}{M_N m_\sigma^2}. \quad (163)$$

The overall factor of 3 counts the three constituent quarks in the nucleon. Equation (163) yields a nucleon sigma term of about  $\sigma_\pi = 11.5$  MeV with our value of  $m = 12.2$  MeV in Table I and consistently the model estimation on the parameters  $m_\sigma = 683.1$  MeV and  $g_{\sigma qq} = 3.841$  with  $G_\sigma = 42.32$  GeV<sup>-2</sup> in Appendix B. This is small in comparison to the empirical value  $\sigma_\pi = 60$  MeV [89] (and references therein). Additional contributions to the simple mean-field estimate with only  $\sigma$  exchange, and beyond the constituent quark description for the nucleon, are expected to narrow the difference. For the mass budget to follow, we will make use of the empirical value

The gluon  $C$ -form factor at zero momentum requires the explicit nucleon wave function in the QCD instanton vacuum which we plan to construct. For an estimate, we will use the results from topological models of the nucleon [85,90,91] which are about  $-1$  (see the table below) at the low resolution of  $1/\rho$ . The chiral quark soliton model ( $\chi$ QSM) in [90] is usually argued to emerge from the QCD instanton vacuum in the large  $N_c$  limit [92], at the same resolution.

	$C_q(0)$	$C_g^{\text{ILM}}(0)$ (this work)
$\pi\rho\omega$ soliton [85]	-1.006	-0.0117
Skyrme [91]	-0.896	-0.0102
$\chi$ QSM [90]	-0.97	-0.0112
	$C_q(0)$	$C_g(0)$
ILM (this work)	-0.617	-0.365
Lattice (dipole, 2018) [86]	...	-2.5
Lattice (dipole, 2023) [21]	-0.325(12)	-0.643(21)
Lattice (tripole) [87]	...	-0.485
Measurement (6 GeV) [93]	$-0.408 \pm 0.028 \pm 0.033$	...

To compare with other results, again we can evolve the result from  $\mu_0 = 0.56$  GeV  $\approx 1/\rho$ . For  $C$ -form factor, they obey the same DGLAP equation in (161). Thus, their asymptotic form is given by

$$C_q(0) = C \frac{N_f}{4C_F + N_f}$$

and

$$C_g(0) = C \frac{4C_F}{4C_F + N_f},$$

where  $C \equiv C(0) = D/4$  is the intrinsic charge related to the mechanical property inside the nucleon, also known as  $D$  term [94]. Here, we choose the result estimated from  $\chi$ QSM [90] for  $C_q(0)$ . Evolved to  $\mu = 2$  GeV, the results are shown in the table.

## XI. HADRON MASS IDENTITY

In QCD, the breaking of conformal symmetry is captured by the trace anomaly (30). By Poincaré symmetry, all squared hadron masses satisfy the mass identity

$$M_H^2 = \frac{1}{2} \langle PS | T_{\mu\mu} | PS \rangle, \quad (164)$$

which is distinct from the mass budgeting sum rule to be discussed below. In particular, (30) gives

$$M_H^2 = -\frac{b}{64\pi^2} \langle PS | g^2 G_{\mu\nu}^a G_{\mu\nu}^a | PS \rangle + \frac{m}{2} \langle PS | \bar{\psi} \psi | PS \rangle. \quad (165)$$

Thus, all hadron masses are composed of

$$M_H = M_{\text{inv}} + \sigma_{\pi H} \quad (166)$$

of the ‘‘invariant’’ mass (fixed by  $\Lambda_{\text{QCD}}$ ) and the chiral breaking mass (sigma term) at some resolution. In quenched QCD (gluodynamics), the hadron mass is the quenched invariant mass  $M_{\text{inv}}^{(0)}$  induced solely by the spontaneous breaking of chiral symmetry and/or confinement from gluons. In QCD, quarks contribute even in the chiral limit. Away from the quenched and chiral limit, the hadronic mass receives additional contributions from the  $\sigma_{\pi H}$  term [24,95].

In the QCD instanton vacuum  $\Lambda_{\text{QCD}}$  at low resolution is played by the mean instanton density at LO. Recall that even the constituent quark mass is fixed by this density, as the mean instanton size is also fixed by this density implicitly through modular interactions. In the QCD instanton vacuum, the mass-breaking terms are of the order of  $\mathcal{O}(mR)$  and small for light quarks. At this low resolution, it is possible to budget the mass carried by the emerging quarks, and the semiclassical gluons that permeate the vacuum, as we now detail.

## XII. NUCLEON MASS SUM RULE

The trace identity (165) reflects on the general fact that all hadron masses in QCD are tied to the quantum breaking of conformal symmetry as we noted earlier and should be enforced by any nonperturbative quantum description, whether numerical such as the lattice or semiclassical such as the QCD instanton vacuum. However, it does not

specifically budget this mass breaking in terms of the emerging constituents in hadrons.

In a strongly interacting theory, the concept of constituents is subtle and resolution dependent. Fortunately, the QCD instanton vacuum emerging from cooled lattice simulations allows for a quantitative description, all within the well-defined framework of semiclassics. In this spirit, a physically motivated proposal to budget the mass was put forth by Ji in [80,96] and since revisited by many [97–99] (and references therein). The ensuing mass composition involves the sum of partonic contributions, some of which may be measurable using DIS experiments. The proposal relies on an invariant decomposition of the energy-momentum tensor (137).

The traceful and traceless part of the energy-momentum tensor (137) correspond to the spin-2 and spin-0 representations of the Lorentz group, respectively, and do not mix under renormalization by symmetry, as we noted earlier. Their renormalization at the instanton size scale  $\rho \approx 0.3$  fm is achieved by cooling through gradient flow, under the constraint of a fixed topological susceptibility. Note that this renormalization scale is softer than the one used in currently fine lattices with  $1/\mu \approx 0.1$  fm ( $\overline{\text{MS}}$  scheme) [26].

With this in mind, the corresponding Hamiltonian in Minkowski signature follows from the 00 component of (137):

$$\begin{aligned}
 H_G &= \int d^3x \bar{T}_{00}^g = \int d^3x \frac{1}{2}(E^2 + B^2), \\
 H_Q &= \int d^3x \left( \bar{T}_{00}^q - \frac{3}{4} m \bar{\psi} \psi \right) = \int d^3x \bar{\psi} \gamma \cdot i \overleftrightarrow{D} \psi, \\
 H_A &= \int d^3x \frac{1}{4} \left( \frac{\beta(g^2)}{4g^2} G^2 \approx -\frac{b}{32\pi^2} g^2 G^2 \right), \\
 H_m &= \int d^3x m \bar{\psi} \psi.
 \end{aligned} \tag{167}$$

We rearranged the quark mass term so that the nucleon mass budget is then

$$\begin{aligned}
 M_N &= \frac{\langle P | H_G + H_Q + H_A + H_m | P \rangle}{\langle P | P \rangle} \\
 &\equiv M_G^N + M_Q^N + M_A^N + M_m^N
 \end{aligned} \tag{168}$$

with the identification

$$M_{\text{inv}} = M_G^N + M_Q^N + M_A^N. \tag{169}$$

Using (156), we note that the forward matrix element of the gluonic  $H_G$  contribution in (167) vanishes at NLO in the QCD instanton vacuum. Hence, at the resolution of the order of the inverse instanton size, we have

$$\begin{aligned}
 \frac{M_Q^N}{M_N} &= \frac{3}{4} \left( A_q(0) - \frac{\sigma_{\pi N}}{M_N} \right) \approx 69.19\%, \\
 \frac{M_G^N}{M_N} &= \frac{3}{4} A_g(0) \approx 1.01\%, \\
 \frac{M_A^N}{M_N} &= \frac{1}{4} \left( 1 - \frac{\sigma_{\pi N}}{M_N} \right) \approx 23.40\%, \\
 \frac{M_m^N}{M_N} &= \frac{\sigma_{\pi N}}{M_N} \approx 6.39\%
 \end{aligned} \tag{170}$$

using the empirical pion-nucleon sigma term [24,25]. Equation (170) shows that, in the QCD instanton vacuum, about 69% of the nucleon mass stems from the valence quarks (hopping zero modes), 23.4% from the gluon condensate (displaced vacuum instanton field), and 1%

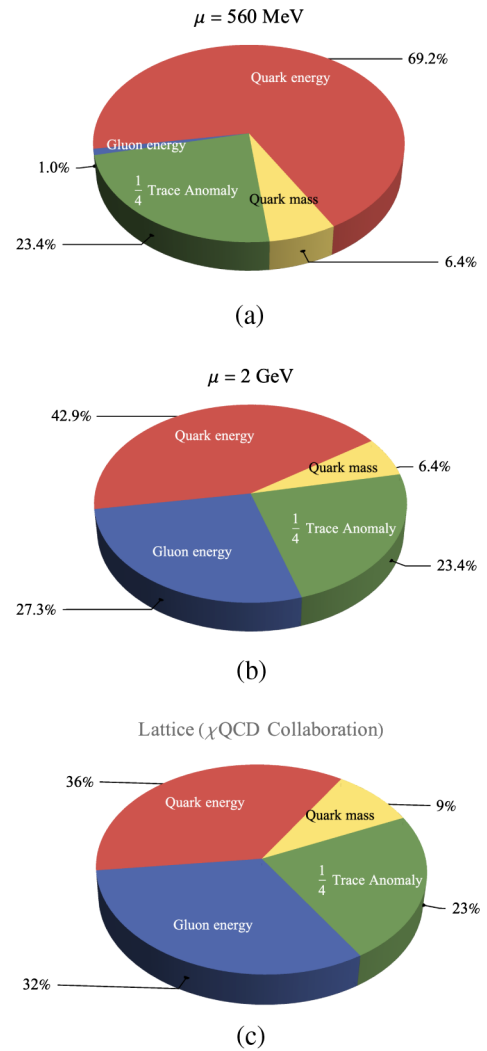


FIG. 13. Mass decomposition using Ji’s nucleon mass sum rule, in the QCD instanton vacuum at the resolution  $\mu = 560$  MeV  $\sim 1/\rho$  (a) and after DGLAP evolution at a resolution  $\mu = 2$  GeV (b). (c) Mass decomposition using Ji’s nucleon mass sum rule, at a resolution of  $\mu = 2$  GeV from the lattice collaboration [26].

from emerging valence gluons. This is illustrated in Fig. 13(a). The nucleon is composed mostly of quark constituents hopping and scooping the vacuum gluon fields. This result is consistent with the one observed in [37].

The budgeting of the nucleon mass evolves as the energy scale varies. At  $\mu = 2$  GeV, the valence quark and gluon energy contribution redistributes as illustrated in Fig. 13(b). The budgeting of the nucleon mass in (171) from the QCD instanton vacuum is consistent with the one reported on the lattice in [26] as illustrated in Fig. 13(c). Under DGLAP evolution, the gluons carry a larger energy fraction at the expense of the quarks:

$$\begin{aligned}\frac{M_Q^N}{M_N} &\approx 42.91\%, \\ \frac{M_G^N}{M_N} &\approx 27.29\%.\end{aligned}\quad (171)$$

### XIII. NUCLEON SPIN SUM RULE

The spin structure of the nucleon has been addressed both empirically and theoretically by many, and we refer to the review in [100] for an exhaustive account and references. Here, we will address it in the QCD instanton vacuum following recent estimates by one of us [37], using Ji's nucleon spin decomposition [101]:

$$S_N = \frac{1}{2}\Sigma_q + L_q + J_g, \quad (172)$$

where  $S_N = 1/2$  is the nucleon spin.

#### A. Intrinsic quark spin $\Sigma_q$

The quark intrinsic spin

$$\Sigma_q = \int d^3\vec{x} \bar{\psi} \vec{\gamma} \gamma^5 \psi \quad (173)$$

captures the isoscalar axial charge inside the nucleon, which is best described by the hadronic matrix element of the flavor-singlet axial current:

$$\langle PS | \bar{\psi} \gamma_\mu \gamma^5 \psi | PS \rangle = 2\Sigma_q S_\mu. \quad (174)$$

Here,  $S_\mu$  is the spin vector of the nucleon with the normalization  $S^2 = -M_N^2$  and  $P \cdot S = 0$ .

The quark intrinsic spin  $\Sigma_q$  is tied to the pseudoscalar gluon operator by the ABJ anomaly [102]

$$\partial_\mu \bar{\psi} \gamma_\mu \gamma^5 \psi = \frac{N_f}{16\pi^2} g^2 G_{\mu\nu}^a \tilde{G}_{\mu\nu}^a + 2m \bar{\psi} i \gamma^5 \psi. \quad (175)$$

The quark intrinsic spin consists of the anomalous gluonic contribution plus the explicit breaking of the  $U(1)$  axial symmetry by the quark current mass  $m$ :

$$\begin{aligned}\frac{\langle PS | \partial_\mu \bar{\psi} \gamma_\mu \gamma^5 \psi | PS \rangle}{2M_N s_v} &= 2M_N \Sigma_q = \frac{N_f}{16\pi^2} \frac{\langle PS | g^2 G_{\mu\nu}^a \tilde{G}_{\mu\nu}^a | PS \rangle}{2M_N s_v} \\ &+ 2m \frac{\langle PS | \bar{\psi} i \gamma^5 \psi | PS \rangle}{2M_N s_v}.\end{aligned}\quad (176)$$

Thus, the intrinsic quark spin can be decomposed into [68] (and references therein)

$$\Sigma_q = \Delta\tilde{q} - N_f \Delta g, \quad (177)$$

where

$$\frac{\langle PS | m \bar{\psi} i \gamma^5 \psi | PS \rangle}{2M_N s_v} = M_N \Delta\tilde{q} \quad (178)$$

and

$$\Delta g = -\tilde{G}_N(0). \quad (179)$$

	$\Sigma_q$
ILM (quenched, 2 GeV)	0.65
ILM (unquenched with two flavors, 2 GeV)	0.105
EMC (1987) [103–105]	0.12 ± 0.17
COMPASS ( $\sqrt{3}$ GeV) [106]	0.35 ± 0.03(stat) ± 0.05(syst)
HERMES ( $\sqrt{5}$ GeV) [107]	0.33 ± 0.011(theo) ± 0.025(exp) ± 0.028(evol)
Lattice (2 GeV, helicity quasi-PDF) [108]	0.467(58)
Lattice (2 GeV, axial form factor) [109]	0.392(26)
Lattice (2 GeV, spin decomposition) [29]	0.382(30)
Lattice [110]	0.30(6)

In the quenched and LO in the instanton density, the intrinsic spin is saturated by the ABJ anomaly contribution. This is achieved in the QCD instanton vacuum at LO in the pseudoparticle density, with the intrinsic quark spin fixed by the quenched topological susceptibility  $\chi_t^{(0)}$ :

$$\Sigma_q^{(0)} = -N_f \Delta g = N_f \frac{M_q(0) \chi_t^{(0)}}{M_N \bar{N}} = \frac{M_q(0) f_\pi^2 M_1^2}{M_N 2n_{I+\bar{I}}} \rightarrow 0.65. \quad (180)$$

The singlet squared mass follows from the Witten-Veneziano relation (39). The rightmost result uses  $M_q(0)/M_N \sim 1/3$  [68] and the Witten-Veneziano relation (39).

In the unquenched and NLO instanton density, there is mixing with the emergent constituent quarks. As a result, the intrinsic spin gets modified:

$$\begin{aligned} \Sigma_q &= N_f \frac{M_q(0) \chi_t}{M_N \bar{N}} + \left[ 1 + \frac{N_f}{N_c} \left( \frac{2\kappa}{\rho^2 m^{*2}} \right) + \frac{N_f}{2N_c(N_c^2 - 1)} \right. \\ &\quad \times \left. \left( \frac{2\kappa}{\rho^2 m^{*2}} \right)^2 3\rho^2 m^2 T_{II} \right] \Delta \tilde{q} \\ &\quad - \frac{1}{8N_c(N_c^2 - 1)} \left( \frac{2\kappa}{\rho^2 m^{*2}} \right)^2 \rho^2 m^2 T_{IA} \Sigma_q \rightarrow 0.1048 \end{aligned} \quad (181)$$

with the unquenched and large volume topological susceptibility  $\chi_t$  given in (105). The rightmost estimate follows by saturating the pseudoscalar and flavor-singlet nucleon form factor, by the  $\eta'$  exchange. In the QCD instanton vacuum, the exchange is given by

$$M_N \Delta \tilde{q} \equiv \frac{\langle PS | m \bar{\psi} i \gamma^5 \psi | PS \rangle}{2M_N s_v} = 3m \times \frac{M_q(0) g_{\eta' qq}^2 / G_{\eta'}}{M_N m_{\eta'}^2}. \quad (182)$$

The overall factor of 3 counts the three constituent quarks in the nucleon. Equation (182) yields a value of explicit chiral symmetry breaking about  $\Delta \tilde{q} = 0.0119$ . Here, we used the empirical value  $m = 0.122$  MeV in Table I and the consistent model parameters  $m_{\eta'} = 681.6$  MeV and  $g_{\eta' qq} = 1.686$  with  $G_{\eta'} = 8.417$  GeV<sup>-2</sup> in Appendix B.

Note that if we were to use a quark-diquark description of the proton or neutron as a strongly correlated quark-diquark state, with a tight scalar-isoscalar diquark  $[ud]_S$  and weaker axial-vector flavor-triplet diquark  $[ud]_A$  [6], then the proton  $SU(6)$  wave functions can be repacked in quark-diquark contributions as [111]

$$\begin{aligned} p \uparrow &= \frac{1}{\sqrt{18}} \left( 3[ud]_S u \uparrow + 2[uu]_A^+ d \downarrow - \sqrt{2}[uu]_A^0 d \uparrow \right. \\ &\quad \left. - \sqrt{2}[ud]_A^+ u \downarrow + [ud]_A^0 u \uparrow \right). \end{aligned} \quad (183)$$

This would suggest that for the proton the  $u$ -quark and  $d$ -quark spin are opposite, with a ratio

$$\left| \frac{\Sigma_d}{\Sigma_u} \right| = \frac{1}{4} \quad (184)$$

and, in particular,  $\Sigma_u = 0.0286$  and  $\Sigma_d = -0.0071$ , with  $\Sigma_q = \Sigma_u + \Sigma_d = 0.0215$ . In this  $SU(6)$  repacking, the discrepancy with (181) stems from the left out diquarks. A more realistic diquark wave function for the nucleon in the ILM will be addressed elsewhere.

At this stage, it is worth noting that, while the topological charge fluctuations in the 4-volume are screened in the QCD instanton vacuum as per our discussion, the topological charge fluctuations in small subvolumes are finite; see [71] for a definition. In the QCD instanton vacuum with light quarks, they were found to be numerically Poissonian [71]:

$$\lim_{V \rightarrow 0} \frac{\langle \Delta N^2(V) \rangle}{V} = n_{I+A} \quad (185)$$

with the unquenched singlet pseudoscalar mass  $M_1$  now given by

$$M_1^2 \rightarrow \frac{2N_f}{f^2} \lim_{V \rightarrow 0} \frac{\langle \Delta N^2(V) \rangle}{V} = \frac{2N_f}{f^2} n_{I+A}, \quad (186)$$

which is finite even in the chiral limit and in agreement with the result in [70,112]. This is supported by the fact that the  $\eta'$  mass is large in nature, which is unquenched QCD. Since the world volume of a hadron in the QCD instanton vacuum can be considered as a vanishingly small subvolume, it is plausible to use (186) in our analysis of the intrinsic spin. This leads to the result that the quenched and unquenched results for the intrinsic spin are mostly unchanged.

	$J_q$	$J_g$
ILM (this work, 2 GeV)	0.318	0.182
Lattice (ETMC) [29]	0.285(45)	0.187(46)
Lattice ( $\chi$ QCD) [28]	0.265(32)	0.230(25)

## B. Quark and gluon orbital momenta

The quark orbital angular momentum (OAM) is given by

$$L_q = \int d^3 \vec{x} \bar{\psi} \gamma^0 \vec{x} \times i \vec{D} \psi. \quad (187)$$

Combined with the intrinsic quark spin (173), we have the quark total angular momentum

$$J_q = \frac{1}{2}\Sigma_q + L_q. \quad (188)$$

The quark total angular momentum  $J_q$  is calculated by the forward hadronic matrix element of the traceless part of the quark  $0j$  EMT:

$$\begin{aligned} J_q &= \frac{\langle PS | \int d^3\vec{x} \epsilon^{3ij} x^i \bar{T}_q^{0j} | PS \rangle}{\langle PS | PS \rangle} \\ &= e^{3ij} i \partial_q^j \frac{\langle P' S | \bar{T}_q^{0j} | PS \rangle}{\langle PS | PS \rangle}, \end{aligned} \quad (189)$$

where  $\partial_q^j$  refers to the derivative with respect to the momentum transfer, followed by the zero momentum transfer limit. Similarly, the angular momentum carried by the gluons is

$$J_g = \int d^3\vec{x} \vec{x} \times (\vec{E}^a \times \vec{B}^a), \quad (190)$$

which translates to the forward hadronic matrix element:

$$\begin{aligned} J_g &= \frac{\langle PS | \int d^3\vec{x} \epsilon^{3ij} x^i \bar{T}_g^{0j} | PS \rangle}{\langle PS | PS \rangle} \\ &= e^{3ij} i \partial_q^j \frac{\langle P' S | \bar{T}_g^{0j} | PS \rangle}{\langle PS | PS \rangle}. \end{aligned} \quad (191)$$

Using (156), it follows that (191) is penalized by the instanton density in the forward limit, at NLO in the instanton density expansion. Hence, at the resolution of the order of the inverse instanton size, Ji's spin sum rule is given by

$$\begin{aligned} \frac{\frac{1}{2}\Sigma_q}{S_N} &= \Delta\tilde{q} - \frac{g^2}{8\pi^2} N_f \Delta g \approx 65\%, \\ \frac{L_q}{S_N} &= A_q(0) + B_q(0) - \frac{\frac{1}{2}\Sigma_q}{S_N} \approx 33.7\%, \\ \frac{J_g}{S_N} &= A_g(0) + B_g(0) \approx 1.3\%. \end{aligned} \quad (192)$$

In the case of the unquenched QCD in the instanton vacuum with two flavors, we have the topological susceptibility screened:

$$\begin{aligned} \frac{\frac{1}{2}\Sigma_q}{S_N} &= \Delta\tilde{q} - \frac{g^2}{8\pi^2} N_f \Delta g \approx 10.5\%, \\ \frac{L_q}{S_N} &= A_q(0) + B_q(0) - \frac{\frac{1}{2}\Sigma_q}{S_N} \approx 88.2\%, \\ \frac{J_g}{S_N} &= A_g(0) + B_g(0) \approx 1.4\% \end{aligned} \quad (193)$$

at the low resolution of  $1/\rho \approx 560$  MeV. Here, we assumed  $B_q(0) = 0$  [27]; hence,  $B_g(0) = 0$  from (157).

Equation (192) shows that, in the QCD instanton vacuum, about 65% of the nucleon spin stems from the spin of the valence quarks as they hop and mix with the vacuum topological charge fluctuations, 34% stems from their OAM, and only 1% stems from the emerging valence gluons as the topological charge fluctuates in small subvolumes.

The budgeting of the nucleon spin evolves as the energy scale varies. For the quenched QCD instanton vacuum at  $\mu = 2$  GeV, the valence quark OAM and gluon angular momentum redistributes as

$$\begin{aligned} \frac{\frac{1}{2}\Sigma_q}{S_N} &\approx 65\%, \\ \frac{L_q}{S_N} &\approx -1.4\%, \\ \frac{J_g}{S_N} &\approx 36.4\%. \end{aligned} \quad (194)$$

For the QCD instanton vacuum with two flavors, we have

$$\begin{aligned} \frac{\frac{1}{2}\Sigma_q}{S_N} &\approx 10.5\%, \\ \frac{L_q}{S_N} &\approx 53.1\%, \\ \frac{J_g}{S_N} &\approx 36.4\%. \end{aligned} \quad (195)$$

In the QCD instanton vacuum, the intrinsic spin does not renormalize, as it captures the vacuum topological susceptibility scooped by the nucleon, in the small volume limit. As a result, DGLAP evolution enhances the gluon contribution at the sole expense of the quark orbital contribution, both of which are not topological in our analysis.

The results for Ji's spin decomposition in the QCD instanton vacuum are illustrated in Figs. 14(a) (quenched) and 14(b) (unquenched) at  $\mu = 0.64$  GeV (left) and at  $\mu = 2$  GeV after DGLAP evolution (right). They are compared to the reported results from the  $\chi$ -QCD Collaboration [28] in Fig. 14(c) (left) and from the ETMC Collaboration [29] in Fig. 14(b) (right).

While the gluonic contributions are comparable to the one reported by both lattice collaborations, there is a

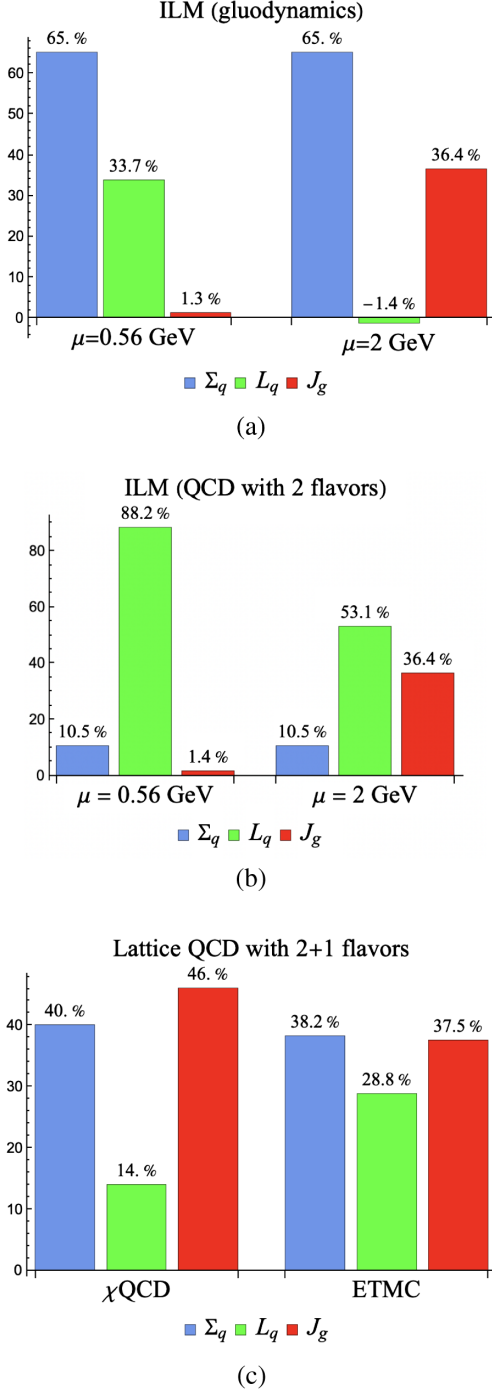


FIG. 14. (a) Spin decomposition using Ji's sum rule, in the quenched QCD instanton vacuum at  $\mu = 0.56$  GeV (left) and  $\mu = 2$  GeV (right). (b) Spin decomposition using Ji's sum rule, in the  $N_f = 2$  QCD instanton vacuum at  $\mu = 0.56$  GeV (left) and  $\mu = 2$  GeV (right). (c) Spin decomposition using Ji's sum rule at a resolution of  $\mu = 2$  GeV, from the Lattice Collaboration  $\chi$ QCD [28] (left) and the ETMC [29] (right).

difference in the way the quarks are carrying the spin. In the lattice, the intrinsic spin to OAM ratio is about 3 : 1 ( $\chi$ QCD) and 2 : 1 (ETMC), which is to be compared to 1 : 1 in the QCD instanton vacuum with two flavors. The origin is the

substantial depletion of the intrinsic spin at low resolution, owing to the strong screening of the large volume topological susceptibility. Although we suggested earlier that the small volume topological susceptibility remains large and may cause the intrinsic spin to be larger even in the unquenched case, our analysis shows that it would lead to a considerably large ratio for the intrinsic spin to OAM as illustrated in Fig. 14(a) (left). This shows the importance of studying and reporting on both the large and small volume topological susceptibilities, when reporting the results for the spin composition of hadrons, using QCD lattice simulations.

#### XIV. CONCLUSION

The QCD instanton vacuum is well supported by current lattice QCD simulations. When the zero-point gauge fluctuations are removed numerically by cooling using the gradient flow method [113,114], the QCD vacuum is found to be populated by topological lumps of gauge fields. These lumps are tunneling gauge configurations describing instanton and anti-instanton pseudoparticles or failed tunneling gauge molecules made of instanton-anti-instanton pairs.

Deep in the cooling procedure, the corresponding gauge fields are strong and localized, with a mean size of  $\rho = \frac{1}{3}$  fm and a mean density  $n_{I+A} = 1$  fm<sup>-4</sup>. Confinement is likely caused by center vortices through percolating long  $Z_{N_c}$  strings of about 4 fm<sup>-2</sup>, with topologically active branch points, the likely anchors of the pseudoparticles.

Hadrons in the QCD vacuum are small ripples propagating in the QCD vacuum. At the resolution of  $\rho = \frac{1}{3}$  fm, the composition and properties of the low-lying hadrons can be fairly approximated in the QCD instanton vacuum, where their bound state structure and small sizes make them less prone to disordering by the long center vortices. This is less so for their excited states, which are larger in size and more prone to flux piercing and the string tension. Throughout, we have assumed that this is the case and pursued all the analyses of the gluons in hadrons solely in the context of the QCD instanton vacuum.

At medium resolution and in LO in the instanton density, the pseudoparticle strong gauge fields dominate the gluonic content of the forward matrix elements. The scalar and pseudoscalar gluon matrix elements receive contributions from their number fluctuations at LO and from pairs of pseudoparticles at NLO. We have shown that the off-forward gluonic scalar and pseudoscalar matrix elements are readily expressed in terms of the pseudoparticle moduli, essentially the fermionic zero modes in the form of multi-flavor effective vertices after averaging over the core moduli. The same carries to higher-dimensional gluonic operators, as we have shown for the  $C$ -even and  $C$ -odd dimension-6 gluon operators. The latter map on leading

twist contributions in diffractive  $C$ -even and  $C$ -odd vector meson production.

The self-dual character of the pseudoparticles shows that only pairs of pseudoparticles or molecules can contribute at NLO to the traceless part of the QCD energy-momentum tensor. The trace part is anomalous and receives contributions in LO from the pseudoparticles. We have shown how they contribute to the gluonic form factors in hadrons, in the form of effective fermionic operators, once the modular integration is carried out. The results allow for a detailed budgeting of the quark and gluon contributions to the nucleon mass and spin, at low resolution. Their evolution at higher resolution is in good agreement with the current lattice simulations. The comparison would be enhanced if the lattice collaboration [28,29] could also report their large and small volume topological susceptibilities, along with their nucleon spin results.

### ACKNOWLEDGMENTS

We thank Christian Weiss for discussions. This work is supported by the Office of Science, U.S. Department of Energy under Contract No. DE-FG-88ER40388, and in part within the framework of the Quark-Gluon Tomography

(QGT) Topical Collaboration, under Contract No. DE-SC0023646.

### APPENDIX A: EMERGENT EFFECTIVE 'T HOOFT INTERACTIONS WITH GLUONS IN SIA

The effective Lagrangian following from (50) after averaging over the instanton moduli with fermionic zero modes in the SIA yield emergent multiflavor interactions with gluon insertions. The latter follow by LSZ reduction of the instanton profile. To characterize these interactions, we use the bookkeeping in  $1/N_c$ .

For a single instanton with  $N_f$  quarks and  $N_g$  gluons, the vertices in (45) give rise to an effective 't Hooft interaction coupling

$$G_{f+g} \sim \frac{n_{I+A}}{2} \frac{1}{N_c^{N_f+N_g}} \left( \frac{4\pi^2 \rho^2}{m^*} \right)^{N_f} \left( \frac{2\pi^2 \rho^2}{g} \right)^{N_g}$$

characteristic of a vacuum contribution. Note that each gluon insertion from the instanton tail is further suppressed by the instanton size. In the SIA, the effective interactions are given by

$$\mathcal{L}_{\text{eff}} = \bar{\psi}(i\partial - m)\psi - \frac{1}{4}(G_{\mu\nu}^a)^2 + \frac{n_{I+A}}{2} \frac{4\pi^2 \rho^2}{m^*} \mathcal{V}_{N_f=1} + \frac{n_{I+A}}{2} \left( \frac{4\pi^2 \rho^2}{m^*} \right)^2 \mathcal{V}_{N_f=2} + \mathcal{O}\left( \frac{n_{I+A}}{2} \left( \frac{4\pi^2 \rho^2}{m^*} \right)^3 \right), \quad (\text{A1})$$

where the one-body interaction is defined as

$$\begin{aligned} \mathcal{V}_{N_f=1} = & -\frac{1}{N_c} \bar{\psi}\psi + \frac{1}{N_c^2 - 1} \left( \frac{2\pi^2 \rho^2}{g} \right) \bar{\psi} \sigma_{\mu\nu} \frac{\lambda^a}{2} \psi G_{\mu\nu}^a - \frac{1}{N_c(N_c^2 - 1)} \left( \frac{2\pi^2 \rho^2}{g} \right)^2 f^{abc} \bar{\psi} \sigma_{\mu\nu} \lambda^a \psi G_{\mu\rho}^b G_{\nu\rho}^c \\ & - \frac{1}{N_c(N_c^2 - 1)} \left( \frac{2\pi^2 \rho^2}{g} \right)^2 \left( \delta^{bc} \bar{\psi}\psi + \frac{N_c}{2(N_c + 2)} d^{abc} \bar{\psi} \lambda^a \psi \right) G_{\mu\nu}^b G_{\mu\nu}^c \\ & - \frac{1}{N_c(N_c^2 - 1)} \left( \frac{2\pi^2 \rho^2}{g} \right)^2 \left( \delta^{bc} \bar{\psi} \gamma^5 \psi + \frac{N_c}{2(N_c + 2)} d^{abc} \bar{\psi} \lambda^a \gamma^5 \psi \right) G_{\mu\nu}^b \tilde{G}_{\mu\nu}^c \\ & + \frac{1}{6(N_c^2 - 1)} \left( \frac{2\pi^2 \rho^2}{g} \right)^3 \left( \frac{8}{N_c^2} f^{abc} \bar{\psi}\psi + \frac{12}{N_c^2 - 4} d^{dae} f^{bce} \bar{\psi} \lambda^d \psi \right) G_{\mu\nu}^a G_{\nu\rho}^b G_{\rho\mu}^c \\ & + \frac{1}{6(N_c^2 - 1)} \left( \frac{2\pi^2 \rho^2}{g} \right)^3 \left( \frac{8}{N_c^2} f^{abc} \bar{\psi} \gamma^5 \psi + \frac{12}{N_c^2 - 4} d^{dae} f^{bce} \bar{\psi} \lambda^d \gamma^5 \psi \right) \tilde{G}_{\mu\nu}^a G_{\nu\rho}^b G_{\rho\mu}^c \\ & + \frac{1}{6(N_c^2 - 1)} \left( \frac{2\pi^2 \rho^2}{g} \right)^3 \left( \frac{3}{(N_c^2 - 1)} \delta^{ab} \delta^{cd} + \frac{3N_c}{(N_c - 4)(N_c + 2)} d^{abe} d^{cde} + \frac{6}{N_c^2} f^{ace} f^{bde} \right) \bar{\psi} \sigma_{\mu\nu} \lambda^a \psi G_{\mu\nu}^b G_{\rho\lambda}^c G_{\rho\lambda}^d \\ & + \frac{1}{6(N_c^2 - 1)} \left( \frac{2\pi^2 \rho^2}{g} \right)^3 \left( \frac{3}{(N_c^2 - 1)} \delta^{ab} \delta^{cd} + \frac{3N_c}{(N_c - 4)(N_c + 2)} d^{abe} d^{cde} + \frac{6}{N_c^2} f^{ace} f^{bde} \right) \bar{\psi} \sigma_{\mu\nu} \lambda^a \gamma^5 \psi G_{\mu\nu}^b \tilde{G}_{\rho\lambda}^c G_{\rho\lambda}^d \\ & + \mathcal{O}\left( \left( \frac{2\pi^2 \rho^2}{g} \right)^4 \right) \end{aligned} \quad (\text{A2})$$

and the two-body interaction is defined as

$$\begin{aligned}
\mathcal{V}_{N_f=2} = & \frac{2N_c - 1}{16N_c(N_c^2 - 1)} [(\bar{\psi}\psi)^2 - (\bar{\psi}\tau^a\psi)^2 - (\bar{\psi}i\gamma^5\psi)^2 + (\bar{\psi}i\gamma^5\tau^a\psi)^2] + \frac{1}{32N_c(N_c^2 - 1)} [(\bar{\psi}\sigma_{\mu\nu}\psi)^2 - (\bar{\psi}\sigma_{\mu\nu}\tau^a\psi)^2] \\
& - \frac{1}{N_c(N_c^2 - 1)} \left( \frac{2\pi^2\rho^2}{g} \right) \left[ \bar{u}_R u_L \bar{d}_R \sigma_{\mu\nu} \frac{\lambda^a}{2} d_L + \bar{u}_R \sigma_{\mu\nu} \frac{\lambda^a}{2} u_L \bar{d}_R d_L \right] G_{\mu\nu}^a \\
& - \frac{1}{(N_c + 2)(N_c^2 - 1)} \left( \frac{2\pi^2\rho^2}{g} \right) d^{abc} \left[ \bar{u}_R \frac{\lambda^a}{2} u_L \bar{d}_R \sigma_{\mu\nu} \frac{\lambda^b}{2} d_L + \bar{u}_R \sigma_{\mu\nu} \frac{\lambda^a}{2} u_L \bar{d}_R \frac{\lambda^b}{2} d_L \right] G_{\mu\nu}^c \\
& - \frac{1}{(2N_c)(N_c^2 - 1)} \left( \frac{2\pi^2\rho^2}{g} \right) f^{abc} \left[ \bar{u}_R \sigma_{\mu\rho} \frac{\lambda^a}{2} u_L \bar{d}_R \sigma_{\nu\rho} \frac{\lambda^b}{2} d_L + \bar{u}_R \sigma_{\mu\rho} \frac{\lambda^a}{2} u_L \bar{d}_R \sigma_{\nu\rho} \frac{\lambda^b}{2} d_L \right] (G_{\mu\nu}^c - \tilde{G}_{\mu\nu}^c) \\
& + \mathcal{O}\left(\left(\frac{2\pi^2\rho^2}{g}\right)^2\right). \tag{A3}
\end{aligned}$$

The emergent couplings with constitutive quarks and gluons follow by color averaging, after pertinent fermionic lines closing in the SIA. More specifically, in the color average, each of the  $UU^\dagger$  pair gives a  $1/N_c$  factor in the large  $N_c$  limit. Therefore, the power counting of each vertex  $1/N_c^{N_f+N_g}$  is given by the flavor number  $N_f$  and the gluon number  $N_g$ . That is, the more quarks and gluons involved in the instanton, the more  $1/N_c$  suppression. Here, we show the one-body interaction with one to three gluons involved and the two-body interaction with one gluon involved. Higher-order interactions follow the same reasoning but are more involved. Using 14(c) in the mean-field approximation yields the SIA determinantal mass

$$m_f^* = m_f + \frac{n_{I+A}}{2} \frac{4\pi^2\rho^2}{m_f^*} \langle \mathcal{V}_{N_f=1} \rangle. \tag{A4}$$

## APPENDIX B: $\sigma$ AND $\eta'$ IN HADRONIC MATRIX ELEMENTS

In this Appendix, we will estimate the meson-quark effective couplings in the  $\sigma$  and  $\eta'$  channels for the hadronic matrix elements of  $\bar{\psi}\psi$  and  $\bar{\psi}i\gamma^5\psi$ , appearing in the gravitational form factors.

The quark part of the effective Lagrangian in the instanton vacuum in (50) determines the meson mass spectrum and meson-quark effective coupling in the QCD instanton vacuum. For that, we need to go beyond the SIA, by resumming the contributions to the quark propagator that includes both the close and far pseudoparticles.

The corresponding effective Lagrangian with induced vertices from unpaired ( $I$ ,  $A$ ) and paired ( $IA$ ) pseudoparticles is given by [60]

$$\begin{aligned}
\mathcal{L}_{\text{tHooft}} = & \bar{\psi}(i\not{\partial} - M)\psi + \frac{G_\sigma}{2} (\bar{\psi}\psi)^2 + \frac{G_{a_0}}{2} (\bar{\psi}\tau^a\psi)^2 + \frac{G_{\eta'}}{2} (\bar{\psi}i\gamma^5\psi)^2 + \frac{G_\pi}{2} (\bar{\psi}i\gamma^5\tau^a\psi)^2 \\
& - \frac{G_\omega}{2} (\bar{\psi}\gamma_\mu\psi)^2 - \frac{G_\rho}{2} (\bar{\psi}\gamma_\mu\tau^a\psi)^2 - \frac{G_{f_1}}{2} (\bar{\psi}\gamma_\mu\gamma^5\psi)^2 - \frac{G_{a_1}}{2} (\bar{\psi}\gamma_\mu\gamma^5\tau^a\psi)^2. \tag{B1}
\end{aligned}$$

As we noted earlier, it is the constituent mass  $M \equiv M_q(0) = 395.17$  MeV in (43), as opposed to the determinantal mass  $m^*$ , that enters the analysis of the long-range hadronic correlations. The induced 't Hooft couplings are

$$\begin{aligned}
G_\sigma = \frac{G_I}{4N_c^2} + \frac{4G_{IA}}{N_c^2}, & \quad G_{a_0} = -\frac{G_I}{4N_c^2} + \frac{4G_{IA}}{N_c^2}, & \quad G_\pi = \frac{G_I}{4N_c^2} + \frac{4G_{IA}}{N_c^2}, & \quad G_{\eta'} = -\frac{G_I}{4N_c^2} + \frac{4G_{IA}}{N_c^2}, \\
G_\omega = \frac{G_{IA}}{N_c^2}, & \quad G_\rho = \frac{G_{IA}}{N_c^2}, & \quad G_{a_1} = \frac{G_{IA}}{N_c^2}, & \quad G_{f_1} = -3\frac{G_{IA}}{N_c^2}.
\end{aligned}$$

The coupling constant of each channel is fixed by two parameters  $G_I$  and  $G_{IA}$ , directly determined from the QCD instanton vacuum with  $\rho = 0.31$  fm and  $n_{I+A} = 1$  fm $^{-4}$ . For two flavors, the values are given by

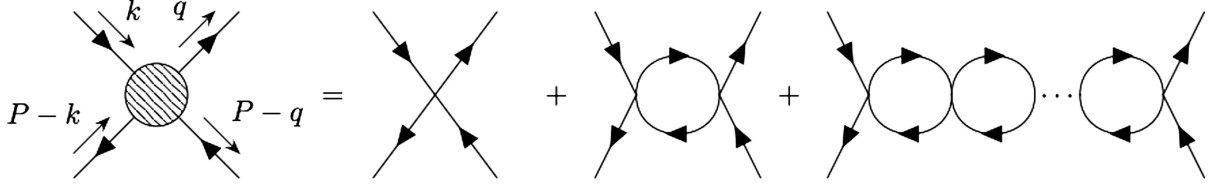


FIG. 15.  $\sigma, \eta'$  Bethe-Salpeter kernels in the QCD instanton vacuum, in leading order in the  $1/N_c$  book-keeping approximation.

$$G_I = \frac{n_{I+A}}{2} \left( \frac{4\pi^2 \rho^2}{m^*} \right)^2 = 610.3 \text{ GeV}^{-2}, \quad m_\sigma = 683.1 \text{ MeV}. \quad (\text{B5})$$

$$G_{IA} = \frac{G_I^2}{8} \left\langle \left( \frac{T_{IA}}{4\pi^2 \rho^2} \right)^2 \right\rangle = 57.08 \text{ GeV}^{-2}.$$

Since  $n_{I+A}$  is of the order of  $N_c$ , both  $G_I$  and  $G_{IA}$  are of the same order in the  $1/N_c$  bookkeeping. The quark hopping integral  $T_{IA} = \int d^4x \phi_I^\dagger(x - z_I) i \not{\partial} \phi_A(x - z_A)$  in the IA molecule is defined by the overlap between the quark zero modes in (41).

With this in mind, the bubble chain in Fig. 15 with the scalar 't Hooft interaction in (B1) yields the gaplike equation for the  $\sigma$  meson mass

$$1 = G_\sigma \Pi_{SS}(m_\sigma^2), \quad (\text{B2})$$

where the scalar to scalar vacuum polarization function is defined as

$$\Pi_{SS}(P^2) = -2iN_c \times \int \frac{d^4k}{(2\pi)^4} \text{tr}[S_{\text{ILM}}(k) S_{\text{ILM}}(k-P)] \mathcal{F}(k) \mathcal{F}(P-k). \quad (\text{B3})$$

The effective Euclidean quark propagator in the QCD instanton vacuum involves the running quark mass (not the determinantal mass) [59,60]

$$S_{\text{ILM}}(k) = \frac{i \not{k} + M_q(k)}{k^2 + M_q(k)^2}. \quad (\text{B4})$$

With (B2), the sigma mass is obtained:

The sigma meson-quark effective coupling can also be determined by

$$g_{\sigma qq}^2 = \left( \frac{\partial \Pi_{SS}(P^2)}{\partial P^2} \right)^{-1} \Big|_{P^2=m_\sigma^2} \rightarrow 3.841. \quad (\text{B6})$$

In the pseudoscalar-flavor-singlet channel, the chiral Ward identity is violated, and the pseudoscalar and axial vector mix. The  $\eta'$  mass follows from the resummation in Fig. 15, in leading order in the  $1/N_c$  bookkeeping. Using the emerging 't Hooft interaction in the pseudoscalar and axial vector channels, the mass of the two-flavor meson follows from the gaplike equation with  $\eta'$ - $f_1$  mixing:

$$1 = G_{\eta'} \Pi_{PP}(m_{\eta'}^2) + G_{f_1} \Pi_{AA}^{(l)}(m_{\eta'}^2) - G_{\eta', \pi} G_{f_1} \Pi_{PA}(m_{\eta'}^2) \Pi_{AP}(m_{\eta', \pi}^2). \quad (\text{B7})$$

The corresponding  $\eta'$  mass is

$$m_{\eta'} = 681.7 \text{ MeV}, \quad (\text{B8})$$

which is comparable to the scalar mass (B5). This is to be compared to the two-flavor  $m_{\eta'} = 772 \text{ MeV}$  reported on the lattice [115]. The interactions in (B1) are mostly repulsive in the scalar and  $\eta'$  channels and attractive in the pion and  $a_0$  channels, hence the heavy  $\eta'$ .

The meson-quark effective coupling in the pseudoscalar channel is adjusted by the mixing from the axial vectors:

$$g_{\eta' qq}^2 = \frac{G_{\eta'} - G_{f_1} + G_{\eta'} G_{f_1} (\Pi_{PP} - \Pi_{AA}^{(l)})}{G_{\eta'} (1 - G_{f_1} \Pi_{AA}^{(l)}) \frac{\partial \Pi_{PP}}{\partial P^2} + G_{f_1} (1 - G_{\eta'} \Pi_{PP}) \frac{\partial \Pi_{AA}^{(l)}}{\partial P^2} - 2G_{\eta'} G_{f_1} \Pi_{PA} \frac{\partial \Pi_{PA}}{\partial P^2}} \Big|_{P^2=m_{\eta'}^2} \rightarrow 1.686. \quad (\text{B9})$$

The vacuum polarization functions regarding the mixing are defined as

$$\Pi_{PP}(P^2) = -2iN_c \int \frac{d^4k}{(2\pi)^4} \text{tr}[S_{\text{ILM}}(k) i\gamma^5 S_{\text{ILM}}(k-P) i\gamma^5] \mathcal{F}(k) \mathcal{F}(P-k), \quad (\text{B10})$$

$$\Pi_{PA}^\mu(P^2) = -2iN_c \int \frac{d^4k}{(2\pi)^4} \text{tr}[S_{\text{ILM}}(k)i\gamma^5 S_{\text{ILM}}(k-P)\gamma^\mu\gamma^5]\mathcal{F}(k)\mathcal{F}(P-k) = i\Pi_{PA}(P^2) \frac{P^\mu}{\sqrt{P^2}} \quad (\text{B11})$$

with  $\Pi_{AP}^\mu = (\Pi_{PA}^\mu)^*$  its complex conjugate and

$$\begin{aligned} \Pi_{AA}^{\mu\nu}(P^2) &= -2iN_c \int \frac{d^4k}{(2\pi)^4} \text{tr}[S_{\text{ILM}}(k)\gamma^\mu\gamma^5 S_{\text{ILM}}(k-P)\gamma^\nu\gamma^5]\mathcal{F}(k)\mathcal{F}(P-k) \\ &= -\Pi_{AA}^{(i)}(P^2) \left( g^{\mu\nu} - \frac{P^\mu P^\nu}{P^2} \right) - \Pi_{AA}^{(l)}(P^2) \frac{P^\mu P^\nu}{P^2}. \end{aligned} \quad (\text{B12})$$

### APPENDIX C: INSTANTON FIELD IN SINGULAR GAUGE

In singular gauge, the instanton gauge field  $A_\mu^a(x)$  is given by

$$A_\mu^a(x - z_I, \rho, U_I) = R^{ab}(U_I)A_\mu^b(x - z_I), \quad (\text{C1})$$

The gauge profile is defined in (57), and  $R^{ab}(U_I) = \frac{1}{2}\text{Tr}(\tau^a U_I \tau^b U_I^\dagger)$ , where  $\tau^a$  is an  $N_c \times N_c$  matrices with the  $2 \times 2$  Pauli matrices embedded in the upper left corner. For the anti-instanton field, we substitute  $\bar{\eta}_{\mu\nu}^a$  by  $\eta_{\mu\nu}^a$  and flip the sign in front of the Levi-Cevita tensor,  $\epsilon_{\mu\nu\rho\lambda} \rightarrow -\epsilon_{\mu\nu\rho\lambda}$ . The instanton moduli is captured by the rigid color rotation, instanton location, and size.

The field strength associated to (C1) reads

$$G_{\mu\nu}^a[A_I] = R^{ab}(U_I)G_{\mu\nu}^b(x - z_I) \quad (\text{C2})$$

with the corresponding field strength profile

$$\begin{aligned} G_{\mu\nu}^a(x) &= \frac{1}{g} \frac{8\rho^2}{x^2(x^2 + \rho^2)^2} \left[ \bar{\eta}_{\mu\rho}^a \left( \frac{x_\rho x_\nu}{x^2} - \frac{1}{4} \delta_{\rho\nu} \right) \right. \\ &\quad \left. - \bar{\eta}_{\nu\rho}^a \left( \frac{x_\rho x_\mu}{x^2} - \frac{1}{4} \delta_{\rho\mu} \right) \right]. \end{aligned} \quad (\text{C3})$$

In the sum ansatz, the gluonic field strength for the multi-instanton configuration can be split into single-instanton fields and crossing terms typical of non-Abelian fields:

$$G_{\mu\nu}^a[A_{\text{inst}}] = \sum_I G_{\mu\nu}^a[A_I] + \sum_{I \neq J} G_{\mu\nu}^a[A_I, A_J]. \quad (\text{C4})$$

The non-Abelian gauge crossing term between two instantons can be expressed as

$$\begin{aligned} G_{\mu\nu}^a[A_I, A_J] &= gR^{a'd'}(U_I)\epsilon^{a'bc}R^{cd}(U_I^\dagger U_J) \\ &\quad \times [A_\mu^b(x - z_I)A_\nu^d(x - z_J) \\ &\quad - A_\nu^b(x - z_I)A_\mu^d(x - z_J)]. \end{aligned} \quad (\text{C5})$$

The 't Hooft symbol in Euclidean space is defined as

$$\bar{\eta}_{\mu\nu}^a = \frac{1}{4i} \text{Tr}[\tau^a (\tau_\mu^- \tau_\nu^+ - \tau_\nu^- \tau_\mu^+)], \quad (\text{C6})$$

$$\eta_{\mu\nu}^a = \frac{1}{4i} \text{Tr}[\tau^a (\tau_\mu^+ \tau_\nu^- - \tau_\nu^+ \tau_\mu^-)], \quad (\text{C7})$$

where the Pauli four-vector is defined as  $\tau_\mu^\pm = (\vec{\tau}, \mp i)$ . The conversion to Minkowski space is follows by adding extra  $i$ 's to each fourth component of the Lorentz indices. Thus, the 't Hooft symbol in Minkowski space is defined as [54]

$$\eta_{\mu\nu}^a = \begin{cases} \epsilon^{a\mu\nu}, & \mu \neq 0, \nu \neq 0, \\ i\delta_\mu^a, & \mu \neq 0, \nu = 0, \\ -i\delta_\nu^a, & \mu = 0, \nu \neq 0 \end{cases} \quad (\text{C8})$$

and its conjugate

$$\bar{\eta}_{\mu\nu}^a = \begin{cases} \epsilon^{a\mu\nu}, & \mu \neq 0, \nu \neq 0, \\ -i\delta_\mu^a, & \mu \neq 0, \nu = 0, \\ i\delta_\nu^a, & \mu = 0, \nu \neq 0. \end{cases} \quad (\text{C9})$$

### APPENDIX D: TWO-INSTANTON CONFIGURATIONS ON THE GLUONIC OPERATORS

The gluonic operators for the multi-instanton configuration can be constructed using the gluonic field strength following from the sum ansatz. Throughout, we will limit the discussion to instanton pairs. The consideration of higher clusters goes beyond the scope of this work.

#### 1. Two-gluon operators

In the case of the two-gluon operators, we have three typical instanton pair configurations:

$$\begin{aligned} G_{\mu\alpha}^a[A_J]G_{\nu\alpha}^a[A_K] &= \frac{1}{2} \text{tr}(\tau^a U_{JK} \tau^b U_{JK}^\dagger) G_{\mu\alpha}^a(x - z_J) \\ &\quad \times G_{\nu\alpha}^b(x - z_K), \end{aligned} \quad (\text{D1})$$

$$G_{\mu\alpha}^a[A_J]G_{\nu\alpha}^a[A_J, A_K] = \frac{1}{2} \text{tr}(\tau^a U_{JK} \tau^b U_{JK}^\dagger) \epsilon^{abcd} G_{\mu\alpha}^c(x-z_J) [A_\nu^d(x-z_J) A_\alpha^b(x-z_K) - A_\alpha^d(x-z_J) A_\nu^b(x-z_K)], \quad (\text{D2})$$

$$G_{\mu\alpha}^a[A_J, A_K]G_{\nu\alpha}^a[A_J, A_K] = \frac{1}{2} \text{tr}(\tau^a U_{JK} \tau^b U_{JK}^\dagger) \frac{1}{2} \text{tr}(\tau^c U_{JK} \tau^d U_{JK}^\dagger) [A_\mu^a(x-z_J) A_\alpha^b(x-z_K) - A_\alpha^a(x-z_J) A_\mu^b(x-z_K)] \\ \times [A_\nu^c(x-z_J) A_\alpha^d(x-z_K) - A_\alpha^c(x-z_J) A_\nu^d(x-z_K)]. \quad (\text{D3})$$

## 2. C-odd three-gluon operators

In the case of the  $C$ -odd three-gluon operators, we have two typical instanton pair configurations:

$$d^{abc} G_{\mu\nu}^a[A_J] G_{\rho\alpha}^b[A_J] G_{\lambda\alpha}^c[A_K] = \frac{1}{2} \text{tr}(\mathbb{1}_2 U_{JK} \tau^a U_{JK}^\dagger) G_{\mu\nu}^b(x-z_J) G_{\rho\alpha}^b(x-z_J) G_{\lambda\alpha}^a(x-z_K), \quad (\text{D4})$$

$$d^{abc} G_{\mu\nu}^a[A_J] G_{\rho\alpha}^b[A_J, A_K] G_{\lambda\alpha}^c[A_K] = \frac{1}{2} \text{tr}(\mathbb{1}_2 U_{JK} \tau^a U_{JK}^\dagger) \frac{1}{2} \text{tr}(\tau^b U_{JK} \tau^c U_{JK}^\dagger) \epsilon^{ade} G_{\mu\nu}^d(x-z_J) [A_\rho^e(x-z_J) A_\alpha^b(x-z_K) \\ - A_\alpha^e(x-z_J) A_\rho^b(x-z_K)] G_{\lambda\alpha}^c(x-z_K). \quad (\text{D5})$$

## 3. C-even three-gluon operators

In the case of the  $C$ -even three-gluon operators, we have two typical instanton pair configurations:

$$f^{abc} G_{\mu\nu}^a[A_J] G_{\nu\lambda}^b[A_J] G_{\lambda\mu}^c[A_K] = \frac{1}{2} \text{tr}(\tau^a U_{JK} \tau^b U_{JK}^\dagger) \epsilon^{acd} G_{\mu\nu}^c(x-z_J) G_{\nu\lambda}^d(x-z_J) G_{\lambda\mu}^b(x-z_K), \quad (\text{D6})$$

$$f^{abc} G_{\mu\nu}^a[A_J] G_{\nu\lambda}^b[A_J, A_K] G_{\lambda\mu}^c[A_K] = \frac{1}{2} \text{tr}(\tau^a U_{JK} \tau^b U_{JK}^\dagger) \frac{1}{2} \text{tr}(\tau^c U_{JK} \tau^d U_{JK}^\dagger) \{ [G_{\mu\nu}^a(x-z_J) A_\nu^c(x-z_J) \\ - \delta^{ac} G_{\mu\nu}^e(x-z_J) A_\nu^e(x-z_J)] A_\lambda^b(x-z_K) G_{\lambda\mu}^d(x-z_K) \\ - [G_{\mu\nu}^a(x-z_J) A_\lambda^c(x-z_J) - \delta^{ac} G_{\mu\nu}^e(x-z_J) A_\lambda^e(x-z_J)] A_\nu^b(x-z_K) G_{\lambda\mu}^d(x-z_K) \}. \quad (\text{D7})$$

We now detail the steps in the calculation of the gluonic operators in the instanton ensemble to include correlations between instantons.

## 4. Color averages

In the case of a two-instanton configuration  $J, K$ , the color structure of the gluonic operators depends on only the relative color rotation  $U_{JK} = U_J^\dagger U_K$ . Only a few color structures are involved in the calculation of the color averages, which we now list.

$$\mathbf{a.} \quad \frac{1}{2} \text{tr}(\tau^a U_{JK} \tau^b U_{JK}^\dagger)$$

$$\int dU_J dU_K \frac{1}{2} \text{tr}(\tau^a U_{JK} \tau^b U_{JK}^\dagger) \Theta_J \Theta_K = \frac{1}{2N_c(N_c^2-1)} \left( \frac{m^*}{4\pi^2 \rho^2} \right)^{2N_f-2} \\ \times \left[ \bar{\psi}(z_J) \frac{1 \mp \gamma^5}{2} \frac{1}{4} \bar{\eta}_{\alpha\beta}^a(J) \sigma_{\alpha\beta} S(z_J - z_K) \frac{1}{4} \bar{\eta}_{\rho\lambda}^b(K) \sigma_{\rho\lambda} \frac{1 \mp \gamma^5}{2} \psi(z_K) \right. \\ \left. + \bar{\psi}(z_K) \frac{1 \mp \gamma^5}{2} \frac{1}{4} \bar{\eta}_{\rho\lambda}^b(K) \sigma_{\rho\lambda} S(z_K - z_J) \frac{1}{4} \bar{\eta}_{\alpha\beta}^a(J) \sigma_{\alpha\beta} \frac{1 \mp \gamma^5}{2} \psi(z_J) \right], \quad (\text{D8})$$

where the 't Hooft symbol is defined as  $\eta_{\mu\nu}^a(J) = \bar{\eta}_{\mu\nu}^a$  if  $J \in I$  (instanton) and  $\eta_{\mu\nu}^a(J) = \eta_{\mu\nu}^a$  if  $J \in A$  (anti-instanton). If the instanton pair is an instanton–anti-instanton molecule, the averaging produces a chiral-conserving quark operator, and a chiral-flipping quark operator otherwise.

(i) *II* cluster

When the pair carries like topological charge, i.e.,  $JK = II$  or  $AA$ ,

$$\int dU_J dU_K \frac{1}{2} \text{tr}(\tau^a U_{JK} \tau^b U_{JK}^\dagger) \Theta_I \Theta_J = \frac{1}{2N_c(N_c^2 - 1)} \left( \frac{m^*}{4\pi^2 \rho^2} \right)^{2N_f - 2} \frac{1}{8} \text{tr}\{S(z_J - z_K)\} \\ \times \delta^{ab} \left[ \bar{\psi}(z_J) \frac{1 \mp \gamma^5}{2} \psi(z_K) + \bar{\psi}(z_K) \frac{1 \mp \gamma^5}{2} \psi(z_J) \right]. \quad (\text{D9})$$

(ii) *IA* cluster

When the pair or molecule carries unlike topological charge, i.e.,  $JK = IA$  or  $AI$ ,

$$\int dU_J dU_K \frac{1}{2} \text{tr}(\tau^a U_{JK} \tau^b U_{JK}^\dagger) \Theta_J \Theta_K = -\frac{1}{2N_c(N_c^2 - 1)} \left( \frac{m^*}{4\pi^2 \rho^2} \right)^{2N_f - 2} \frac{1}{8} \text{tr}\{S(z_J - z_K) \gamma_\rho\} \bar{\eta}_{\rho\beta}^a \eta_{\lambda\beta}^b \\ \times \left[ \bar{\psi}(z_J) \gamma_\lambda \frac{1 \pm \gamma^5}{2} \psi(z_K) - \bar{\psi}(z_K) \gamma_\lambda \frac{1 \mp \gamma^5}{2} \psi(z_J) \right]. \quad (\text{D10})$$

$$\mathbf{b.} \quad \frac{1}{2} \text{tr}(\tau^a U_{JK} \tau^b U_{JK}^\dagger) \frac{1}{2} \text{tr}(\tau^c U_{JK} \tau^d U_{JK}^\dagger)$$

$$\int dU_J dU_K \frac{1}{2} \text{tr}(\tau^a U_{JK} \tau^b U_{JK}^\dagger) \frac{1}{2} \text{tr}(\tau^c U_{JK} \tau^d U_{JK}^\dagger) \Theta_J \Theta_K \\ = \frac{1}{2N_c^2(N_c^2 - 1)} \left( \frac{m^*}{4\pi^2 \rho^2} \right)^{2N_f - 2} \epsilon^{ace} \epsilon^{bdf} \left[ \bar{\psi}(z_J) \frac{1 \mp \gamma^5}{2} \frac{1}{4} \bar{\eta}_{\alpha\beta}^e(J) \sigma_{\alpha\beta} S(z_J - z_K) \frac{1}{4} \bar{\eta}_{\rho\lambda}^f(K) \sigma_{\rho\lambda} \frac{1 \mp \gamma^5}{2} \psi(z_K) \right. \\ \left. + \bar{\psi}(z_K) \frac{1 \mp \gamma^5}{2} \frac{1}{4} \bar{\eta}_{\rho\lambda}^f(K) \sigma_{\rho\lambda} S(z_K - z_J) \frac{1}{4} \bar{\eta}_{\alpha\beta}^e(J) \sigma_{\alpha\beta} \frac{1 \mp \gamma^5}{2} \psi(z_J) \right] \\ + \frac{1}{2N_c^2(N_c^2 - 1)} \left( \frac{m^*}{4\pi^2 \rho^2} \right)^{2N_f - 2} \left( 2 + \frac{N_c - 2}{4(N_c + 2)} \right) \delta^{ac} \delta^{bd} \\ \times \left[ \bar{\psi}(z_J) \frac{1 \mp \gamma^5}{2} S(z_J - z_K) \frac{1 \mp \gamma^5}{2} \psi(z_K) + \bar{\psi}(z_K) \frac{1 \mp \gamma^5}{2} S(z_K - z_J) \frac{1 \mp \gamma^5}{2} \psi(z_J) \right]. \quad (\text{D11})$$

This type of color structure is down by  $1/N_c$  in the two-gluon operators. Therefore, they can be neglected in the  $1/N_c$  counting.

(i) *II* cluster

When the pair carries like topological charge, i.e.,  $JK = II$  or  $AA$ ,

$$\int dU_J dU_K \frac{1}{2} \text{tr}(\tau^a U_{JK} \tau^b U_{JK}^\dagger) \frac{1}{2} \text{tr}(\tau^c U_{JK} \tau^d U_{JK}^\dagger) \Theta_J \Theta_K = \frac{1}{2N_c(N_c^2 - 1)} \left( \frac{m^*}{4\pi^2 \rho^2} \right)^{2N_f - 2} \frac{1}{8} \text{tr}\{S(z_J - z_K)\} \\ \times \left[ \frac{1}{N_c} \epsilon^{ace} \epsilon^{bde} + \left( \frac{4}{N_c} + \frac{N_c - 2}{2N_c(N_c + 2)} \right) \delta^{ac} \delta^{bd} \right] \\ \times \left[ \bar{\psi}(z_J) \frac{1 \mp \gamma^5}{2} \psi(z_J) + \bar{\psi}(z_J) \frac{1 \mp \gamma^5}{2} \psi(z_J) \right]. \quad (\text{D12})$$

(ii) *IA* clusterWhen the pair or molecule carries unlike topological charge, i.e.,  $JK = IA$  or  $AI$ ,

$$\begin{aligned}
& \int dU_J dU_K \frac{1}{2} \text{tr}(\tau^a U_{JK} \tau^b U_{JK}^\dagger) \frac{1}{2} \text{tr}(\tau^c U_{JK} \tau^d U_{JK}^\dagger) \Theta_J \Theta_K \\
&= \frac{1}{2N_c(N_c^2 - 1)} \left( \frac{m^*}{4\pi^2 \rho^2} \right)^{2N_f - 2} \frac{1}{8} \text{tr}\{S(z_I - z_J) \gamma_\rho\} \left[ \bar{\eta}_{\rho\beta}^e \eta_{\lambda\beta}^f \frac{1}{N_c} \epsilon^{ace} \epsilon^{bdf} + \delta_{\rho\lambda} \left( \frac{4}{N_c} + \frac{N_c - 2}{2N_c(N_c + 2)} \right) \delta^{ac} \delta^{bd} \right] \\
&\quad \times \left[ \bar{\psi}(z_I) \gamma_\lambda \frac{1 \pm \gamma^5}{2} \psi(z_J) - \bar{\psi}(z_J) \gamma_\lambda \frac{1 \mp \gamma^5}{2} \psi(z_I) \right]. \tag{D13}
\end{aligned}$$

**c.**  $\frac{1}{2} \text{Tr}(\mathbb{1}_2 U_{JK} \tau^a U_{JK}^\dagger)$ 

$$\begin{aligned}
\int dU_J dU_K \frac{1}{2} \text{Tr}(\mathbb{1}_2 U_{JK} \tau^a U_{JK}^\dagger) \Theta_J \Theta_K &= -\frac{N_c - 2}{2N_c^2(N_c^2 - 1)} \left( \frac{m^*}{4\pi^2 \rho^2} \right)^{2N_f - 2} \frac{1}{4} \bar{\eta}_{\mu\nu}^a(K) \left[ \bar{\psi}(z_J) \frac{1 \mp \gamma^5}{2} S(z_J - z_K) \sigma_{\mu\nu} \frac{1 \mp \gamma^5}{2} \psi(z_K) \right. \\
&\quad \left. + \bar{\psi}(z_K) \frac{1 \mp \gamma^5}{2} \sigma_{\mu\nu} S(z_K - z_J) \frac{1 \mp \gamma^5}{2} \psi(z_J) \right]. \tag{D14}
\end{aligned}$$

(i) *II* clusterWhen the pair carries like topological charge, i.e.,  $JK = II$  or  $AA$ ,

$$\begin{aligned}
\int dU_J dU_K \frac{1}{2} \text{Tr}(\mathbb{1}_2 U_{JK} \tau^a U_{JK}^\dagger) \Theta_J \Theta_K &= -\frac{N_c - 2}{2N_c^2(N_c^2 - 1)} \left( \frac{m^*}{4\pi^2 \rho^2} \right)^{2N_f - 2} \frac{1}{8} \text{tr}\{S(z_J - z_K)\} \frac{1}{2} \bar{\eta}_{\mu\nu}^a(K) \\
&\quad \times \left[ \bar{\psi}(z_J) \sigma_{\mu\nu} \frac{1 \mp \gamma^5}{2} \psi(z_K) + \bar{\psi}(z_K) \sigma_{\mu\nu} \frac{1 \mp \gamma^5}{2} \psi(z_J) \right]. \tag{D15}
\end{aligned}$$

(ii) *IA* clusterWhen the pair or molecule carries unlike topological charge, i.e.,  $JK = IA$  or  $AI$ ,

$$\begin{aligned}
\int dU_J dU_K \frac{1}{2} \text{Tr}(\mathbb{1}_2 U_{JK} \tau^a U_{JK}^\dagger) \Theta_J \Theta_K &= -\frac{N_c - 2}{2N_c^2(N_c^2 - 1)} \left( \frac{m^*}{4\pi^2 \rho^2} \right)^{2N_f - 2} \frac{i}{4} \text{tr}\{S(z_J - z_K) \gamma_\mu\} \frac{1}{2} \bar{\eta}_{\mu\nu}^a(K) \\
&\quad \times \left[ \bar{\psi}(z_J) \gamma_\nu \frac{1 \pm \gamma^5}{2} \psi(z_K) + \bar{\psi}(z_K) \gamma_\nu \frac{1 \mp \gamma^5}{2} \psi(z_J) \right]. \tag{D16}
\end{aligned}$$

**d.**  $\frac{1}{2} \text{tr}(\mathbb{1}_2 U_{JK} \tau^a U_{JK}^\dagger) \frac{1}{2} \text{tr}(\tau^b U_{JK} \tau^c U_{JK}^\dagger)$ 

$$\begin{aligned}
\int dU_J dU_K \frac{1}{2} \text{tr}(\mathbb{1}_2 U_{JK} \tau^a U_{JK}^\dagger) \frac{1}{2} \text{tr}(\tau^b U_{JK} \tau^c U_{JK}^\dagger) \Theta_J \Theta_K &= -\frac{N_c - 2}{2N_c^2(N_c^2 - 1)} \frac{1}{4(N_c + 2)} \frac{1}{4} \bar{\eta}_{\mu\nu}^a(J) \delta^{bc} \\
&\quad \times \left[ \bar{\psi}(z_J) \frac{1 \mp \gamma^5}{2} \sigma_{\mu\nu} S(z_J - z_K) \frac{1 \mp \gamma^5}{2} \psi(z_K) \right. \\
&\quad \left. + \bar{\psi}(z_K) \frac{1 \mp \gamma^5}{2} S(z_K - z_J) \sigma_{\mu\nu} \frac{1 \mp \gamma^5}{2} \psi(z_J) \right]. \tag{D17}
\end{aligned}$$

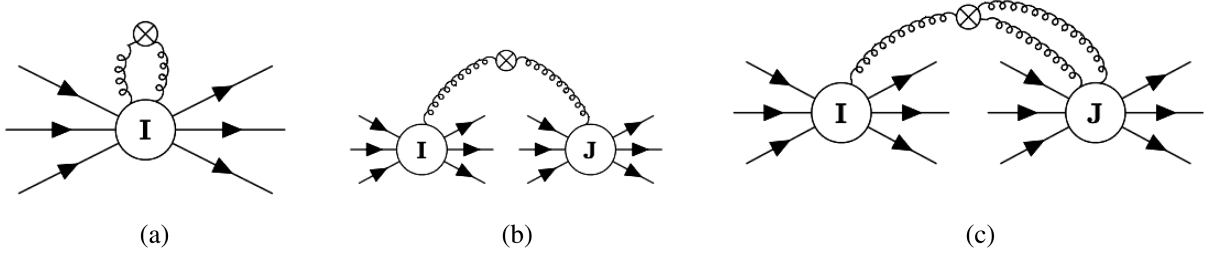


FIG. 16. (a) The diagram of  $\mathcal{O}[I]$  in the multi-instanton expansion of the two-gluon operator  $\mathcal{O}_{2g}$ . Each dashed line connected to the instanton represents the classical background field. (b) The diagram of  $\mathcal{O}[I]$  in the multi-instanton expansion of the two-gluon operator  $\mathcal{O}_{2g}$ . Each dashed line connected to the instanton represents the classical background field. (c) The effective two-(anti-)instanton operators  $\mathcal{O}_{3g++,+--}$ , which represents all of the gluons in the operator  $\mathcal{O}_{3g}[A]$  are plane waves, one of the gluon plane waves are connected to the instanton  $I$ , and the remaining two-gluon plane waves are connected to  $J$ . The conjugate diagram could be obtained by  $I \leftrightarrow J$ .

(i)  $II$ ,  $AA$  cluster

When the pair carries like topological charge, i.e.,  $JK = II$  or  $AA$ ,

$$\begin{aligned} & \int dU_J dU_K \frac{1}{2} \text{tr}(\mathbb{1}_2 U_{JK} \tau^a U_{JK}^\dagger) \frac{1}{2} \text{tr}(\tau^b U_{JK} \tau^c U_{JK}^\dagger) \Theta_J \Theta_K \\ &= -\frac{N_c - 2}{2N_c^2(N_c^2 - 1)} \frac{1}{4(N_c + 2)} \left( \frac{m^*}{4\pi^2 \rho^2} \right)^{2N_f - 2} \frac{1}{8} \text{tr}\{S(z_J - z_K)\} \frac{1}{2} \bar{\eta}_{\mu\nu}^a(J) \delta^{bc} \\ & \quad \times \left[ \bar{\psi}(z_I) \sigma_{\mu\nu} \frac{1 \mp \gamma^5}{2} \psi(z_J) + \bar{\psi}(z_J) \sigma_{\mu\nu} \frac{1 \mp \gamma^5}{2} \psi(z_I) \right]. \end{aligned} \quad (\text{D18})$$

(ii)  $IA$  cluster

When the pair or molecule carries unlike topological charge, i.e.,  $JK = IA$  or  $AI$ ,

$$\begin{aligned} & \int dU_J dU_K \frac{1}{2} \text{tr}(\mathbb{1}_2 U_{JK} \tau^a U_{JK}^\dagger) \frac{1}{2} \text{tr}(\tau^b U_{JK} \tau^c U_{JK}^\dagger) \Theta_J \Theta_K \\ &= -\frac{N_c - 2}{2N_c^2(N_c^2 - 1)} \frac{1}{4(N_c + 2)} \left( \frac{m^*}{4\pi^2 \rho^2} \right)^{2N_f - 2} \frac{i}{4} \text{tr}\{S(z_J - z_K) \gamma_\mu\} \frac{1}{2} \bar{\eta}_{\mu\nu}^a(J) \delta^{bc} \\ & \quad \times \left[ \bar{\psi}(z_J) \gamma_\nu \frac{1 \pm \gamma^5}{2} \psi(z_K) + \bar{\psi}(z_K) \gamma_\nu \frac{1 \mp \gamma^5}{2} \psi(z_J) \right]. \end{aligned} \quad (\text{D19})$$

## APPENDIX E: GLUONS CAPTURED BY THE INSTANTON TAILS

When strict factorization is enforced on hadronic kernels and Feynman-like graphs are used, it may be more appropriate to evaluate the hadronic matrix elements using the effective vertices in  $S_{\text{eff}}$  in (50), with the LSZ reduced gluons. This is graphically illustrated by the Feynman diagrams in Figs. 16(a)–16(c), where the gluonic lines denote the LSZ reduced gluons.

We note that, in the ensemble averaging described earlier, the dashed gluons are moduli gluons, as opposed

to the LSZ reduced gluons in this section. The latter are sourced only by small size pseudoparticles in the QCD vacuum, while the former are for any pseudoparticle size in the QCD vacuum.

With this in mind and using the  $1/N_c$  bookkeeping, the one-body interaction is seen to dominate matrix elements, with the rest of the  $N_f - 1$  flavors looped up. Therefore, in the following calculations, we will retain only the one-body induced interaction.

For the gluonic scalar  $G_{\mu\nu}^a G_{\mu\nu}^a$ , the result of the Feynman diagram in Fig. 16(a) reads

$$\langle P' | G_{\mu\nu}^a G_{\mu\nu}^a | P \rangle = -\frac{G}{N_c} \left( \frac{m^*}{4\pi^2 \rho^2} \right)^{N_f-1} \langle P' | \bar{\psi} \psi | P \rangle \int d^4 x \left( \frac{2\pi^2 \rho^2}{g} \right)^2 D_{\mu\nu\rho\lambda}(x) D_{\mu\nu\rho\lambda}(x) e^{-iq \cdot x}, \quad (\text{E1})$$

where the Euclidean gluon propagator connecting the instanton and the effective vertices is defined by

$$\begin{aligned} D_{\mu\nu\rho\lambda}(x) &= \int \frac{d^4 q}{(2\pi)^4} \mathcal{F}_g(\rho q) \frac{1}{q^2} (q_\mu q_\rho \delta_{\nu\lambda} - q_\nu q_\rho \delta_{\mu\lambda} - q_\mu q_\lambda \delta_{\nu\rho} + q_\nu q_\lambda \delta_{\mu\rho}) \theta(1/\rho^2 - q^2) e^{iq \cdot x} \\ &= -\frac{1}{4\pi^2 x} \left( \frac{x_\mu x_\rho}{x^2} \delta_{\nu\lambda} - \frac{x_\nu x_\rho}{x^2} \delta_{\mu\lambda} - \frac{x_\mu x_\lambda}{x^2} \delta_{\nu\rho} + \frac{x_\nu x_\lambda}{x^2} \delta_{\mu\rho} \right) \int_0^\infty dq q^2 \mathcal{F}_g(\rho q) \theta(1/\rho^2 - q^2) J_3(qx) \\ &\quad + \frac{1}{2\pi^2 x} (\delta_{\mu\rho} \delta_{\nu\lambda} - \delta_{\mu\lambda} \delta_{\nu\rho}) \int_0^\infty dq q^2 \mathcal{F}_g(\rho q) \theta(1/\rho^2 - q^2) \frac{J_2(qx)}{qx}. \end{aligned} \quad (\text{E2})$$

The gluon emitted from the instanton carries the instanton gluonic form factor, while the gluon absorbed by the operator is cut by the hard cutoff  $1/\rho$ .

The calculation can be extended to second order in the instanton density. The result of the Feynman diagram in Fig. 16(b) depends on the topological charges of the  $IJ$  pairs. The pairs with the same topological charges such as the  $II$  or  $AA$  pair yield a chiral-conserving quark operator. The result reads

$$\begin{aligned} \langle P' | G_{\mu\nu}^a G_{\rho\lambda}^a | P \rangle |_{II,AA} &= \frac{G^2}{N_c(N_c^2 - 1)} \left( \frac{m^*}{4\pi^2 \rho^2} \right)^{2(N_f-1)} \left( \frac{2\pi^2 \rho^2}{g} \right)^2 \int d^4 z_I d^4 z_J \frac{1}{4} \text{tr} \{ S(z_I - z_J) \} \\ &\quad \times D_{\mu\nu\rho\lambda}(x - z_I) D_{\mu\nu\rho\lambda}(x - z_J) \langle P' | \left[ \bar{\psi}(z_I) \frac{1 \mp \gamma^5}{2} \psi(z_J) + \bar{\psi}(z_J) \frac{1 \mp \gamma^5}{2} \psi(z_I) \right] | P \rangle. \end{aligned} \quad (\text{E3})$$

Similarly, the pairs with opposite topological charges in the  $IA$  or  $AI$  molecules yield a chiral-flipping quark operator given by

$$\begin{aligned} \langle P' | G_{\mu\nu}^a G_{\rho\lambda}^a | P \rangle |_{IA,AI} &= -\frac{G^2}{N_c(N_c^2 - 1)} \left( \frac{m^*}{4\pi^2 \rho^2} \right)^{2(N_f-1)} \left( \frac{2\pi^2 \rho^2}{g} \right)^2 \int d^4 z_I d^4 z_J \frac{1}{4} \text{tr} \{ S(z_I - z_J) \gamma_\rho \} \\ &\quad \times [D_{\mu\nu\rho\alpha}(x - z_I) D_{\mu\nu\lambda\alpha}(x - z_J) + D_{\mu\nu\lambda\alpha}(x - z_I) D_{\mu\nu\rho\alpha}(x - z_J)] \\ &\quad \times \langle P' | \left[ \bar{\psi}(z_I) \gamma_\lambda \frac{1 \pm \gamma^5}{2} \psi(z_J) - \bar{\psi}(z_J) \gamma_\lambda \frac{1 \mp \gamma^5}{2} \psi(z_I) \right] | P \rangle. \end{aligned} \quad (\text{E4})$$

The localized form of the pseudoparticles in the QCD instanton vacuum allows for the use of the  $R$  expansion or local approximation, in the evaluation of the double integral over the position of the pseudoparticles, with the result to second order in the instanton density

$$\begin{aligned} \langle P' | g^2 G_{\mu\nu}^a G_{\mu\nu}^a | P \rangle &= \left[ -\frac{G}{N_c} \left( \frac{m^*}{4\pi^2 \rho^2} \right)^{N_f-1} + \frac{G^2}{N_c(N_c^2 - 1)} \left( \frac{m^*}{4\pi^2 \rho^2} \right)^{2(N_f-1)} \frac{1}{m^*} \right] \langle P' | \bar{\psi} \psi | P \rangle \\ &\quad \times (2\pi^2)^2 \int d^4 x D_{\mu\nu\rho\lambda}(x) D_{\mu\nu\rho\lambda}(x) e^{-i\rho q \cdot x} \\ &\quad - \frac{G^2}{N_c(N_c^2 - 1)} \left( \frac{m^*}{4\pi^2 \rho^2} \right)^{2(N_f-1)} \rho^2 T_{IA}(\rho m^*) \langle P' | \bar{\psi} \gamma_\rho \overleftrightarrow{\partial}_\lambda \psi | P \rangle \\ &\quad \times (2\pi^2)^2 \int d^4 x [D_{\mu\nu\rho\alpha}(x) D_{\mu\nu\lambda\alpha}(x) + D_{\mu\nu\lambda\alpha}(x) D_{\mu\nu\rho\alpha}(x)] e^{-i\rho q \cdot x} + \mathcal{O}(G^3). \end{aligned} \quad (\text{E5})$$

The quark hopping integral is given in (88).

The calculation can be extended to the three-gluon operators. Here, we detail it for the  $C$ -even operator. As expected, there is no contribution from a single pseudoparticle. The Feynman diagram in Fig. 16(c) with like pairs the pairs  $II$  or  $AA$  yields the chiral-conserving quark operator:

$$\begin{aligned}
\langle P' | d^{abc} G_{\mu\nu}^a G_{\rho\alpha}^b G_{\lambda\alpha}^c | P \rangle |_{II,AA} &= -\frac{N_c - 2}{2N_c^2(N_c^2 - 1)} G^2 \left( \frac{m^*}{4\pi^2 \rho^2} \right)^{2(N_f - 1)} \left( \frac{2\pi^2 \rho^2}{g} \right)^3 \int d^4 z_I d^4 z_J \frac{1}{4} \text{tr} \{ S(z_I - z_J) \} \\
&\times [D_{\mu\nu\beta\gamma}(x - z_J) D_{\rho\alpha\delta\sigma}(x - z_I) D_{\lambda\alpha\delta\sigma}(x - z_I) + 2D_{\rho\alpha\beta\gamma}(x - z_J) D_{\mu\nu\delta\sigma}(x - z_I) D_{\lambda\alpha\delta\sigma}(x - z_I) \\
&+ (\rho \leftrightarrow \lambda) + (I \leftrightarrow J)] \langle P' | \left[ \bar{\psi}(z_I) \sigma_{\beta\gamma} \frac{1 \mp \gamma^5}{2} \psi(z_I) + \bar{\psi}(z_J) \sigma_{\beta\gamma} \frac{1 \mp \gamma^5}{2} \psi(z_J) \right] | P \rangle. \quad (E6)
\end{aligned}$$

For the unlike pairs, the result gives the chiral-flipping quark operator:

$$\begin{aligned}
\langle P' | d^{abc} G_{\mu\nu}^a G_{\rho\alpha}^b G_{\lambda\alpha}^c | P \rangle |_{IA,AI} &= -\frac{N_c - 2}{2N_c^2(N_c^2 - 1)} G^2 \left( \frac{m^*}{4\pi^2 \rho^2} \right)^{2(N_f - 1)} \left( \frac{2\pi^2 \rho^2}{g} \right)^3 \int d^4 z_I d^4 z_J \frac{i}{2} \text{tr} \{ S(z_I - z_J) \gamma_\beta \} \\
&\times [D_{\mu\nu\beta\gamma}(x - z_J) D_{\delta\sigma\rho\alpha}(x - z_I) D_{\delta\sigma\lambda\alpha}(x - z_I) + 2D_{\rho\alpha\beta\gamma}(x - z_J) D_{\mu\nu\delta\sigma}(x - z_I) D_{\lambda\alpha\delta\sigma}(x - z_I) \\
&+ (\rho \leftrightarrow \lambda) - (I \leftrightarrow J)] \langle P' | \left[ \bar{\psi}(z_I) \gamma_\gamma \frac{1 \pm \gamma^5}{2} \psi(z_I) + \bar{\psi}(z_J) \gamma_\gamma \frac{1 \mp \gamma^5}{2} \psi(z_J) \right] | P \rangle. \quad (E7)
\end{aligned}$$

The Euclidean gluon propagator connecting the instanton and the operators is given in (E2).

Similarly, in the forward limit, we can average over the local operator around the neighborhood of one of the instanton field shared by the operator. Therefore, after averaging the gluonic operator over four-dimensional Euclidean space, the profile functions depends only on the relative distance between two instantons. Again, the effective fermionic operator is nonlocal. Using the  $R$  expansion or local approximation, the result is

$$\begin{aligned}
\langle P' | g^3 d^{abc} G_{\mu\nu}^a G_{\rho\alpha}^b G_{\lambda\alpha}^c | P \rangle &= -\frac{N_c - 2}{N_c^2(N_c^2 - 1)} G^2 \left( \frac{m^*}{4\pi^2 \rho^2} \right)^{2(N_f - 1)} \frac{2}{\rho^2 m^*} \langle P' | \bar{\psi} \sigma_{\beta\gamma} \psi | P \rangle \\
&\times (2\pi^2)^3 \int d^4 x e^{-i\rho q \cdot x} [D_{\mu\nu\beta\gamma}(x) D_{\rho\alpha\delta\sigma}(x) D_{\lambda\alpha\delta\sigma}(x) + 2D_{\rho\alpha\beta\gamma}(x) D_{\mu\nu\delta\sigma}(x) D_{\lambda\alpha\delta\sigma}(x) + (\rho \leftrightarrow \lambda)] \\
&- \frac{N_c - 2}{N_c^2(N_c^2 - 1)} G^2 \left( \frac{m^*}{4\pi^2 \rho^2} \right)^{2(N_f - 1)} \rho^2 T_{IA}(\rho m^*) \langle P' | \bar{\psi} \gamma_\gamma \psi | P \rangle \\
&\times (2\pi^2)^3 \int d^4 x e^{-i\rho q \cdot x} \frac{\partial}{\partial x'_\beta} [D_{\mu\nu\beta\gamma}(x) D_{\rho\alpha\delta\sigma}(x') D_{\lambda\alpha\delta\sigma}(x') + 2D_{\rho\alpha\beta\gamma}(x) D_{\mu\nu\delta\sigma}(x') D_{\lambda\alpha\delta\sigma}(x') \\
&- D_{\mu\nu\beta\gamma}(x') D_{\delta\sigma\rho\alpha}(x) D_{\delta\sigma\lambda\alpha}(x) - 2D_{\rho\alpha\beta\gamma}(x') D_{\mu\nu\delta\sigma}(x) D_{\lambda\alpha\delta\sigma}(x) + (\rho \leftrightarrow \lambda)] |_{x=x'}. \quad (E8)
\end{aligned}$$

The quark hopping integral  $T_{IA}(\rho m^*)$  is given in (88).

## APPENDIX F: GRAND CANONICAL ENSEMBLE

To account for the fluctuations of the topological charges in the present description using an ensemble of pseudo-particles, we need to extend it to a grand canonical ensemble. For that, we will allow for the number sum  $N = N_+ + N_-$  and the number difference  $\Delta N = N_+ - N_-$  to fluctuate, with a universal distribution  $\mathbb{P}(N_+, N_-)$  fixed by low-energy theorems for  $N$  and a topological variance  $\chi_t$  for  $\Delta N$  [6,15,37,68]:

$$\mathbb{P}(N_+, N_-) \propto \left( \frac{\bar{N}^N}{N!} \right)^{b/4} \frac{1}{\sqrt{2\pi\chi_t}} \exp \left( -\frac{\Delta N^2}{2\chi_t} \right) \quad (F1)$$

with  $\chi_t = \langle \Delta N^2 \rangle$  and  $b = \frac{11}{3} N_c - \frac{2}{3} N_f$ . The average instanton number is consistent with the parameters  $\bar{N} = \langle N \rangle$ , and the mean topological charge is null  $Q_t = \langle \Delta N \rangle = 0$ . As a

result, most of the operators we encountered earlier can be further averaged:

$$\langle \mathcal{O} \rangle = \sum_{N_+, N_-} \mathbb{P}(N_+, N_-) \langle \mathcal{O} \rangle_{N_\pm} \equiv \overline{\langle \mathcal{O} \rangle}_{N_\pm}. \quad (F2)$$

The averaging is carried over the configurations with fixed  $N_\pm$  (canonical ensemble average), followed by an averaging over the distribution (F1).

Since the multiflavor emergent coupling  $G(1 \pm \delta) = N_\pm / \langle \theta_\pm \rangle_{\text{eff}}$  is fixed by the saddle point approximation in the canonical ensemble, we can expand  $\langle \mathcal{O} \rangle_{\text{eff}}$  in (65), in terms of connected diagrams with different orders of instanton numbers  $N_\pm$ . Therefore, the total fixed- $N_\pm$  ensemble average can be written as a certain function expanded in terms of instanton numbers  $N_\pm$ :

$$\langle \mathcal{O}[A] \rangle_{N_{\pm}} = \mathcal{O}(N_+, N_-). \quad (\text{F3})$$

All vacuum expectation values  $\langle \mathcal{O}[A] \rangle$  in the grand canonical ensemble can be expressed as

$$\langle \mathcal{O}[A] \rangle = \overline{\mathcal{O}(N_+, N_-)}. \quad (\text{F4})$$

With this in mind, the evaluation of the hadronic matrix elements can be formally written as a large- $T$  reduction of a

three-point function:

$$\frac{\langle h | \mathcal{O} | h \rangle}{\langle h | h \rangle} = \lim_{T \rightarrow \infty} \frac{\langle J_h^\dagger(T/2) \mathcal{O} J_h(-T/2) \rangle_{\text{con}}}{\langle J_h^\dagger(T/2) J_h(-T/2) \rangle}, \quad (\text{F5})$$

where  $J_h(t)$  is a pertinent source for the hadronic state  $h$ . The averaging of the connected three-point function reads

$$\begin{aligned} \langle J_h^\dagger(T/2) \mathcal{O}[A] J_h(-T/2) \rangle_{\text{con}} &= \langle J_h^\dagger(T/2) \mathcal{O}[A] J_h(-T/2) \rangle - \langle \mathcal{O}[A] \rangle \langle J_h^\dagger(T/2) J_h(-T/2) \rangle_{\text{con}} \\ &= \sum_{N_+, N_-} \mathbb{P}(N_+, N_-) (\mathcal{O}(N_+, N_-) - \overline{\mathcal{O}(N_+, N_-)}) \langle J_h^\dagger(T/2) J_h(-T/2) \rangle_{N_{\pm}} \\ &\quad + \langle J_h^\dagger(T/2) : \mathcal{O}[\psi, \bar{\psi}] : J_h(-T/2) \rangle_{\text{eff}}, \end{aligned} \quad (\text{F6})$$

where  $: \mathcal{O}[\psi, \bar{\psi}] :$  denotes the effective quark operator connected to the hadronic sources. The quark contributions are usually penalized by  $1/N_c$  counting, as they are rooted in the quark-instanton interaction.

To extract the nontrivial contribution from the disconnected diagrams, we need to consider the fluctuations. In the  $1/N_c$  bookkeeping, the dominant contributions are given by

$$\begin{aligned} \frac{\langle P | \mathcal{O}[A] | P \rangle}{\langle P | P \rangle} &= \sum_{N_+, N_-} \mathbb{P}(N_+, N_-) (\mathcal{O}(N_+, N_-) - \overline{\mathcal{O}(N_+, N_-)}) \\ &\quad \times \lim_{T \rightarrow \infty} \left[ (N - \bar{N}) \left( \frac{\partial}{\partial N} \ln \langle J_h^\dagger(T/2) J_h(-T/2) \rangle_{\text{eff}} \right)_{N=\bar{N}} + \Delta N \left( \frac{\partial}{\partial \Delta N} \ln \langle J_h^\dagger(T/2) J_h(-T/2) \rangle_{\text{eff}} \right)_{\Delta N=0} \right] \end{aligned} \quad (\text{F7})$$

with the number sum  $N = N_+ + N_-$ , the number difference  $\Delta N = N_+ - N_-$ , the mean number  $\bar{N} = \langle N \rangle$ , and the mean topological charge  $Q_t = \langle \Delta N \rangle = 0$ .

To show how the three-point function is determined, we will consider a few examples. When the gluonic operator is proportional to the total instanton number,

$$\mathcal{O}(N_+, N_-) = \alpha N / V.$$

For asymptotic Euclidean times

$$\langle J_h^\dagger(T/2) J_h(-T/2) \rangle_{\text{eff}} \rightarrow e^{-M_h(N_+, N_-)T},$$

the matrix element at the leading  $1/N_c$  is tied to the topological compressibility:

$$\langle P | \mathcal{O}[A] | P \rangle = -2M_h^2 \alpha \left[ \frac{\langle (N - \bar{N})^2 \rangle_{\mathbb{P}}}{\bar{N}} \right] \bar{N} \frac{\partial \ln M_h}{\partial \bar{N}}. \quad (\text{F8})$$

In particular, for the nucleon, the mass is related to the instanton density by the scaling relation

$$M_N = C \left( \frac{\bar{N}}{V} \right)^{1/4} + \sigma_{\pi N}$$

so that

$$\langle P | \mathcal{O}[A] | P \rangle = -2M_N^2 \alpha \frac{1}{4} \left[ \frac{\langle (N - \bar{N})^2 \rangle_{\mathbb{P}}}{\bar{N}} \right] \left( 1 - \frac{\sigma_{\pi N}}{M_N} \right). \quad (\text{F9})$$

When the gluonic operator is proportional to the number difference, say,  $\mathcal{O}(N_+, N_-) = \alpha \Delta N / V$ , a rerun of the preceding reasoning gives

$$\langle P | \mathcal{O}[A] | P \rangle = -2M_h^2 \alpha \chi_t \frac{\partial \ln M_h}{\partial \Delta N}. \quad (\text{F10})$$

For a polarized nucleon consisting of quark-scalar-diquark [68],

$$M_N(\Delta N) = M_N - M_N s_v \frac{\Delta N}{\bar{N}}$$

so that

$$\langle P|\mathcal{O}[A]|P\rangle = 2M_N^2 \alpha \frac{\chi_t}{N} s_v. \quad (\text{F11})$$

This calculation can be extended to the constituent quark model and  $SU(6)$  quark-diquark model.

### APPENDIX G: AVERAGING THE INSTANTON INTERACTIONS OVER THE $SU(3)$ ROTATIONS

One way to carry out the color averaging in the effective instanton interaction  $\det_{\pm}$  is by determinantal reduction [116]:

$$\int dU \prod_{i=1}^{N_c} U_{a_i b_i} = \frac{1}{N_c!} \epsilon_{a_1 \dots a_{N_c}} \epsilon_{b_1 \dots b_{N_c}} \quad (\text{G1})$$

and

$$U_{ba}^{\dagger} = \frac{1}{(N_c - 1)!} \epsilon_{aa_1 \dots a_{N_c-1}} \epsilon_{bb_1 \dots b_{N_c-1}} U_{a_1 b_1} \dots U_{a_{N_c-1} b_{N_c-1}}, \quad (\text{G2})$$

where  $\epsilon_{a_1 \dots a_{N_c}}$  is the Levi-Civita tensor of rank  $N_c$  with  $\epsilon_{12 \dots N_c} = 1$ .

With these two identities, the color averagings of  $(UU^{\dagger})^p$  with small  $p$  are

$$(1) \quad p = 1—$$

$$\int dUU_{ab}U_{cd}^{\dagger} = \frac{1}{N_c} \delta_{ad} \delta_{cb}; \quad (\text{G3})$$

$$(2) \quad p = 2—$$

$$\begin{aligned} & \int dUU_{a_1 b_1} U_{c_1 d_1}^{\dagger} U_{a_2 b_2} U_{c_2 d_2}^{\dagger} \\ &= \frac{1}{N_c^2 - 1} (\delta_{a_1 d_1} \delta_{a_2 d_2} \delta_{c_1 b_1} \delta_{c_2 b_2} + \delta_{a_1 d_2} \delta_{a_2 d_1} \delta_{c_1 b_2} \delta_{c_2 b_1}) \\ & \quad - \frac{1}{N_c(N_c^2 - 1)} (\delta_{a_1 d_1} \delta_{a_2 d_2} \delta_{c_1 b_2} \delta_{c_2 b_1} \\ & \quad + \delta_{a_1 d_2} \delta_{a_2 d_1} \delta_{c_1 b_1} \delta_{c_2 b_2}); \end{aligned} \quad (\text{G4})$$

$$(3) \quad p = 3—$$

$$\begin{aligned} & \int dUU_{a_1 b_1} U_{c_1 d_1}^{\dagger} U_{a_2 b_2} U_{c_2 d_2}^{\dagger} U_{a_3 b_3} U_{c_3 d_3}^{\dagger} \\ &= \frac{N_c^2 - 2}{N_c(N_c^2 - 4)(N_c^2 - 1)} (\delta_{a_1 d_1} \delta_{a_2 d_2} \delta_{a_3 d_3} \delta_{c_1 b_1} \delta_{c_2 b_2} \delta_{c_3 b_3} + \delta_{a_1 d_2} \delta_{a_2 d_1} \delta_{a_3 d_3} \delta_{c_1 b_2} \delta_{c_2 b_1} \delta_{c_3 b_3} \\ & \quad + \delta_{a_1 d_3} \delta_{a_2 d_2} \delta_{a_3 d_1} \delta_{c_1 b_3} \delta_{c_2 b_2} \delta_{c_3 b_1} + \delta_{a_1 d_1} \delta_{a_3 d_2} \delta_{a_2 d_3} \delta_{c_1 b_1} \delta_{c_3 b_2} \delta_{c_2 b_3} \\ & \quad + \delta_{a_1 d_3} \delta_{a_3 d_2} \delta_{a_2 d_1} \delta_{c_1 b_3} \delta_{c_3 b_2} \delta_{c_2 b_1} + \delta_{a_1 d_2} \delta_{a_2 d_3} \delta_{a_3 d_1} \delta_{c_1 b_2} \delta_{c_2 b_3} \delta_{c_3 b_1}) \\ & \quad - \frac{1}{(N_c^2 - 4)(N_c^2 - 1)} (\delta_{a_1 d_1} \delta_{a_2 d_2} \delta_{a_3 d_3} \delta_{c_1 b_2} \delta_{c_2 b_1} \delta_{c_3 b_3} + \delta_{a_1 d_2} \delta_{a_2 d_1} \delta_{a_3 d_3} \delta_{c_1 b_1} \delta_{c_2 b_2} \delta_{c_3 b_3} \\ & \quad + \delta_{a_1 d_1} \delta_{a_2 d_2} \delta_{a_3 d_3} \delta_{c_1 b_3} \delta_{c_2 b_2} \delta_{c_3 b_1} + \delta_{a_1 d_3} \delta_{a_2 d_2} \delta_{a_3 d_1} \delta_{c_1 b_1} \delta_{c_2 b_2} \delta_{c_3 b_3} + \delta_{a_1 d_1} \delta_{a_2 d_2} \delta_{a_3 d_3} \delta_{c_1 b_1} \delta_{c_3 b_2} \delta_{c_2 b_3} \\ & \quad + \delta_{a_1 d_1} \delta_{a_3 d_2} \delta_{a_2 d_3} \delta_{c_1 b_1} \delta_{c_3 b_2} \delta_{c_2 b_3} + \delta_{a_1 d_3} \delta_{a_3 d_2} \delta_{a_2 d_1} \delta_{c_1 b_3} \delta_{c_3 b_2} \delta_{c_2 b_1} + \delta_{a_1 d_1} \delta_{a_3 d_2} \delta_{a_2 d_3} \delta_{c_1 b_3} \delta_{c_3 b_2} \delta_{c_2 b_1} \\ & \quad + \delta_{a_1 d_1} \delta_{a_3 d_2} \delta_{a_2 d_3} \delta_{c_1 b_3} \delta_{c_3 b_2} \delta_{c_2 b_1} + \delta_{a_1 d_2} \delta_{a_2 d_3} \delta_{a_3 d_1} \delta_{c_1 b_1} \delta_{c_3 b_2} \delta_{c_2 b_3} + \delta_{a_1 d_2} \delta_{a_2 d_3} \delta_{a_3 d_1} \delta_{c_3 b_1} \delta_{c_2 b_2} \delta_{c_1 b_3} \\ & \quad + \delta_{a_1 d_2} \delta_{a_2 d_3} \delta_{a_3 d_1} \delta_{c_1 b_2} \delta_{c_2 b_1} \delta_{c_3 b_3} + \delta_{a_1 d_1} \delta_{a_3 d_2} \delta_{a_2 d_3} \delta_{c_1 b_2} \delta_{c_2 b_3} \delta_{c_3 b_1} \\ & \quad + \delta_{a_1 d_1} \delta_{a_3 d_2} \delta_{a_2 d_3} \delta_{c_1 b_2} \delta_{c_2 b_3} \delta_{c_3 b_1} + \delta_{a_1 d_1} \delta_{a_3 d_2} \delta_{a_2 d_3} \delta_{c_1 b_2} \delta_{c_2 b_3} \delta_{c_3 b_1}) \\ & \quad + \frac{2}{N_c(N_c^2 - 4)(N_c^2 - 1)} (\delta_{a_1 d_2} \delta_{a_2 d_3} \delta_{a_3 d_1} \delta_{c_1 b_1} \delta_{c_2 b_2} \delta_{c_3 b_3} + \delta_{a_1 d_1} \delta_{a_2 d_2} \delta_{a_3 d_3} \delta_{c_1 b_2} \delta_{c_2 b_3} \delta_{c_3 b_1} \\ & \quad + \delta_{a_1 d_3} \delta_{a_3 d_2} \delta_{a_2 d_1} \delta_{c_1 b_1} \delta_{c_2 b_2} \delta_{c_3 b_3} + \delta_{a_1 d_1} \delta_{a_2 d_2} \delta_{a_3 d_3} \delta_{c_1 b_3} \delta_{c_3 b_2} \delta_{c_2 b_1} + \delta_{a_1 d_2} \delta_{a_2 d_3} \delta_{a_3 d_1} \delta_{c_1 b_3} \delta_{c_3 b_2} \delta_{c_2 b_1} \\ & \quad + \delta_{a_1 d_3} \delta_{a_3 d_2} \delta_{a_2 d_1} \delta_{c_1 b_2} \delta_{c_2 b_3} \delta_{c_3 b_1} + \delta_{a_1 d_1} \delta_{a_3 d_2} \delta_{a_2 d_3} \delta_{c_3 b_2} \delta_{c_2 b_2} \delta_{c_1 b_3} + \delta_{a_1 d_1} \delta_{a_3 d_2} \delta_{a_2 d_3} \delta_{c_1 b_2} \delta_{c_2 b_1} \delta_{c_3 b_3} \\ & \quad + \delta_{a_1 d_3} \delta_{a_3 d_2} \delta_{a_2 d_1} \delta_{c_1 b_2} \delta_{c_2 b_1} \delta_{c_3 b_3} + \delta_{a_1 d_3} \delta_{a_3 d_2} \delta_{a_2 d_1} \delta_{c_1 b_2} \delta_{c_2 b_1} \delta_{c_3 b_3} + \delta_{a_1 d_2} \delta_{a_2 d_3} \delta_{a_3 d_1} \delta_{c_1 b_1} \delta_{c_3 b_2} \delta_{c_2 b_3} \\ & \quad + \delta_{a_1 d_2} \delta_{a_2 d_3} \delta_{a_3 d_1} \delta_{c_3 b_1} \delta_{c_2 b_2} \delta_{c_1 b_3}). \end{aligned} \quad (\text{G5})$$

However, for large values of  $p$ , this averaging method is tedious. Since  $N_c \otimes N_c = 1 \oplus (N_c^2 - 1)$ , the group integral practically reduces to finding all projections of the product of adjoint representations onto the singlet for  $SU(N_c)$ . The result can be obtained by using the graphical color projection rules [117–119], with the following results:

(1)  $p = 2$ —

$$\int dUU_{a_1 b_1} U_{c_1 d_1}^\dagger U_{a_2 b_2} U_{c_2 d_2}^\dagger = \frac{1}{N_c^2} \delta_{a_1 d_1} \delta_{a_2 d_2} \delta_{c_1 b_1} \delta_{c_2 b_2} + \frac{1}{4(N_c^2 - 1)} \lambda_{a_1 d_1}^\alpha \lambda_{a_2 d_2}^\alpha \lambda_{c_1 b_1}^\beta \lambda_{c_2 b_2}^\beta; \quad (\text{G6})$$

(2)  $p = 3$ —

$$\begin{aligned} \int dUU_{a_1 b_1} U_{c_1 d_1}^\dagger U_{a_2 b_2} U_{c_2 d_2}^\dagger U_{a_3 b_3} U_{c_3 d_3}^\dagger &= \frac{1}{N_c^3} \delta_{a_1 d_1} \delta_{a_2 d_2} \delta_{a_3 d_3} \delta_{c_1 b_1} \delta_{c_2 b_2} \delta_{c_3 b_3} \\ &+ \frac{1}{4N_c(N_c^2 - 1)} (\lambda_{a_1 d_1}^\alpha \lambda_{a_2 d_2}^\alpha \delta_{a_3 d_3} \lambda_{c_1 b_1}^\beta \lambda_{c_2 b_2}^\beta \delta_{c_3 b_3} + \delta_{a_1 d_1} \lambda_{a_2 d_2}^\alpha \lambda_{a_3 d_3}^\alpha \delta_{c_1 b_1} \lambda_{c_2 b_2}^\beta \lambda_{c_3 b_3}^\beta + \lambda_{a_1 d_1}^\alpha \delta_{a_2 d_2} \lambda_{a_3 d_3}^\alpha \lambda_{c_1 b_1}^\beta \delta_{c_2 b_2} \lambda_{c_3 b_3}^\beta) \\ &+ \frac{1}{4(N_c^2 - 1)} \left( \frac{N_c}{2(N_c^2 - 4)} d^{\alpha\beta\gamma} d^{\alpha'\beta'\gamma'} \lambda_{a_1 d_1}^\alpha \lambda_{a_2 d_2}^\beta \lambda_{a_3 d_3}^\gamma \lambda_{c_1 b_1}^{\alpha'} \lambda_{c_2 b_2}^{\beta'} \lambda_{c_3 b_3}^{\gamma'} + \frac{1}{2N_c} f^{\alpha\beta\gamma} f^{\alpha'\beta'\gamma'} \lambda_{a_1 d_1}^\alpha \lambda_{a_2 d_2}^\beta \lambda_{a_3 d_3}^\gamma \lambda_{c_1 b_1}^{\alpha'} \lambda_{c_2 b_2}^{\beta'} \lambda_{c_3 b_3}^{\gamma'} \right); \end{aligned} \quad (\text{G7})$$

(3)  $p = 4$ —

$$\begin{aligned} \int dUU_{a_1 b_1} U_{c_1 d_1}^\dagger U_{a_2 b_2} U_{c_2 d_2}^\dagger U_{a_3 b_3} U_{c_3 d_3}^\dagger U_{a_4 b_4} U_{c_4 d_4}^\dagger &= \frac{1}{N_c^4} \delta_{a_1 d_1} \delta_{a_2 d_2} \delta_{a_3 d_3} \delta_{a_4 d_4} \delta_{c_1 b_1} \delta_{c_2 b_2} \delta_{c_3 b_3} \delta_{c_4 b_4} \\ &+ \left[ \frac{1}{N_c} \delta_{a_4 d_4} \delta_{c_4 b_4} \left( \int dUU_{a_1 b_1} U_{c_1 d_1}^\dagger U_{a_2 b_2} U_{c_2 d_2}^\dagger U_{a_3 b_3} U_{c_3 d_3}^\dagger - \frac{1}{N_c^3} \delta_{a_1 d_1} \delta_{a_2 d_2} \delta_{a_3 d_3} \delta_{c_1 b_1} \delta_{c_2 b_2} \delta_{c_3 b_3} \right) + \text{permutations} \right] \\ &+ \lambda_{a_1 d_1}^\alpha \lambda_{a_2 d_2}^\beta \lambda_{a_3 d_3}^\gamma \lambda_{a_4 d_4}^\delta \lambda_{c_1 b_1}^{\alpha'} \lambda_{c_2 b_2}^{\beta'} \lambda_{c_3 b_3}^{\gamma'} \lambda_{c_4 b_4}^{\delta'} \left[ \frac{1}{16(N_c^2 - 1)^2} (\delta^{\alpha\beta} \delta^{\gamma\delta} \delta^{\alpha'\beta'} \delta^{\gamma'\delta'} + \delta^{\alpha\gamma} \delta^{\beta\delta} \delta^{\alpha'\gamma'} \delta^{\beta'\delta'} + \delta^{\alpha\delta} \delta^{\beta\gamma} \delta^{\alpha'\delta'} \delta^{\beta'\gamma'}) \right. \\ &+ \frac{1}{4(N_c^2 - 1)} \left( \frac{N_c^2}{4(N_c^2 - 4)^2} d^{\alpha\beta\epsilon} d^{\gamma\delta\epsilon} d^{\alpha'\beta'\rho} d^{\gamma'\delta'\rho} + \frac{1}{4(N_c^2 - 4)} d^{\alpha\beta\epsilon} f^{\gamma\delta\epsilon} d^{\alpha'\beta'\epsilon'} f^{\gamma'\delta'\epsilon'} + \frac{1}{4(N_c^2 - 4)} f^{\alpha\beta\epsilon} d^{\gamma\delta\epsilon} f^{\alpha'\beta'\epsilon'} d^{\gamma'\delta'\epsilon'} \right. \\ &\left. \left. + \frac{1}{4N_c^2} f^{\alpha\beta\epsilon} f^{\gamma\delta\epsilon} f^{\alpha'\beta'\epsilon'} f^{\gamma'\delta'\epsilon'} \right) \right]. \end{aligned} \quad (\text{G8})$$

- 
- [1] A. Athenodorou, Ph. Boucaud, F. De Soto, J. Rodríguez-Quintero, and S. Zafeiropoulos, Instanton liquid properties from lattice QCD, *J. High Energy Phys.* **02** (2018) 140.
- [2] A. A. Belavin, Alexander M. Polyakov, A. S. Schwartz, and Yu. S. Tyupkin, Pseudoparticle Solutions of the Yang-Mills Equations, *Phys. Lett.* **59B**, 85 (1975).
- [3] Curtis G. Callan, Jr., R. F. Dashen, and David J. Gross, The structure of the gauge theory vacuum, *Phys. Lett.* **63B**, 334 (1976).
- [4] Curtis G. Callan, Jr., Roger F. Dashen, and David J. Gross, Toward a theory of the strong interactions, *Phys. Rev. D* **17**, 2717 (1978).
- [5] Edward V. Shuryak, The role of instantons in quantum chromodynamics. I. Physical vacuum, *Nucl. Phys.* **B203**, 93 (1982).
- [6] Thomas Schäfer and Edward V. Shuryak, Instantons in QCD, *Rev. Mod. Phys.* **70**, 323 (1998).
- [7] Edward Shuryak and Ismail Zahed, Hadronic structure on the light front. I. Instanton effects and quark-antiquark effective potentials, *Phys. Rev. D* **107**, 034023 (2023).
- [8] Thomas Schäfer and Edward V. Shuryak, Glueballs and instantons, *Phys. Rev. Lett.* **75**, 1707 (1995).
- [9] M. Kacir, M. Prakash, and I. Zahed, Hadrons and QCD instantons: A bosonized view, *Acta Phys. Pol. B* **30**, 287 (1999), [arXiv:hep-ph/9602314](https://arxiv.org/abs/hep-ph/9602314).

- [10] T. Schäfer and V. Zetocha, Instantons and the spin of the nucleon, *Phys. Rev. D* **69**, 094028 (2004).
- [11] Ioannis Iatrakis, Adith Ramamurti, and Edward Shuryak, Collective string interactions in AdS/QCD and high-multiplicity pA collisions, *Phys. Rev. D* **92**, 014011 (2015).
- [12] Edward Shuryak, Lectures on nonperturbative QCD (Non-perturbative topological phenomena in QCD and related theories), [arXiv:1812.01509](https://arxiv.org/abs/1812.01509).
- [13] B. Duran *et al.*, Determining the gluonic gravitational form factors of the proton, *Nature (London)* **615**, 813 (2023).
- [14] Zein-Eddine Meziani, Gluonic gravitational form factors of the proton, in *Proceedings of the 25th International Spin Symposium* (2024); [arXiv:2403.08423](https://arxiv.org/abs/2403.08423).
- [15] Dmitri Diakonov, Maxim V. Polyakov, and C. Weiss, Hadronic matrix elements of gluon operators in the instanton vacuum, *Nucl. Phys.* **B461**, 539 (1996).
- [16] Stanley J. Brodsky and Glennys R. Farrar, Scaling laws at large transverse momentum, *Phys. Rev. Lett.* **31**, 1153 (1973).
- [17] A. V. Radyushkin, Deep elastic processes of composite particles in field theory and asymptotic freedom, [arXiv:hep-ph/0410276](https://arxiv.org/abs/hep-ph/0410276).
- [18] G. M. Huber *et al.* (Jefferson Lab Collaboration), Charged pion form-factor between  $Q^2 = 0.60\text{-GeV}^2$  and  $2.45\text{-GeV}^2$ . II. Determination of, and results for, the pion form-factor, *Phys. Rev. C* **78**, 045203 (2008).
- [19] D. Brömmel *et al.* (QCDSF/UKQCD Collaboration), The Pion form-factor from lattice QCD with two dynamical flavours, *Eur. Phys. J. C* **51**, 335 (2007).
- [20] Bigeng Wang, Fangcheng He, Gen Wang, Terrence Draper, Jian Liang, Keh-Fei Liu, and Yi-Bo Yang ( $\chi$ QCD Collaboration), Trace anomaly form factors from lattice QCD, [arXiv:2401.05496](https://arxiv.org/abs/2401.05496).
- [21] Daniel C. Hackett, Dimitra A. Pefkou, and Phiala E. Shanahan, Gravitational form factors of the proton from lattice QCD, [arXiv:2310.08484](https://arxiv.org/abs/2310.08484).
- [22] Y. Chen *et al.*, Glueball spectrum and matrix elements on anisotropic lattices, *Phys. Rev. D* **73**, 014516 (2006).
- [23] Wei Sun, Long-Cheng Gui, Ying Chen, Ming Gong, Chuan Liu, Yu-Bin Liu, Zhaofeng Liu, Jian-Ping Ma, and Jian-Bo Zhang, Glueball spectrum from  $N_f = 2$  lattice QCD study on anisotropic lattices, *Chin. Phys. C* **42**, 093103 (2018).
- [24] Martin Hoferichter, Jacobo Ruiz de Elvira, Bastian Kubis, and Ulf-G. Meißner, Remarks on the pion–nucleon  $\sigma$ -term, *Phys. Lett. B* **760**, 74 (2016).
- [25] J. M. Alarcón, Brief history of the pion–nucleon sigma term, *Eur. Phys. J. Spec. Top.* **230**, 1609 (2021).
- [26] Yi-Bo Yang, Jian Liang, Yu-Jiang Bi, Ying Chen, Terrence Draper, Keh-Fei Liu, and Zhaofeng Liu, Proton mass decomposition from the QCD energy momentum tensor, *Phys. Rev. Lett.* **121**, 212001 (2018).
- [27] Kiminad A. Mamo and Ismail Zahed,  $J/\psi$  near threshold in holographic QCD: A and D gravitational form factors, *Phys. Rev. D* **106**, 086004 (2022).
- [28] Gen Wang, Yi-Bo Yang, Jian Liang, Terrence Draper, and Keh-Fei Liu ( $\chi$ QCD Collaboration), Proton momentum and angular momentum decompositions with overlap fermions, *Phys. Rev. D* **106**, 014512 (2022).
- [29] C. Alexandrou, S. Bacchio, M. Constantinou, J. Finkenrath, K. Hadjiyiannakou, K. Jansen, G. Koutsou, H. Panagopoulos, and G. Spanoudes, Complete flavor decomposition of the spin and momentum fraction of the proton using lattice QCD simulations at physical pion mass, *Phys. Rev. D* **101**, 094513 (2020).
- [30] Dmitri Diakonov, Chiral symmetry breaking by instantons, in *Proceedings of the International School of Physics "Enrico Fermi"* (1996), 130, 397.
- [31] Maciej A. Nowak, Mannque Rho, and I. Zahed, *Chiral Nuclear Dynamics* (World Scientific Publishing Company, Singapore, 1996).
- [32] Christopher Michael and P. S. Spencer, Instanton size distributions from calibrated cooling, *Nucl. Phys. B, Proc. Suppl.* **42**, 261 (1995).
- [33] Christopher Michael and P. S. Spencer, Cooling and the SU(2) instanton vacuum, *Phys. Rev. D* **52**, 4691 (1995).
- [34] Derek B. Leinweber, Visualizations of the QCD vacuum, in *Proceedings of the Workshop on Light-Cone QCD and Nonperturbative Hadron Physics* (1999), pp. 138–143; [arXiv:hep-lat/0004025](https://arxiv.org/abs/hep-lat/0004025).
- [35] P. J. Moran and D. B. Leinweber, Buried treasure in the sand of the QCD vacuum, in *Proceedings of the QCD Downunder II* (2008); [arXiv:0805.4246](https://arxiv.org/abs/0805.4246).
- [36] M. C. Chu, J. M. Grandy, S. Huang, and John W. Negele, Correlation functions of hadron currents in the QCD vacuum calculated in lattice QCD, *Phys. Rev. D* **48**, 3340 (1993).
- [37] Ismail Zahed, Mass sum rule of hadrons in the QCD instanton vacuum, *Phys. Rev. D* **104**, 054031 (2021).
- [38] V. A. Novikov, Mikhail A. Shifman, A. I. Vainshtein, and Valentin I. Zakharov, Are all hadrons alike?, *Nucl. Phys.* **B191**, 301 (1981).
- [39] Edward Witten, Current algebra theorems for the U(1) Goldstone boson, *Nucl. Phys.* **B156**, 269 (1979).
- [40] G. Veneziano, U(1) without instantons, *Nucl. Phys.* **B159**, 213 (1979).
- [41] Gerard 't Hooft, Computation of the quantum effects due to a four-dimensional pseudoparticle, *Phys. Rev. D* **14**, 3432 (1976); **18**, 2199(E) (1978).
- [42] J. J. M. Verbaarschot and I. Zahed, Spectral density of the QCD Dirac operator near zero virtuality, *Phys. Rev. Lett.* **70**, 3852 (1993).
- [43] Hartmut Wittig, QCD on the lattice, in *Particle Physics Reference Library: Volume 1: Theory and Experiments*, edited by Herwig Schopper (Springer Cham, Cham, Switzerland, 2020), pp. 137–262.
- [44] P. V. Pobylitsa, The quark propagator and correlation functions in the instanton vacuum, *Phys. Lett. B* **226**, 387 (1989).
- [45] Arthur Kock, Yizhuang Liu, and Ismail Zahed, Pion and kaon parton distributions in the QCD instanton vacuum, *Phys. Rev. D* **102**, 014039 (2020).
- [46] Thomas Schäfer, Edward V. Shuryak, and J. J. M. Verbaarschot, Baryonic correlators in the random instanton vacuum, *Nucl. Phys.* **B412**, 143 (1994).
- [47] V. Bernard, U. G. Meissner, and I. Zahed, Decoupling of the pion at finite temperature and density, *Phys. Rev. D* **36**, 819 (1987).

- [48] S. P. Klevansky, The Nambu-Jona-Lasinio model of quantum chromodynamics, *Rev. Mod. Phys.* **64**, 649 (1992).
- [49] Craig D. Roberts, David G. Richards, Tanja Horn, and Lei Chang, Insights into the emergence of mass from studies of pion and kaon structure, [arXiv:2102.01765](https://arxiv.org/abs/2102.01765).
- [50] Jeff Greensite, Confinement from center vortices: A review of old and new results, *EPJ Web Conf.* **137**, 01009 (2017).
- [51] James C. Biddle, Waseem Kamleh, and Derek B. Leinweber, Visualization of center vortex structure, *Phys. Rev. D* **102**, 034504 (2020).
- [52] James C. Biddle, Waseem Kamleh, and Derek B. Leinweber, Visualisations of centre vortices, *EPJ Web Conf.* **245**, 06010 (2020).
- [53] Maciej A Nowak, Mannque Rho, and Ismail Zahed, *Chiral Nuclear Dynamics* (World Scientific, Singapore, 1996), 10.1142/1681.
- [54] A. I. Vainshtein, Valentin I. Zakharov, V. A. Novikov, and Mikhail A. Shifman, ABC's of instantons, *Sov. Phys. Usp.* **25**, 195 (1982).
- [55] N. I. Kochelev, Anomalous quark chromomagnetic moment induced by instantons, *Phys. Lett. B* **426**, 149 (1998).
- [56] Dmitri Diakonov and V. Yu. Petrov, Instanton based vacuum from Feynman variational principle, *Nucl. Phys.* **B245**, 259 (1984).
- [57] Thomas Schäfer and Edward V. Shuryak, The interacting instanton liquid in QCD at zero and finite temperature, *Phys. Rev. D* **53**, 6522 (1996).
- [58] P. Faccioli and Edward V. Shuryak, Systematic study of the single instanton approximation in QCD, *Phys. Rev. D* **64**, 114020 (2001).
- [59] Wei-Yang Liu, Edward Shuryak, and Ismail Zahed, Hadronic structure on the light-front. VII. Pions and kaons and their partonic distributions, *Phys. Rev. D* **107**, 094024 (2023).
- [60] Wei-Yang Liu, Edward Shuryak, and Ismail Zahed, Hadronic structure on the light-front VIII. Light scalar and vector mesons, [arXiv:2307.16302](https://arxiv.org/abs/2307.16302).
- [61] B. L. Ioffe, Condensates in quantum chromodynamics, *Phys. At. Nucl.* **66**, 30 (2003).
- [62] S. Aoki *et al.* (Flavour Lattice Averaging Group), FLAG review 2019: Flavour lattice averaging group (FLAG), *Eur. Phys. J. C* **80**, 113 (2020).
- [63] Yachao Qian and Ismail Zahed, Spin physics through QCD instantons, *Ann. Phys. (Amsterdam)* **374**, 314 (2016).
- [64] Dmitri Diakonov, Instantons at work, *Prog. Part. Nucl. Phys.* **51**, 173 (2003).
- [65] Edward Shuryak and Ismail Zahed, Nonperturbative quark-antiquark interactions in mesonic form factors, *Phys. Rev. D* **103**, 054028 (2021).
- [66] C. Weiss, Nucleon matrix element of Weinberg's CP-odd gluon operator from the instanton vacuum, *Phys. Lett. B* **819**, 136447 (2021).
- [67] Xiangdong Ji, Yizhuang Liu, and Ismail Zahed, Mass structure of hadrons and light-front sum rules in the  $t$  Hooft model, *Phys. Rev. D* **103**, 074002 (2021).
- [68] Ismail Zahed, Spin sum rule of the nucleon in the QCD instanton vacuum, *Symmetry* **14**, 932 (2022).
- [69] Martin Luscher and Filippo Palombi, Universality of the topological susceptibility in the SU(3) gauge theory, *J. High Energy Phys.* **09** (2010) 110.
- [70] I. Zahed, QCD instantons in vacuum and matter, *Nucl. Phys.* **B427**, 561 (1994).
- [71] Edward V. Shuryak and J. J. M. Verbaarschot, Screening of the topological charge in a correlated instanton vacuum, *Phys. Rev. D* **52**, 295 (1995).
- [72] P. Di Vecchia and G. Veneziano, Chiral dynamics in the large  $n$  limit, *Nucl. Phys.* **B171**, 253 (1980).
- [73] J. Gasser and H. Leutwyler, Chiral perturbation theory: Expansions in the mass of the strange quark, *Nucl. Phys.* **B250**, 465 (1985).
- [74] H. Leutwyler and Andrei V. Smilga, Spectrum of Dirac operator and role of winding number in QCD, *Phys. Rev. D* **46**, 5607 (1992).
- [75] Romuald A. Janik, Maciej A. Nowak, Gabor Papp, and Ismail Zahed, U(1) problem at finite temperature, *AIP Conf. Proc.* **494**, 408 (1999).
- [76] J. P. Ma, Diffractive photoproduction of  $\eta_c$ , *Nucl. Phys.* **A727**, 333 (2003).
- [77] Florian Hechenberger, Kiminad A. Mamo, and Ismail Zahed, Threshold production of  $\eta_{c,b}$  using holographic QCD, [arXiv:2401.12162](https://arxiv.org/abs/2401.12162).
- [78] Adam Freese and Ian C. Cloët, Gravitational form factors of light mesons, *Phys. Rev. C* **100**, 015201 (2019); **105**, 059901(E) (2022).
- [79] Xiangdong Ji, Proton mass decomposition: Naturalness and interpretations, *Front. Phys. (Beijing)* **16**, 64601 (2021).
- [80] Xiang-Dong Ji, Breakup of hadron masses and energy—momentum tensor of QCD, *Phys. Rev. D* **52**, 271 (1995).
- [81] Kiminad A. Mamo and Ismail Zahed, Diffractive photoproduction of  $J/\psi$  and  $\Upsilon$  using holographic QCD: Gravitational form factors and GPD of gluons in the proton, *Phys. Rev. D* **101**, 086003 (2020).
- [82] Yoshitaka Hatta, Abha Rajan, and Kazuhiro Tanaka, Quark and gluon contributions to the QCD trace anomaly, *J. High Energy Phys.* **12** (2018) 008.
- [83] D. J. Gross and Frank Wilczek, Asymptotically free gauge theories. 2, *Phys. Rev. D* **9**, 980 (1974).
- [84] H. David Politzer, Setting the scale for predictions of asymptotic freedom, *Phys. Rev. D* **9**, 2174 (1974).
- [85] Ju-Hyun Jung, Ulugbek Yakshiev, and Hyun-Chul Kim, Energy—momentum tensor form factors of the nucleon within a  $\pi$ - $\rho$ - $\omega$  soliton model, *J. Phys. G* **41**, 055107 (2014).
- [86] P. E. Shanahan and W. Detmold, Gluon gravitational form factors of the nucleon and the pion from lattice QCD, *Phys. Rev. D* **99**, 014511 (2019).
- [87] Dimitra A. Pefkou, Daniel C. Hackett, and Phiala E. Shanahan, Gluon gravitational structure of hadrons of different spin, *Phys. Rev. D* **105**, 054509 (2022).
- [88] Tie-Jiun Hou *et al.*, New CTEQ global analysis of quantum chromodynamics with high-precision data from the LHC, *Phys. Rev. D* **103**, 014013 (2021).
- [89] P. Schweitzer, The Sigma term form-factor of the nucleon in the large- $N_c$  limit, *Phys. Rev. D* **69**, 034003 (2004).
- [90] M. Wakamatsu, On the D-term of the nucleon generalized parton distributions, *Phys. Lett. B* **648**, 181 (2007).
- [91] C. Cebulla, K. Goeke, J. Ossmann, and P. Schweitzer, The nucleon form-factors of the energy momentum tensor in the Skyrme model, *Nucl. Phys.* **A794**, 87 (2007).

- [92] Dmitri Diakonov, Instantons and baryon dynamics, in *Proceedings of the 9th International Conference on the Structure of Baryons* (2002), pp. 153–164; [arXiv:hep-ph/0205054](#).
- [93] V.D. Burkert, L. Elouadrhiri, and F.X. Girod, The pressure distribution inside the proton, *Nature (London)* **557**, 396 (2018).
- [94] Maxim V. Polyakov and Peter Schweitzer, Forces inside hadrons: Pressure, surface tension, mechanical radius, and all that, *Int. J. Mod. Phys. A* **33**, 1830025 (2018).
- [95] James V. Steele, Hidenaga Yamagishi, and Ismail Zahed, The Pion—nucleon sigma term and the Goldberger-Treiman discrepancy, [arXiv:hep-ph/9512233](#).
- [96] Xiang-Dong Ji, A QCD analysis of the mass structure of the nucleon, *Phys. Rev. Lett.* **74**, 1071 (1995).
- [97] Cédric Lorcé, On the hadron mass decomposition, *Eur. Phys. J. C* **78**, 120 (2018).
- [98] Craig D. Roberts, On mass and matter, *AAPPS Bull.* **31**, 6 (2021).
- [99] Andreas Metz, Barbara Pasquini, and Simone Rodini, Revisiting the proton mass decomposition, *Phys. Rev. D* **102**, 114042 (2021).
- [100] Alexandre Deur, Stanley J. Brodsky, and Guy F. De Téra mond, The spin structure of the nucleon, *Rep. Prog. Phys.* **82**, 076201 (2019).
- [101] Xiang-Dong Ji, Gauge-invariant decomposition of nucleon spin, *Phys. Rev. Lett.* **78**, 610 (1997).
- [102] Stephen L. Adler, Axial vector vertex in spinor electrodynamics, *Phys. Rev.* **177**, 2426 (1969).
- [103] J. Ashman *et al.* (European Muon Collaboration), An investigation of the spin structure of the proton in deep inelastic scattering of polarized muons on polarized protons, *Nucl. Phys.* **B328**, 1 (1989).
- [104] Stanley J. Brodsky, John R. Ellis, and Marek Karliner, Chiral symmetry and the spin of the proton, *Phys. Lett. B* **206**, 309 (1988).
- [105] John R. Ellis and Marek Karliner, Nucleon spin, in *Proceedings of the Workshop on the Prospects of Spin Physics at HERA* (1995), pp. 141–152; [arXiv:hep-ph/9510402](#).
- [106] V. Yu. Alexakhin *et al.* (COMPASS Collaboration), The deuteron spin-dependent structure function  $g_1^d$  and its first moment, *Phys. Lett. B* **647**, 8 (2007).
- [107] A. Airapetian *et al.* (HERMES Collaboration), Precise determination of the spin structure function  $g_1$  of the proton, deuteron and neutron, *Phys. Rev. D* **75**, 012007 (2007).
- [108] Constantia Alexandrou, Martha Constantinou, Kyriakos Hadjiyiannakou, Karl Jansen, and Floriano Manigrasso, Flavor decomposition of the nucleon unpolarized, helicity, and transversity parton distribution functions from lattice QCD simulations, *Phys. Rev. D* **104**, 054503 (2021).
- [109] C. Alexandrou, S. Bacchio, M. Constantinou, K. Hadjiyiannakou, K. Jansen, and G. Koutsou, Quark flavor decomposition of the nucleon axial form factors, *Phys. Rev. D* **104**, 074503 (2021).
- [110] Keh-Fei Liu, Quark and glue components of the proton spin from lattice calculation, *Int. J. Mod. Phys. Conf. Ser.* **40**, 1660005 (2016).
- [111] Mauro Anselmino, Enrico Predazzi, Svante Ekelin, Sverker Fredriksson, and D.B. Lichtenberg, Diquarks, *Rev. Mod. Phys.* **65**, 1199 (1993).
- [112] Reinhard Alkofer, Maciej A. Nowak, J. J. M. Verbaarschot, and I. Zahed, Pseudoscalars in the instanton liquid model, *Phys. Lett. B* **233**, 205 (1989).
- [113] Martin Luscher, Trivializing maps, the Wilson flow and the HMC algorithm, *Commun. Math. Phys.* **293**, 899 (2010).
- [114] Martin Luscher and Peter Weisz, Perturbative analysis of the gradient flow in non-Abelian gauge theories, *J. High Energy Phys.* **02** (2011) 051.
- [115] Petros Dimopoulos *et al.*, Topological susceptibility and  $\eta'$  meson mass from  $N_f = 2$  lattice QCD at the physical point, *Phys. Rev. D* **99**, 034511 (2019).
- [116] Michael Creutz, On invariant integration over  $SU(N)$ , *J. Math. Phys. (N.Y.)* **19**, 2043 (1978).
- [117] S. Chernyshev, Maciej A. Nowak, and I. Zahed, Heavy hadrons and QCD instantons, *Phys. Rev. D* **53**, 5176 (1996).
- [118] Maciej A. Nowak, J. J. M. Verbaarschot, and I. Zahed, Flavor mixing in the instanton vacuum, *Nucl. Phys.* **B324**, 1 (1989).
- [119] Nicholas Miesch, Edward Shuryak, and Ismail Zahed, Baryons and tetraquarks using instanton-induced interactions, [arXiv:2308.05638](#).